Study of different texture zeros of neutrino mass matrices in seesaw mechanism and their group symmetry realization

Priyanka Kumar

Department of Physics

Cotton College (currently Cotton University)

This thesis is submitted to

Gauhati University as requirement for the degree of

Doctor of Philosophy

Faculty of Science

March 2020

Certificate

This is to certify that the thesis entitled "**Study of different texture zeros of neutrino mass matrices in seesaw mechanism and their group symmetry realization**" is the result of research work of Ms. Priyanka Kumar, carried under my supervision and submitted to Gauhati University for the award of the degree of Doctor of Philosophy in Physics.

Dr. Mahadev Patgiri, Supervisor

March 2020

Members of the Research Advisory Committee:

Declaration

I hereby declare that the thesis entitled "**Study of different texture zeros of neutrino mass matrices in seesaw mechanism and their group symmetry realization**" is the result of my own research work which has been carried out under the guidance of Dr. Mahadev Patgiri of Cotton University. I further declare that this thesis as a whole or any part thereof has not been submitted to any university (or institute) for the award of any degree or diploma.

This thesis contains less than 90,000 (ninety thousand) words excluding bibliography and captions.

Priyanka Kumar

Priyanka Kumar

March 2020

Dedicated to my loving parents

Nagendra Kumar (Father)

&

Meera Choudhury (Mother)

Acknowledgements

In this section, I take the opportunity to thank all the people who have directly or indirectly helped me throughout my journey in successful completion of this thesis.

First of all, I would like to express my sincere thanks to my respected Supervisor Dr. Mahadev Patgiri, Associate Professor, Department of Physics, Cotton University, for his intellectual, invaluable and excellent guidance throughout my PhD work. His kind support, immense knowledge and inspirational contribution have greatly helped me at each and every stage of my research tenure. Without his resourceful supervision, this thesis would not have been possible. Words will always fall short to express my heartfelt gratitude and immense respect I have for him.

I would to like to express my sincere regards to Prof. Debojit Sarma, Department of Physics, Cotton University, for his encouraging words, educative discussions and valuable suggestions in different aspects of my PhD work.

My deepest gratitude to Prof. Ngangkham Nimai Singh, Department of Physics, Manipur University for his advice, encouragement and critical suggestions of my work. All the fruitful discussions with him have always motivated me and developed my interests to work in diverse fields of particle physics.

I would like to thank Prof. Ganesh C. Wary, Head of the Department of Physics, Cotton University, for his kind support, encouraging words and providing all the necessary research

facilities in the Department. I am thankful to all the faculty members and non teaching staff of the Department of Physics, Cotton University for their valuable suggestions and constant support throughout these years.

My sincere thanks to Dr. Mrinal K. Das, Associate Professor, Department of Physics, Tezpur University, whom I visited and learnt various aspects of particle physics. I thank him for providing all the necessary help during my stay at the University as a visiting research scholar.

I am thankful to Dr. Subhankar Roy, Assistant Professor, Department of Physics, Gauhati University, who has always motivated me and helped me in various aspects of my PhD work. His critical and beneficiary suggestions have always provoked me to have a deep understanding of the subject.

My heartfelt thanks to my friends Luxmi, Devanand, Sangeeta, Partha, Manas Da, Jitu Da, Manashree for their motivation, support and making this period very memorable.

My heartfelt thanks to my closest friend and my support system, Sneha and Gunajit for being the constant source of inspiration.

I shall always remain thankful to my dear little sister Pritysmita (Buli) for playing the perfect role of a critics as well as a mentor and keeping me motivated throughout this venture. I express my love and affection to her.

Last but not the least, I express my deepest gratitude to my loving and encouraging parents. Without their unconditional love, unfailing support, care and sacrifices, this thesis would never have been possible. I shall forever remain indebted to them.

Abstract

In this thesis, we explore the different texture zero models of neutrino mass matrices in presence of an additional eV-scale sterile neutrino. The presence of an additional flavor of neutrino of eV-scale was first hinted by the LSND experiment, which is now popularly known as the LSND anomaly. In the (3+1) scenario, that is, three active and one light sterile neutrino the system becomes more complicated and constrained. For theoretical understanding of the eV scale sterile neutrino and their admixture with the three active neutrinos, we consider the Minimal Extended Seesaw (MES) mechanism. MES mechanism is an extension to the canonical type-I seesaw mechanism with an additional gauge singlet chiral field 'S'. The construction of MES mechanism is such that an eV scale sterile neutrino naturally appears without the need to include any Yukawa coupling or mass scale for sterile neutrino. Neutrino mass matrix m_ν in MES is built from (3×3) form of Dirac neutrino mass matrix M_D, (3×3) form of Majorana neutrino mass matrix M_R and (1×3) row matrix M_S which couples the singlet field 'S' with the three right-handed neutrinos.

In our work, we study the texture zeros of neutrino mass matrices within the context of MES mechanism. We consider different zero textures of M_D, M_R and M_S which finally propagates as zeros of m_ν in MES. We explore the zero textures of both $m_\nu^{3\times 3}$ and $m_\nu^{4\times 4}$ in our study. Accordingly we consider the (3×3) and (4×4) form of neutrino mass matrix of MES mechanism. We restrict ourselves to phenomenologically predictive scenarios :

(4+4) scheme, (5+3) scheme and (6+2) scheme where the digit within the pairs represent the number of zeros of M_D and M_R respectively along with suitable zero textures of M_S. There are a large number of combinations of M_D, M_R and M_S within the predictive scenario which leads to the desired zero texture of $m_\nu^{3\times3}$ and $m_\nu^{4\times4}$. However, S_3 group permutation between the different combinations of M_D, M_R and M_S leads to only a minimum number of basic cases. On realizing the textures we arrive at certain correlations between the neutrino mass matrix elements. We check the viability of the textures by scanning their respective correlations under recent neutrino oscillation data. For viability check of $m_\nu^{4\times4}$ we consider different constrained ranges of the Dirac and Majorana CP phases and discuss the role played by the CP phases in determining the viability of the textures. Textures which are allowed within 3σ range of experimental data are then realized via suitable Abelian flavor symmetry group Z_n by extending the Standard Model with few scalar fields. We also find that S_3 symmetric textures follows a definite pattern of symmetry realization. We demonstrate how symmetry realization of the S_3 symmetric textures can be obtained by a simple interchange of Z_n transformation of the right-handed neutrino singlets of the basic combination.

Table of contents

List of figures

List of tables

1

INTRODUCTION

1.1 A brief overview on neutrinos

The horizon of our knowledge for understanding of the underlying working principles of the universe has been dramatically expanded by the theoretical and experimental efforts and achievements for the last few decades. In the journey of such scientific endeavour in various fields for unearthing the mysteries, new challenges pose in the way of formulation of theories as well as experimentations. One of such interesting challenges in particle physics is massive neutrinos. In 1930, W. Pauli first proposed a concept of $\frac{1}{2}$ spin, zero electric charge and zero mass particle called neutrino for understanding the continuous energy spectrum of the β

decay process, otherwise, the finger would have pointed to the question of validity of the celebrated principle of conservation of energy. Almost 26 years after Pauli's proposition of neutrino, in 1956, F. Reines and C. Cowan [1] could detect anti-neutrino in a nuclear reactor through inverse beta decay reaction :

$$\bar{\nu}_e + p \rightarrow e^+ + n. \tag{1.1}$$

Later in 1962 the muon neutrino was discovered at Brookhaven National Laboratory [2] whereby it was observed that neutrinos produced in association with muons behave differently as those produced in association with electrons. The third type of neutrino - ν_τ was discovered in 2001 at the DONUT ("Direct Observation of Nu Tau") experiment at Fermilab [3].

The myth of neutrinos being massless was finally broken in the late 1990's by various neutrino experiments [4–13] which observed that neutrinos produced with a particular flavor eigenstate, oscillate to a different flavor after propagating a macroscopic distance. This quantum mechanical phenomenon, known as "neutrino oscillation", gives us the insight that neutrino flavor or weak eigenstates for interactions are different from their mass eigenstates implying that neutrinos do mix and thus have a non zero mass. Since neutrinos are massless in the Standard Model of electroweak theory, the strong experimental evidence of neutrino oscillations indicating neutrinos being massive is new physics beyond Standard Model. Although the oscillation experiments have shown neutrinos to be massive, but their masses are in about sub-eV scale, that is, several times smaller than the mass of an electron. The smallness of neutrino mass still remains to be an enigma and is believed to open the doors for new and unexplored area of physics related to such small mass scales beyond Standard Model. It is also believed that a deeper understanding of these elusive neutrinos may hold a clue to the long standing problem of the fermion mass generation as well as some long standing cosmological issues.

Besides the three active neutrino species at the sub-eV scale, there could be a possibility of the existence of additional light sterile neutrino states at the eV scale, which may be solution for the anomalous results of the LSND experiment [14, 15]. Subsequently a number of other experiments [16–19] have been performed, but their results could not rule out the LSND anomaly. In such scenario, the proposition of at least one light sterile neutrino has been gathering attentions of both theoretical and experimental physicists. The presence of such eV scale sterile neutrinos shall be a new challenge in particle physics and shall also have implications to other fields like astrophysics and cosmology.

The study of neutrino masses, mixing and number of species is important for enhancing the clarity of our understanding of some phenomena or beginning of new search in unknown terrain of physics which have been summarised with no exhaustive list in the following. Neutrinos are a unique tool for searching various aspects of physics on scales ranging from 10^{-33} to 10^{28}cm. (i) Applications in particle physics include: νN, μN, eN scattering for existence/properties of quarks and QCD; weak decays for Fermi theory, parity violation, mixing; neutral current, electroweak unification, field theory etc.; neutrino mass for constraint on TeV scale physics, grand unification, superstrings, extra dimensions. (ii) Similarly applications in astrophysics and cosmology include: core of Sun, atmospheric neutrinos, violent events like GRBs, AGNs etc.; large scale structure (dark matter); nucleosynthesis of small atomic number (big bang) to large atomic number (supernova) via stable atomic number for iron (steller); baryogenesis for matter-antimatter asymmetry of the early universe.

1.2 Experimental evidences and neutrino oscillations

It is clear beyond any doubt from the solar and atmospheric observations in a number of experiments like Homestake, Gallex, SAGE, Super-Kamiokande (SK) and SNO collaborations that neutrinos change their identities (flavors) on transit from one place to another. These gave rise to the solar and atmospheric neutrino anomalies and the LSND anomaly

after the LSND experiment at Los Alamos National Laboratory. The first watershed proof of neutrino oscillations was the results of the Superkamiokande experiment (SK) [9] in 1998 that observed an up-down asymmetry of high energy events generated by atmospheric neutrinos (ν_μ) and thereby providing a model independent proof of oscillation of atmospheric neutrinos. Similarly, the Sudbury Neutrino Observatory (SNO) was the first experiment which gave the first clear evidence for solar neutrino (ν_e) oscillation [7, 8]. Apart from the natural sources there are a number of short and long base line laboratory experiments where neutrinos are produced in accelerators and reactors. K2K (KEK to Kamioka) is the first long baseline neutrino accelerator experiment [11] which was designed to confirm the oscillation of atmospheric neutrinos detected at Super-K experiment. Results from K2K were found to be consistent with the oscillation of atmospheric neutrinos reported by SK collaboration. There are a number of other neutrino oscillation experiments like Daya Bay [20, 21], Double CHOOZ [22], KamLAND [23], MINOS [24], NOνA [25], RENO [26], T2K [27] and so on, which not only have given clear evidence of neutrino oscillation but have also provided precise and solid information regarding the oscillation parameters. There are a few completed/ongoing (or future plan) non-oscillation experiments [28–33] required to measure the mass scale, Dirac or Majorana, hierarchy of mass orderings of the three active neutrinos etc. of which information and measurements are not possible in the oscillation experiments.

In the oscillation experiments, neutrinos are detected in charged-current (CC) weak interaction processes with weak eigenstates or flavors : ν_e, ν_μ, ν_τ. The neutrino mass matrix, in general, is not diagonal which implies that neutrino flavor eigenstates (ν_e, ν_μ, ν_τ) are different from the mass eigenstates (ν_1, ν_2, ν_3). Therefore, the probability that a neutrino with flavor eigenstate $|\nu_\alpha\rangle$ to be in the same eigenstate will oscillate with time.

A neutrino flavor eigenstate $|\nu_\alpha\rangle$ produced with a definite flavor at time $t = 0$, after travelling some distance L evolves as:

$$|\nu_\alpha(t)\rangle = \sum_{i=1}^{n} U^*_{\alpha i} |\nu_i(t)\rangle = \sum_{i=1}^{n} U^*_{\alpha i} e^{-iE_i t} |\nu_i\rangle . \tag{1.2}$$

Here n represents the number of light neutrino species, U is a unitary matrix, known as the neutrino mixing matrix which relates the neutrino flavor eigenstates with mass eigenstates.

Probability of flavor transition from flavor eigenstate $\nu_\alpha \to \nu_\beta$ is given by

$$P_{\alpha\beta} = |\langle \nu_\beta | \nu_\alpha(t) \rangle|^2 = \sum_{i,j} U^*_{\alpha i} U_{\beta i} U_{\alpha j} U^*_{\beta j} e^{-i(E_i - E_j)t}. \tag{1.3}$$

For ultrarelativistic limit for tiny neutrino mass, we can approximate $p_i >> m_i$, $p_i \approx p_j$ and $|\vec{p}| \simeq E$ and $E_i \simeq p_i + \frac{m_i^2}{2p_i}$, $E_i - E_j \simeq \frac{\Delta m^2_{ij}}{2E}$ and $t \approx L$. Using orthogonality condition of mass eigenstates, the transition probability in Eq. (1.3) can be rewritten as

$$P_{\alpha\beta} = \delta_{\alpha\beta} - 4\sum_{i>j} Re(U^*_{\alpha i} U_{\beta i} U_{\alpha j} U^*_{\beta j}) \sin^2 \Delta_{ij} + 2\sum_{i>j} Im(U^*_{\alpha i} U_{\beta i} U_{\alpha j} U^*_{\beta j}) \sin 2\Delta_{ij}, \tag{1.4}$$

where

$$\Delta_{ij} \equiv \frac{(m_i^2 - m_j^2)L}{4E} \equiv 1.27 \frac{\Delta m^2_{ij}}{eV^2} \frac{L/E}{m/MeV}. \tag{1.5}$$

and Δm^2_{ij} represents the mass squared difference of two neutrino mass eigenstates ν_i and ν_j. Transition probability in Eq. (1.4) shows oscillatory behaviour where oscillation length l^{osc}_{ij} is

$$l^{osc}_{ij} = \frac{4\pi E}{\Delta m^2_{ij}} \simeq 2.48m \frac{E(MeV)}{\Delta m^2(eV^2)} \simeq 2.48km \frac{E(GeV)}{\Delta m^2(eV^2)}. \tag{1.6}$$

l^{osc}_{ij} is the distance between any two closest minima or maxima of the transition probability. Eq. (1.4) depicts that, for neutrinos to undergo flavor oscillation, Δm^2_{ij} must be non-vanishing, that is, neutrinos must have different masses. Thus, experimental observation from neutrino oscillation shows that, at least one of the neutrino mass eigenstates $|\nu_i\rangle$ should have non-zero mass, so that there exists at least one non-zero mass difference between any two neutrino mass

eigenstate in accordance with the condition $\Delta m^2_{ij} \neq 0$. Also $U_{\alpha i}U_{\beta i} \neq 0$, that is, they must mix. Furthermore, the oscillation experiment to be sensitive to a given value Δm^2_{ij}, the baseline L and oscillation length l^{osc} should be of the same order $L \sim l^{osc}$, that is, the experiment should be set up with the condition $E/L \approx \Delta m^2_{ij}$. For $L << l^{osc}$ ($E/L >> \Delta m^2$), oscillation effects are negligible because $\sin^2 \Delta_{ij} << 1$. Conversely, for $L >> l^{osc}$, oscillation effects are negligible, due to averaging over neutrino spectrum and the uncertainty over baseline length, leading to the average value $\left\langle \sin^2 \Delta_{ij} \right\rangle = 1/2$.

Two-flavor case

Considering the oscillation between the two species ν_e and ν_μ, mixing matrix U is of 2×2 form as

$$U = \begin{pmatrix} \cos\theta & \sin\theta \\ -\sin\theta & \cos\theta \end{pmatrix}, \tag{1.7}$$

where θ is the mixing angle. Two-flavor oscillation involves only one mass squared difference Δm^2 and the transition probability takes the form

$$P_{\nu_e \to \nu_\mu} = \sin^2 2\theta \sin^2 \left(1.27 \Delta m^2 \frac{L}{E} \right). \tag{1.8}$$

Three-flavor case

For oscillation between the three flavors ν_e, ν_μ, ν_τ, the neutrino mixing matrix U_ν takes a more complicated 3×3 form, which connects the neutrino mass eigenstate (ν_1, ν_2, ν_3) and flavor eigenstate $(\nu_e, \nu_\mu, \nu_\tau)$ as

$$\begin{pmatrix} \nu_e \\ \nu_\mu \\ \nu_\tau \end{pmatrix} = \begin{pmatrix} U_{11} & U_{12} & U_{13} \\ U_{21} & U_{22} & U_{23} \\ U_{31} & U_{32} & U_{33} \end{pmatrix} \begin{pmatrix} \nu_1 \\ \nu_2 \\ \nu_3 \end{pmatrix}. \tag{1.9}$$

In the flavor basis, the flavor eigenstate for charged lepton coincides with its mass eigenstate. Thus, the charged lepton mixing matrix ($U_l^\dagger$) is diagonal. Thus, the total lepton mixing matrix $U = U_l^\dagger U_\nu$ coincides with the neutrino mixing matrix U_ν. The standard parametrization of the lepton mixing matrix is given by

$$U_{PMNS} = U.P, \tag{1.10}$$

where

$$U = \begin{pmatrix} c_{12}c_{13} & s_{12}c_{13} & s_{13}e^{-i\delta} \\ -s_{12}c_{23} - c_{12}s_{23}s_{13}e^{i\delta} & c_{12}c_{23} - s_{12}s_{23}s_{13}e^{i\delta} & s_{23}c_{13} \\ s_{12}s_{23} - c_{12}c_{23}s_{13}e^{i\delta} & -c_{12}s_{23} - s_{12}c_{23}s_{13}e^{i\delta} & c_{23}c_{13} \end{pmatrix}, \tag{1.11}$$

and

$$P = \begin{pmatrix} 1 & 0 & 0 \\ 0 & e^{-\frac{i\alpha}{2}} & 0 \\ 0 & 0 & e^{-i(\frac{\beta}{2}-\delta)} \end{pmatrix}. \tag{1.12}$$

The above parametrization consists of three mixing angles $\theta_{12}, \theta_{13}, \theta_{23}$, one Dirac CP violating phase δ and two Majorana CP phases α, β. The three rotation angles are related to the physical observables in the first approximation as: $\theta_{23} = \theta_{atm}$, the atmospheric angle, which can be measured in the atmospheric neutrino oscillation experiments; $\theta_{12} = \theta_{sol}$, solar angle, determined from solar neutrino experiments and $\theta_{13} = \theta_{reactor}$, reactor angle from reactor neutrino oscillation experiments. It is interesting to note that in the above parametrization, Dirac CP phase δ is always associated with the reactor angle θ_{13}, which implies that for vanishing reactor angle δ remains undetermined and hence doesnot appear in the mixing matrix U. A measure of Dirac CP violation is given by Jarlskog rephasing invariant [34] J_{CP} where

$$J_{CP} = Im[U_{e1}U_{\mu 2}U_{e2}^* U_{\mu 1}^*]. \tag{1.13}$$

In accordance with the PDG parametrization J_{CP} takes the following form

$$J_{CP} = s_{12}s_{23}s_{13}c_{12}c_{23}c_{13}^2 \sin\delta. \tag{1.14}$$

From Eq. (1.14) it is obvious that for $J_{CP} \neq 0$, CP violating phase δ as well as all the mixing angles must be non-zero.

1.3 Seesaw mechanism

For the possibility of inter-species oscillations to occur, neutrinos must be massive and do mix among themselves. The mass squared differences and mixing angles measured by the experiments tell that the mass of a neutrino is about six orders of magnitude smaller than that of an electron and two of the three mixing angles are very large. To understand such tiny masses and large mixing angles of neutrinos, the successful neutrino models are so far based on the seesaw mechanism which is briefly discussed below.

In the premise of the Standard Model (SM) of particle physics the neutrino is massless due to the following aspects of the model: (i) the absence of the right-handed partner (ν_R) and (ii) the exactness of $B-L$ global symmetry. There is a possibility of constructing a model relaxing these two assumptions of SM with inclusion of (i) one right-handed neutrinos (N_R) per generation making the SM completely quark-lepton symmetric with the gauge group $SU(2)_L \times SU(2)_R \times U(1)_{B-L}$ [35, 36]. The electric charge takes the form $Q = I_{3L} + I_{3R} + \frac{B-L}{2}$. Hence it can be concluded that below the scale v_R where $SU(2)_R \times U(1)_{B-L}$ breaks down to SM and above the electroweak scale M_W, one can have the relation $\Delta I_{3R} = -\Delta\frac{B-L}{2}$ [37]. This relation has a profound consequence that neutrinos are Majorana particle exhibiting lepton number violating phenomena in nature like $\nu 0\beta\beta$ processes. Seesaw mechanism is based on such ideas and serves to be one of the most simple and attractive model for generating tiny neutrino masses [38–41]. There are three forms of seesaw mechanisms which

are generally used: type-I, type-II and type-III seesaw mechanism. The basic idea of seesaw mechanism is to generate ultra small neutrino mass by inclusion of very heavy external fields, thereby forming a seesaw between both the mass scales. In type-I, type-II and type-III seesaw mechanism, the external heavy fields are the three right-handed neutrino singlets, one scalar Higgs triplet and three $SU(2)_L$ triplet respectively, thereby going beyond the SM in their own way. Our work mainly concentrates on type-I seesaw mechanism and its minimal extension. We shall therefore have a brief discussion on type-I seesaw only.

Type-I seesaw

Here the SM extension is done by including three right-handed neutrinos which are singlets under $SU(2)_L$. Presence of such right-handed neutrinos allow Dirac mass term for neutrinos. In addition, Majorana mass term is also possible for electrically neutral neutrinos.
The total Lagrangian for neutrinos takes the form

$$-\mathscr{L} = \mathscr{L}_{M_D} + \mathscr{L}_{M_R} = M_D \bar{\nu}_R \nu_L + \frac{1}{2}\bar{\nu}_R^c M_R \nu_R + h.c.. \tag{1.15}$$

Here L and R stands for left and right-handedness respectively. M_D, M_R are the complex 3×3 Dirac and symmetric Majorana mass matrices respectively.

Combined M_D and M_R gives rise to the 6×6 Majorana mass matrix M of the form:

$$M = \begin{pmatrix} 0 & M_D \\ M_D^T & M_R \end{pmatrix}. \tag{1.16}$$

The Dirac mass term M_D is of the order of electroweak scale, owing to its origin from *vev* of Higgs field Φ. On the other hand, the Majorana mass term M_R, invariant under $SU(3)_C \times SU(2)_L \times U(1)_Y$, remains unconstrained by gauge symmetry and therefore can have arbitrarily large mass and can be many orders larger than the electroweak scale, that is, $M_R \gg M_D$. The mass matrix M in Eq. (1.16) on block diagonalization leads to the famous

seesaw mechanism

$$m_\nu^{light} = -M_D M_R^{-1} M_D^T. \tag{1.17}$$

The light neutrino mass matrix m_ν in Eq. (1.17) is inversely proportional to the large Majorana mass M_R. The mass scale for M_R is often taken to be of the order of GUT scale, in order to explain sub-eV scale neutrino masses. The smallness of neutrino mass m_ν is a direct consequence of large mass scale of M_R. This is the basic principle of type-I seesaw mechanism.

1.4 Experimental hints beyond 3 light neutrino paradigm

During the last two decades, the neutrino physics has witnessed a tremendous progress in the precision measurement of neutrino parameters like mixing angles $(\theta_{12}, \theta_{13}, \theta_{23})$ and mass squared differences $(\Delta m^2_{21}, |\Delta m^2_{13}|)$ of the three active neutrinos in experiments as well as theoretical formulation of underlying theory to understand the three neutrino paradigm. Physicists around the globe have been putting constant efforts to solve the long standing problems of origin of such a small mass scale, CP violation and mass hierarchy to name a few. Amidst the mysteries that still prevails in the three neutrino paradigm, there are a number of oscillation experiments which yields some intriguing yet controversial results which cannot be explained in the three neutrino framework. Such anomalous results have been found in both appearance and disappearance measurement experiments, some of which are discussed below:

LSND Experiment: Liquid Scintillation Neutrino Detector (LSND) [14, 15] at the Los Alamos Neutron Science Centre was designed for the search of $\bar{\nu}_\mu - \bar{\nu}_e$ oscillation with a baseline of $L \sim 30$m. It uses high intensity proton beam ($\sim 800 MeV$) to produce pions which decays to muons. μ^+ that are produced decays at rest to produce $\bar{\nu}_\mu$. The experiment was set up to search for $\bar{\nu}_e$ which if produced will undergo $\bar{\nu}_e p \to e^+ n$ with the protons present

in the detector. The signal that one looks for is the Cherenkov radiation produced by e^+ in the detector with $(20 < E_e < 60MeV)$ and a 2.2MeV γ produced from neutron capture on a free proton: $np \to d\gamma$. The final LSND oscillation results taken from $1993-1998$ shows a clear excess of $(87 \pm 22.4 \pm 6.0)$ events corresponding to an oscillation probability of $(0.264 \pm 0.067 \pm 0.045)\%$. The oscillation probability between $\bar{\nu}_\mu$ and $\bar{\nu}_e$ however corresponds to mass squared difference $\Delta m^2 \sim 1$ eV^2 which contradicts with the solar and atmospheric mass squared differences in the three neutrino paradigm :$\Delta m^2_{sol} = 7.5 \times 10^{-5}$eV^2 and $\Delta m^2_{atm} = 2.3 \times 10^{-3}$eV^2. This is known as the LSND anomaly which hints towards the presence of an additional neutrino state with mass of the order of eV scale.

MiniBooNE: The Mini Booster Neutrino Experiment [16] at Fermilab has been designed to test the LSND results. The baseline was kept at L$\sim$ 50m but with same L/E as the LSND experiment. Here proton beams of energy $8MeV$ were focussed on a Be target producing pions and kaons which decays to ν_μ and $\bar{\nu}_\mu$. The experiment is capable of running in both the modes: neutrino mode; $\nu_\mu \to \nu_e$ oscillation search and antineutrino mode; $\bar{\nu}_\mu \to \bar{\nu}_e$. Their antineutrino oscillation data are consistent for the range $\Delta m^2 \approx (0.01-1.0)$eV and have some overlap with the LSND antineutrino oscillation data. At low energies, an event excess of 162 ± 47.8 (3.4σ) was observed whose energy distribution was found to be marginally compatible with simple two-neutrino oscillation scenario.

Radiochemical Experiments (*Gallium radioactive source experiments*): The Gallex and SAGE solar neutrino experiments have been tested with intense radioactive sources ^{51}Cr and ^{37}Ar placed in the detector [17, 18]. The ν_e that are produced during the radioactive decay have been detected through the same process employed for solar neutrino detection:

$$\nu_e + {}^{71}Ga \to {}^{71}Ge + e^-. \tag{1.18}$$

It was found that the the ratio of expected to observed counts of ^{71}Ge, averaged between both the experiments was 2.7σ low. On analysing the data in terms of neutrino oscillation

indicates the mass squared difference to be $\Delta m^2 \geq 0.35$ eV^2 at 99% C.L.. This can be interpreted as oscillation between ν_e and some fourth flavor of neutrino and thereby evading detection.

Reactor experiments: Neutrinos from reactor experiments are basically electron antineutrinos emitted from subsequent β-decay of unstable fission fragments. The neutron-rich fission fragments undergoes inverse beta decay reaction $\bar{\nu}_e + p \rightarrow n + e^+$ with the hydrogen present in Liquid scintillator detector.Almost all the energies of the electron antineutrino is carried away by the positron, which serves as a prompt signal. A recent re-evaluation reports an increase in the $\bar{\nu}_e$ flux from reactors upto 3.5%. This small increase in flux although has no effect on KamLAND's solar parameter results, when combined with the previously observed small deficits at smaller distances, results in a larger average deficit of 5.7%. This is known as the *reactor antineutrino anomaly*. Such a deficit can be explained with an additional flavor of neutrino with mass squared difference $|\Delta m^2| \geq 1.5eV^2$ [19].

In addition, recent cosmological data from cosmological microwave background (CMB) and Large Scale Structure (LSS) on weakly interacting relativistic "dark radiation" prefers additional degrees of freedom (d.o.f.) [42]. Light sterile neutrinos beyond SM serves to be the most natural and convincing candidate corresponding to the extra d.o.f.. If this new source of radiation is attributed to addtional neutrino species then WMAP data points towards the bound on the number of neutrinos to be $N_{eff} = 3.84 \pm 0.40$ [43].

The above experimental anomalies can be explained on extending the SM with one (or more) neutrino state with mass at the eV scale. However, LEP data [44] on measurement of Z-line shape, limits the number of light neutrinos coupling to the Z boson to be 3. Thus, the new neutrino state must be a singlet fermion under SM which doesnot participate in weak interactions, that is, the new neutrino state must be 'sterile'. The sterile neutrinos donot take part in ordinary charged and neutral current weak interactions, but mix significantly with the three active neutrinos.

On the other hand, the results provided by KAMREN experiment [45], MINOS experiment [46], ICARUS [47], ν_e – Carbon scattering experiment [48] and Planck data [49] could not support sterile neutrino state, but could not rule out also. The NEOS collaboration [50] has set an upper limit on mixing angle θ_{14} with $\sin^2 2\theta_{14} < 0.1$ for Δm^2_{41} ranging from $(0.2 - 2.3)eV^2$ at 90% C.L..

Recently in May 2018, the MiniBooNE collaboration [51] once again confirmed the excess of events reported by the LSND experiment and the significance of the combined LSND and MiniBooNE excesses was reported to be 6.1σ. Again the ANITA experiment [52], in August 2018, reported that they observed two unusual upgoing air shower events, which are consistent with the τ-lepton decay origin but contradicts the standard neutrino-matter interaction models. Sterile neutrinos can serve as a possible explanation [53] for the unusual upward air shower events at ANITA experiment. All these controversies have raised one's curiosity and posed new challenges so as to develop a particle physics model to accommodate the light sterile neutrino and at the same time to have a consistent cosmological model. Many new oscillation experiments are proposed/planned to testify the status of sterile neutrinos and reach to a definitive conclusion. It has been observed that with recent reactor flux prediction, there has been a considerable improvement in the global fits when five neutrino framework, that is, when two sterile neutrinos are considered [54]. However, an analysis in [55] shows that the viability of a cosmological model with two eV scale sterile neutrinos depends significantly on the choice of the cosmological data sets used in the analysis and the fitting procedures. Their analysis depicts that conclusive statement regarding the viability of a cosmologically consistent model with two sterile neutrinos still cannot be made. The authors of Ref. [56] performed an analysis on both the 3+1 and 3+2 mixing schemes and found a preference of 3+1 framework over 3+2. They found that the parameter goodness of fit obtained in the 3+2 scheme is mainly due to increased number of oscillation parameters as compared to 3+1 scheme and therefore is mainly a statistical effect. Presence

of thermalized sterile neutrinos in early Universe although is compatible with Big-Bang Nucleosynthesis data [57], the presence of more than one sterile neutrino is disfavored [58]. Thus, the four neutrino framework is considered to be the minimal extension and a more consistent cosmological model.

In the context of four neutrino scheme, there are three possible ways of adding a sterile neutrino in the SM mass patterns- (i) 3+1 scheme, with three active neutrinos of sub-eV scale and one sterile neutrino of eV scale [59, 60] (ii) 2+2 scheme, where two different neutrino pairs differ in their mass by eV^2 (iii) 1+3 scheme, where three active neutrinos are in eV scale and one sterile neutrino lighter than the three active neutrinos. The solar and atmospheric data [61] disfavors the 2+2 scheme. Also, the 1+3 scheme is disfavored from cosmology [62, 63]. In our work we shall concentrate on the (3+1) scheme which is considered to be the minimal form.

1.5 Theoretical framework for (3+1) neutrino scheme

In the four-neutrino scenario, the neutrino flavor eigenstate ν_α ($\alpha = e, \mu, \tau, s$) are related to their mass eigenstate ν_i ($i = 1, 2, 3, 4$) via

$$\nu_\alpha = \sum_{i=1}^{4} U_{\alpha i} \nu_i. \tag{1.19}$$

Assuming the charged lepton mass matrix to be diagonal, the complex symmetric 4×4 Majorana neutrino mass matrix in the flavor basis can be written as

$$m_\nu^{4\times4} = V m_\nu^{diag} V^T = \begin{pmatrix} m_{ee} & m_{e\mu} & m_{e\tau} & m_{es} \\ m_{e\mu} & m_{\mu\mu} & m_{\mu\tau} & m_{\mu s} \\ m_{e\tau} & m_{\mu\tau} & m_{\tau\tau} & m_{\tau s} \\ m_{es} & m_{\mu s} & m_{\tau s} & m_{ss} \end{pmatrix}. \tag{1.20}$$

The symmetric Majorana mass matrix $m_\nu^{4\times4}$ contains ten independent mass elements unlike six in the three neutrino scenario. Here, $m_\nu^{diag} = (m_1, m_2, m_3, m_4)$ is the diagonal neutrino mass matrix in the mass basis. Diagonalizing matrix V is the 4×4 PMNS-like leptonic mixing matrix which can be expressed as

$$V = UP. \tag{1.21}$$

Here U represents the mixing matrix for Dirac neutrinos. Apart from the solar (θ_{12}), atmospheric (θ_{23}) and reactor (θ_{13}) mixing angles, the mixing matrix U contains three active-sterile mixing (ASM) angles θ_{14}, θ_{24} and θ_{34} which quantifies the $\nu_s - \nu_e$, $\nu_s - \nu_\mu$ and $\nu_s - \nu_\tau$ mixings respectively, along with three Dirac CP violating phases.

Parametrizing U explicitly as [64]

$$U = (R_{34}\tilde{R}_{24}\tilde{R}_{14})(R_{23}\tilde{R_{13}})R_{12}, \tag{1.22}$$

$R_{ij}/\tilde{R}_{ij}$ are the 4×4 rotation matrix in the ij flavor space and $\delta_{13}, \delta_{14}, \delta_{24}$ are the Dirac CP violating phases

$$R_{34} = \begin{pmatrix} 1 & 0 & 0 & 0 \\ 0 & 1 & 0 & 0 \\ 0 & 0 & c_{34} & s_{34} \\ 0 & 0 & -s_{34} & c_{34} \end{pmatrix}, \quad \tilde{R}_{24} = \begin{pmatrix} 1 & 0 & 0 & 0 \\ 0 & c_{24} & 0 & s_{24}e^{-i\delta_{24}} \\ 0 & 0 & 1 & 0 \\ 0 & -s_{24}e^{i\delta_{24}} & 0 & c_{24} \end{pmatrix}, \tag{1.23}$$

where $c_{ij} = \cos\theta_{ij}$, $s_{ij} = \sin\theta_{ij}$.

The matrix P in Eq. (1.21) is a diagonal matrix with three Majorana phases (α, β, γ) which can be written as

$$P = diag(1, e^{-i\alpha/2}, e^{-i(\beta/2-\delta_{13})}, e^{-i(\gamma/2-\delta_{14})}). \tag{1.24}$$

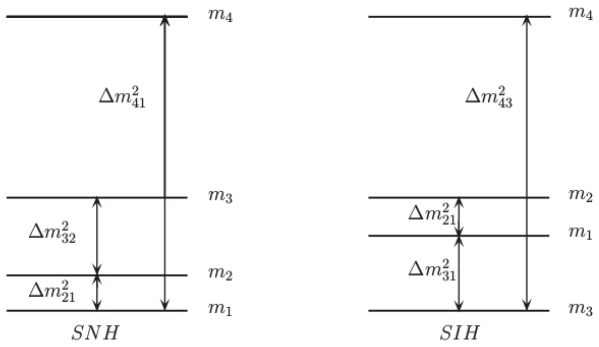

Fig. 1.1 Mass spectrum in 3+1 scheme for normal (SNH) and inverted (SIH) hierarchy.

Apart from the 5 new mixing parameters (3 ASM angles and 2 Dirac CP phases δ_{14}, δ_{24}) mentioned above, the (3+1) model also involves one new mass squared difference $\Delta m^2_{LSND} = \Delta m^2_{41/43}$ between the eV scale sterile neutrino and the light active neutrinos. The additional sterile neutrino along with the three active neutrinos can have two possible mass arrangements: the sterile neutrino mass can either be higher ($\Delta m^2_{41} > 0$) or lower ($\Delta m^2_{41} < 0$) than the mass of the three active neutrinos. In the latter case, the additional sterile state is the lightest while the three active neutrinos are of mass $\simeq$eV each leading to $\sum m \simeq 3eV$ which is inconsistent by cosmological observation [65]. Thus, considering that the sterile neutrino is heavier than the three active neutrinos, the three mass squared difference in the 3+1 picture follows the condition

$$|\Delta m^2_{21}| << |\Delta m^2_{31}| << |\Delta m^2_{41}|. \tag{1.25}$$

As the sign of $|\Delta m^2_{31}|$ is yet to be pinned down, two mass spectra are possible (Fig. 1.1)

(i) Normal hierarchy (SNH) with $m_1 << m_2 << m_3 << m_4$.

(ii) Inverted hierarchy (SIH) with $m_4 >> m_1 \simeq m_2 >> m_3$

1.5.1 Minimal extended seesaw mechanism

In order to accommodate light sterile neutrinos in theory with mass ranging from eV-keV scale, a number of new mechanisms have been proposed [66–75]. A general analysis of the active-sterile mixing have also been studied in Ref. [76]. In the three neutrino scenario seesaw mechanism has played a major role for the theoretical understanding of the smallness of neutrino masses. In the (3+1) framework, the authors of Ref. [67] made a similar approach for generating an eV scale sterile neutrino within the seesaw framework. In the context of type-I seesaw mechanism, an eV scale sterile neutrino can be realized by bringing one of the heavy right-handed neutrinos ($\sim 10^{14}$ GeV) states down to the eV scale [67]. However, such a scenario is quite trivial as the seesaw Lagrangian already has atleast one particle at the desired eV scale and therefore contradicts the seesaw spirit. For accommodating an eV scale sterile neutrino, the authors of Ref. [67] considered an extension of the canonical type-I seesaw mechanism whereby the Standard Model is extended by an additional neutral heavy fermion (heavier than the SM scale), apart from the three right-handed neutrinos. This extended version of the canonical type-I seesaw mechanism is popularly known as **Minimal Extended Seesaw (MES) Mechanism**. In the MES framework, an eV scale sterile neutrino is generated without the priori presence of states with eV scale masses and is therefore more within the seesaw spirit. We now present a details on the MES mechanism in the following which shall be the common formalism of all the chapters thereafter.

For the theoretical understanding of the origin of an eV scale sterile neutrino as well as its mixing with the three active neutrinos, the authors of Ref. [67] studied the minimal extension of canonical type-I seesaw mechanism, popularly known as minimal extended seesaw mechanism (MES). In MES mechanism, the Standard Model is extended with an additional gauge singlet chiral field 'S', apart from the three right-handed neutrinos ($\nu_{eR}, \nu_{\mu R}, \nu_{\tau R}$). Within this scenario, an eV scale sterile neutrino naturally appears, without needing to insert any small mass term for ν_s.

Thus the Lagrangian representing Dirac and Majorana mass terms with sterile neutrino mass term is of the following form [67]

$$-\mathscr{L}_m = \bar{\nu}_L M_D \nu_R + \bar{S}^c M_S \nu_R + \frac{1}{2}\bar{\nu}_R^c M_R \nu_R + h.c.. \tag{1.26}$$

With only one extra gauge singlet field 'S', the mass matrix M_S is a 1×3 row matrix which couples the singlet field 'S' and the three right-handed neutrinos. In the (ν_L, ν_R^c, S^c) basis, the neutrino mass matrix becomes a 7×7 matrix of the following form

$$m_\nu^{7\times 7} = \begin{pmatrix} 0 & M_D & 0 \\ M_D^T & M_R & M_S^T \\ 0 & M_S & 0 \end{pmatrix}. \tag{1.27}$$

On implementing the seesaw approximation $M_R \gg M_S > M_D$ the heavy RH ν are much heavier than the electroweak scale and hence gets decoupled at low energy scale. Block diagonalization of Eq. (1.27) using seesaw approximation reduces the 7×7 neutrino mass matrix in the basis (ν_L, S^c) to a 4×4 mass matrix of the following form:

$$m_\nu^{4\times 4} = -\begin{pmatrix} M_D M_R^{-1} M_D^T & M_D M_R^{-1} M_S^T \\ M_S (M_R^{-1})^T M_D^T & M_S M_R^{-1} M_S^T \end{pmatrix}. \tag{1.28}$$

$m_\nu^{4\times 4}$ in Eq. (1.28) is a square matrix containing four light eigenstates corresponding to three active neutrinos and one sterile neutrino [68] and their masses gets suppresed by a factor M_R^{-1} which is within the seesaw spirit. However, the determinant of the mass matrix $m_\nu^{4\times 4}$ is

zero.

$$\begin{aligned}\det(m_\nu^{4\times4}) &= \det(M_D M_R^{-1} M_D^T)\det[-M_S M_R^{-1} M_S^T \\ &\quad + M_S M_R^{-1} M_D^T (M_D M_R^{-1} M_D^T)^{-1} M_D M_R^{-1} M_S^T] \\ &= \det(M_D M_R^{-1} M_D^T)\det[M_S(M_R^{-1} - M_R^{-1})M_S^T] \\ &= 0.\end{aligned} \tag{1.29}$$

$m_\nu^{4\times4}$ is therefore a matrix of rank 3 which implies that at least one of the active neutrinos is massless. Here, both M_D and M_R are considered to be non-singular.

There can be three possible scenarios [68] for the mass scale of M_S :
1) $M_D \sim M_S$: Within this scenario, $m_\nu^{4\times4}$ is a nearly democratic matrix which implies maximal active-sterile mixing and therefore is incompatible with experimental observations.
2) $M_D > M_S$: Under this scenario, the active neutrinos are heavier than the sterile state. Block diagonalization of Eq. (1.28) then leads to the active-sterile neutrino mass matrix at the leading order of the form $m_\nu = -M_D M_R^{-1} M_D^T$ which is the same as type-I seesaw mechanism and also a vanishing sterile neutrino mass. In view of the experimental observations on active-sterile mass squared differences which is $\sim eV^2$ would then imply that all the three active neutrinos are located at the eV scale. This would lead to a large value of $\sum m_i$ resulting in tensions with standard cosmological constraints. We shall therefore, concentrate on the third and only possible scenario where $M_S > M_D$.

As $M_S > M_D$, the seesaw approximation can be applied once again to Eq. (1.28) to obtain the modified active neutrino mass matrix to its leading term as

$$m_\nu^{3\times3} \sim M_D M_R^{-1} M_S^T (M_S M_R^{-1} M_S^T)^{-1} M_S (M_R^{-1})^T M_D^T - M_D M_R^{-1} M_D^T, \tag{1.30}$$

with the mass of the sterile neutrino as

$$m_s \sim -M_S M_R^{-1} M_S^T . \tag{1.31}$$

The mass matrix M_S being a 1×3 row matrix, prevents the right-hand-side of Eq. (1.30) from vanishing. There would have been an exact cancellation between the two terms of Eq. (1.30) if M_S would have been a square matrix.

The active-sterile neutrino mixing matrix takes the form-

$$V \sim \begin{pmatrix} (1 - \frac{1}{2} R R^+) U & R \\ -R^+ U & 1 - \frac{1}{2} R^+ R \end{pmatrix}, \tag{1.32}$$

where U is the unitary matrix diagonalising the mass matrix $m_\nu^{3\times 3}$.

$$R_{3\times 1} = M_D M_R^{-1} M_S^T (M_S M_R^{-1} M_S^T)^{-1} = (V_{e4}, V_{\mu 4}, V_{\tau 4})^T . \tag{1.33}$$

$R_{3\times 1} = (V_{e4}, V_{\mu 4}, V_{\tau 4})^T$ defines the strength of active-sterile mixing and is essentially suppressed by the ratio $\mathcal{O}(M_D)/\mathcal{O}(M_S)$.

An illustration have also been made in Ref. [67] where one arrives at $m_s \approx 1.3$ eV, $m_\nu \approx 0.05$eV and $R \approx 0.2$, assuming $M_D \approx 10^2$GeV, $M_S \approx 5 \times 10^2$ GeV and $M_R \approx 2 \times 10^{14}$ GeV.

Within the context of MES mechanism, at least three heavy right-handed neutrinos are required so as to suppress the masses of active as well as sterile neutrinos. Two of the heavy right-handed neutrinos generates two massive active neutrinos, while one of them gives rise to the mass of ν_s.

The minimal extended seesaw mechanism is an extension to the canonical type-I seesaw mechanism. Due to the absence of fermionic degrees of freedom, type-II seesaw does not provide the possibility of light sterile neutrinos. Although the neutral components of

fermionic triplets in type-III seesaw plays similar role as the right-handed neutrinos in type-I seesaw, they are not gauge singlets and therefore cannot be accounted for light sterile neutrinos.

1.6 Texture zeros and symmetry realization

Texture zeros

Texture zero models have been successful in explaining the masses and mixings in both the sectors - quarks and leptons. Zeros in the mass matrix elements is the simplest and transparent way of inducing relations among the physical quantities (masses, mixing angles and CP phases) of the mass matrix m_ν and thereby reducing the number of free parameters [77]. A complex symmetric Majorana neutrino mass matrix $m_\nu^{3\times3}$ for three active neutrinos has nine physical quantities : three neutrino masses, three mixing angles, one Dirac CP phase and two Majorana CP phases which leads to four correlation conditions among the physical quantities [78, 79]. One zero in m_ν corresponds to one-zero texture, two zeros in m_ν corresponds to two-zero texture and so on. Free parameters can be further reduced if one considers a vanishing neutrino mass ($m_1 = 0$ (NH) or $m_3 = 0$ (IH)) along with zero textures of m_ν. One vanishing neutrino mass along with one-zero in m_ν imposes only two correlation conditions: one related to the vanishing absolute value and another to the vanishing argument on the parameters-masses, mixing angles and CP phases [80]. More number of zeros implies more correlation conditions, that is, more restrictions on the mass matrix m_ν. In that sense, two-zero textures are more restrictive and thereby lead to more predictive models compared to the one-zero textures. Apart from zero textures of m_ν, there are a number of papers in literature where zeros of m_ν^{-1} are also explored leading to interesting phenomenologies [81].

Zeros in the light neutrino mass matrices can be imposed directly by hand. A complex symmetric neutrino mass matrix $m_\nu^{3\times3}$ has six independent entries. However, in the three

neutrino scenario, the current neutrino oscillation data disfavours the neutrino mass matrices with three or more zeros [78]. There are ${}^6C_3 = 20$ possible three-zero textures of $m_\nu^{3\times3}$, but none of them are compatible with neutrino oscillation data. Similarly, out of 15 possible two-zeros textures of $m_\nu^{3\times3}$, only 7 patterns can withstand the current experimental data [78]. And out of 6 possible one-zero textures [80], 4 textures survive the experimental constraints with inverted mass ordering ($m_3 = 0$), whereas in normal mass ordering ($m_1 = 0$) all the 6 textures are ruled out at 3σ range of experimental values. From a more deeper theoretical front, zeros in the light neutrino mass matrices can also be imposed via type-I seesaw mechanism which is the prime candidate for understanding the smallness of neutrino mass. In the context of type-I seesaw mechanism, the light neutrino mass matrix m_ν is the product of a more basic Dirac neutrino mass matrix M_D and right-handed Majorana neutrino mass matrix M_R. It has been highlighted by many authors [82–84] that zeros of M_D and M_R propagates as zeros in effective neutrino mass matrix m_ν via type-I seesaw mechanism. Thus, considering zeros in M_D and M_R will be more natural than considering zeros in m_ν alone. Apart from type-I seesaw mechanism, zero textures of m_ν have also been investigated in the framework of Inverse seesaw [85–94] mechanism .

A detailed study on texture zeros have also been made in the (3+1) picture, [95–99], that is, three active and one light sterile neutrino. In the (3+1) scenario, the neutrino mass matrix m_ν takes a (4×4) form with 10 independent entries. However, it is to be mentioned that in $m_\nu^{4\times4}$ zeros are allowed only in the active sector of the mass matrix. Zeros in the sterile sector, that is, in the fourth row and column are disfavored by neutrino oscillation data.

Symmetry realization

Texture zero models in general, seems to be quite arbitrary and will not lead to renormalizable models [100]. However, zeros implemented through suitable Abelian symmetries with an extended scalar sector can promote the texture zero schemes into renormalizable field theories

[101]. In our work, for realization of the zero textures of the fermion mass matrices we shall concentrate on discrete Abelian flavor symmetry group Z_n. A group G is said to be Abelian, if all the elements of the group are commutable to each other, that is , $ab = ba$ for any elements a,b in the group G. If $a^n = e$, where e is the identity element of the group, then 'n' is said to be the order of the group and is also defined as the number of elements of the group G. The element 'a', which can generate the whole group elements is called the generator of the group. A discrete Abelian group Z_n has elements $(1, \omega, \omega^2, \omega^3 ....., \omega^{n-1})$ where $\omega^n = 1$ and $\omega = e^{i\frac{2\pi}{n}}$ is the generator of the group.

For a given mass matrix with zeros in arbitrary entries, it is always possible to find suitable Abelian symmetry group Z_n with an extended scalar sector such that the texture zeros originates from these symmetries [101, 102]. Vice versa, Abelian symmetries may also be used to impose zeros in any arbitrary entries of the mass matrix [103, 104]. Apart from Abelian symmetry group, realization of zero textures is also possible by non-abelian flavor symmetry approach [105]. In presence of an additional flavor symmetry (G_{flavor}), the Standard Model symmetry gets extended to

$$G = SU(3)_C \times SU(2)_L \times U(1)_Y \times G_{flavor}, \tag{1.34}$$

with the condition that Lagrangian of the theory continues to remain invariant on leptonic field transformation under the group G_{flavor}.

Considering the Yukawa Lagrangian

$$-\mathscr{L}_Y = \sum_{i,j=1}^{3} \left(Y_{ij} \bar{D}_{L_i} \phi_{ij} l_{R_j} + \tilde{Y}_{ij} \bar{D}_{L_i} \tilde{\phi}_{ij} \nu_{R_j} + \frac{1}{2} W_{ij} \chi_{ij} \bar{\nu}_{R_i} C \bar{\nu}_{R_j}^T \right) + h.c.. \tag{1.35}$$

Here $\bar{D}_L, l_R, \nu_R$ are the left-handed $SU(2)_L$ doublets, right-handed $SU(2)_L$ singlets and right-handed neutrino singlets respectively. ϕ_{ij} represents the Higgs doublet with hypercharge +1 and $\tilde{\phi}_{ij} = i\tau_2 \phi^*$ with hypercharge -1. Y_{ij} are the (3×3) complex Yukawa coupling matrices.

From the Lagrangian in Eq. (1.35) it is evident that one can have a total of nine Higgs doublet $\phi_{ij}(\tilde{\phi}^*_{ij})$ and six gauge singlet scalar χ_{ij}. Their respective non-zero vaccum expectation values $v_{ij}(u^*_{ij})$ and w_{ij} leads to the charged lepton mass matrix $(M_l)_{ij} = v^*_{ij}Y_{ij}$, Dirac neutrino mass matrix $(M_D)_{ij} = u_{ij}\tilde{Y}_{ij}$ and right-handed Majorana neutrino mass matrix $(M_R)_{ij} = w_{ij}W_{ij}$.

General methods for symmetry realization of zero textures has been provided in paper [100], whereby two methods have been propounded for enforcing zeros in fermion mass matrices by means of Abelian symmetry group with an extended scalar sector. However, specific guidelines for minimal symmetry realization of texture zeros are still lacking.

1.7 Present status of neutrino masses and mixings

The parameter space for three active neutrinos include two independent mass squared differences (Δm^2_{12}, Δm^2_{31}), the three mixing angles ($\theta_{12}, \theta_{13}, \theta_{23}$), Dirac CP violating phase δ and Majorana CP violating phases α, β.

• 3σ values of the two mass squared differences are provided below [106]:

$$\Delta m^2_{21} = (6.93 - 7.97) \times 10^{-5} \quad \text{eV}^2. \tag{1.36}$$

$$\begin{aligned} |\Delta m^2_{31}| &= (2.37 - 2.63) \times 10^{-3} \quad \text{eV}^2 \quad \text{(NH)}, \\ &= (2.33 - 2.60) \times 10^{-3} \quad \text{eV}^2 \quad \text{(IH)}. \end{aligned} \tag{1.37}$$

From the experimental data it is evident that the two mass squared difference $\Delta m^2_{solar} = \Delta m^2_{21}$ and $\Delta m^2_{atmospheric} = |\Delta m^2_{31}|$ differ by two orders of magnitude and thus $R_\nu = \frac{\Delta m^2_{21}}{\Delta m^2_{31}} \simeq 10^{-2}$. The sign of $|\Delta m^2_{31}|$ is not yet known and hence the neutrino mass ordering whether normal or inverted still remains to be an open question. Moreover, the absolute mass scale of m_1, m_2, m_3 is yet to be ascertained.

• The three mixing angles θ_{12}, θ_{23}, θ_{13} are constrained within 3σ as [106]:

$$\begin{aligned}
\sin^2\theta_{12} &= (2.50-3.54)\times 10^{-1}, \\
\sin^2\theta_{13} &= (1.85-2.46)\times 10^{-2} \quad \text{(NH)}, \\
&= (1.86-2.48)\times 10^{-2} \quad \text{(IH)}, \\
\sin^2\theta_{23} &= (3.79-6.16)\times 10^{-1} \quad \text{(NH)}, \\
&= (3.83-6.37)\times 10^{-1} \quad \text{(IH)}.
\end{aligned} \tag{1.38}$$

The reactor mixing angle $\theta_{13} \neq 0$ but is comparatively smaller than the other two mixing angles. Octant of the atmospheric mixing angle θ_{23} is yet to be determined and hence can lie either in the first octant ($\theta_{23} < \pi/4$) or second octant ($\theta_{23} > \pi/4$).

• Dirac as well as Majorana CP phases remains unconstrained $(0-2\pi)$ at 3σ range.

• With three active and one eV scale sterile neutrino, the mass squared difference Δm^2_{LSND} and the active-sterile mixing, represented by the fourth row and column in the 4×4 diagonalizing matrix V_{PMNS} are constrained [107–109] within 3σ as:

$$\begin{aligned}
|V_{e4}|^2 &= (0.012-0.047), \\
|V_{\mu 4}|^2 &= (0.005-0.03), \\
|V_{\tau 4}|^2 &< 0.16, \\
\Delta m^2_{LSND} &= (0.87-2.04)\text{eV}^2.
\end{aligned} \tag{1.39}$$

Here $\Delta m^2_{LSND} = (\Delta m^2_{41}$ or $\Delta m^2_{43})$ depending on whether the hierarchy is Normal (Δm^2_{43}) or Inverted (Δm^2_{41}).

1.8 Motivation for present work

Although neutrino physics has witnessed a tremendous progress in last few decades in both theoretical and experimental fronts, neutrinos continue to enthral us with a number of questions, some of which are listed below:

- Why are neutrino masses so tiny compared to other fermions?
- Why are the two mixing angles of neutrinos are large compared to quark mixing?
- What is the absolute mass scale of neutrinos?
- What is the nature of neutrinos: Dirac or Majorana particles?
- How many neutrino species are there?
- What is the mass hierarchy of neutrinos: Normal or Inverted?
- CP violating phases are yet to be determined?
- Are there light sterile states of neutrinos- answer to LSND anomaly?

In theoretical pursuit of understanding of neutrino masses and mixing, the seesaw mechanism has been recognised as the most popular and successful approach in literature. Seesaw models are the neutrino mass matrices constructed from the following fermion mass matrices: the Dirac neutrino mass matrices M_D and heavy right handed Majorana mass matrices M_R as basis of the models. The fermion mass matrices M_D and M_R are not completely known from the point of view of experiments. Under such a scenario, phenomenological approaches for model building have been playing a useful tool for interpreting new experimental data on leptons as well as quarks. It is expected that these approaches will provide hints on the underlying symmetries of the lepton flavor structure and thereby help in constructing a more realistic model for the same.

The phenomenology of the neutrino mass matrices m_ν hints at negligibly small contributions of certain entries compared to others of the matrices. Thus the simplest approach is to consider neutrino mass matrix with zeros in arbitrary entries. Such textures of neutrino mass matrix with independent zero entries in it are popularly known as ‘texture zeros’. Zeros

in arbitrary entries of the fermion mass matrices can also be imposed via discrete Abelian flavor symmetry group Z_n. Flavor symmetries are horizontal symmetries, that is, it unifies fermions of different families, in contrast to GUT symmetry, where the unification takes place vertically among the different members of each family. Flavor symmetry or family symmetry acting on the three families of the SM might prove to be a guiding principle in solving the long standing flavor problem.

Now the motivation of the present work is primarily and broadly based on (i) theoretical understanding of the LSND anomaly in the framework of Minimal Extended Seesaw (MES) as described in the preceding Section, (ii) study of texture zeros of MES neutrino mass matrices acquired from texture zeros of fermion mass matrices involved, (iii) also origin of zeros from flavour symmetry groups.

1.8.1 Layout of the thesis

In **Chapter 2** we re-investigate the one-zero textures in $m_\nu^{3\times3}$ within the (3+1) scheme in the context of MES mechanism. For realization of the one-zero textures of $m_\nu^{3\times3}$ in the context of MES mechanism we consider the zero textures of 3×3 form of M_D, M_R and 1×3 matrix M_S for phenomenologically predictive cases having total number of zeros of M_D and M_R to be eight. With this motivation, we consider the (4+4) scheme, (5+3) scheme and (6+2) scheme, where the digits of a pair represent the number of zeros of M_D and M_R respectively. We also present the S_3 group transformation existing between the different combinations of M_D, M_R and M_S which yields similar phenomenology. The textures which are found to be viable in our study are realized via Abelian symmetry group Z_7 by extending the SM to include few scalar fields.

In **Chapter 3** we study the two-zero textures of $m_\nu^{4\times4}$ in the context of MES mechanism. The 4×4 MES model deals with 3×3 (M_D), 3×3 (M_R) and 1×3 mass matrix (M_S). As

the 4×4 MES matrix is a matrix of rank three so we consider only those two-zero textures which are of rank three which reduces the number of feasible zero textures to 12, out of 15. We consider the (4+4) scheme, that is, 4 zeros in M_D and 4 zeros in M_R along with one/two zero textures of M_S for realization of the 12 two-zero textures of $m_\nu^{4\times4}$. Similar to $m_\nu^{3\times3}$, S_3 group transformation exists among the different textures of M_D, M_R and M_S in $m_\nu^{4\times4}$ as well, all of which shows similar phenomenology. We also discuss the role of Dirac and Majorana CP phases in determining the viability of the textures. Textures which are allowed within 3σ range of experimental values are realized by discrete Abelian symmetry group Z_9 with the extension of standard model to include some scalar fields.

In **Chapter 4** we present the realization of the rank 3 two-zero textures of $m_\nu^{4\times4}$ under MES mechanism considering (5+3) and (6+2) scheme. Correlations of each textures are examined under recent neutrino oscillation data. We also discuss the interplay of Dirac and Majorana CP phases in determining the viability of the textures. S_3 group permutations of M_D, M_R and M_S under (5+3) scheme is also discussed in this chapter. Viable texturesare then realized via Z_9 Abelian symmetry group.

In **Chapter 5** we finally conclude our work of the thesis in this Chapter along with a broad outlines of the scope of the thesis for extension of future research.

2

Study of texture zeros of MES $m_\nu^{3\times3}$ and Z_7 symmetry realization

2.1 Introduction

This chapter is based on the work published in our paper [98]. The procedure of realization of texture zeros of neutrino mass matrices m_ν, the predictive power of such models and the origin of texture zeros from flavor group symmetry have been discussed in the section 1.6 of Chapter 1. In the three neutrino scenario, texture zeros of m_ν have been extensively studied in

literature [110–124]. A complex symmetric neutrino mass matrix $m_\nu^{3\times3}$ with six independent entries can have six possible one-zero textures. However, with one vanishing neutrino mass only four one-zero textures survive the experimental constraints in inverted hierarchical mass ordering, whereas none of the textures survive with normal hierarchical mass ordering [80]. Similarly, out of 15 possible two-zero textures only 7 textures are allowed by experimental data [78]. Zeros in m_ν can also be realized via type-I seesaw mechanism. In the context of type-I seesaw mechanism, zeros of Dirac neutrino mass matrix (M_D) and right-handed Majorana neutrino mass matrix (M_R) propagates [82–84] as zeros in the effective neutrino mass matrix (m_ν). Thus, the study of zero textures of M_D and M_R are more natural than the study of zero textures of m_ν alone. Without giving any emphasis on the number and/or position of zeros of m_ν, the author of Ref. [82] have studied all possible zeros of M_D and M_R in the context of type-I seesaw mechanism for predictive scenario, whereby the sum of zeros of M_D and M_R is eight. Following the similar approach, in this chapter, we explore the zero textures of $m_\nu^{3\times3}$ in the (3+1) scenario, that is, with an additional eV scale sterile neutrino apart from the three active neutrinos. In presence of the sterile species the system becomes more constrained. In the (3+1) scenario, a number of textures previously allowed in three neutrino scenario may be ruled out based on current neutrino data with active-sterile mixings. Remaining allowed textures may be tested in the ongoing or future experiments.

In this chapter we realize the zero textures of $m_\nu^{3\times3}$ in the context of Minimal Extended Seesaw (MES) mechanism for predictive scenario. MES is an extension of the canonical type-I seesaw mechanism, whereby the Standard Model (SM) is extended by an additional gauge singlet chiral field 'S' along with three right-handed neutrinos. This results into a naturally occurring eV scale sterile neutrino without requiring to impose any tiny Yukawa term for ν_s. MES mechanism deals with (3×3) M_D, (3×3) M_R and (1×3) row matrix M_S which couples the singlet field 'S' with the three right-handed neutrinos. For realization of zero textures of m_ν we consider the zero textures of M_D, M_R and M_S which will finally

propagate as zeros in m_ν. Under predictive scenario there are three possible mappings of M_D and M_R along with suitable zero textures of M_S : (i) (4+4) scheme (ii) (5+3) scheme and (iii) (6+2) scheme, where the numbers within a pair represents the number of zeros of M_D and M_R respectively. A similar study was performed by the authors of Ref. [97] whereby they considered the minimal scenario of 5 zeros of M_D and 4 zeros as well as diagonal M_R, which happens to be a few cases of the predictive scenario. We therefore, will not consider the diagonal form of M_R with 5 zeros in M_D in our study.

Interestingly we also find that fermion mass matrices in our study are related to each other via S_3 permutation group under MES mechanism. This eases our job of dealing only with a few basic combinations of M_D, M_R and M_S. Enforcing zeros in m_ν lead to a number of constraint conditions, named as correlations, whereby different mass matrix elements of $m_\nu^{3\times 3}$ are related to each other. We check the viability of each of the textures under recent neutrino oscillation data. We consider a texture to be viable only if it shows consistency with experimental data. We find that out of four experimentally allowed one-zero textures of m_ν only three textures $m_{e\tau} = 0, m_{\mu\mu} = 0$ and $m_{\tau\tau} = 0$ can be realized in the context of predictive scenario and MES mechanism. However, recent neutrino oscillation data allows only one texture $m_{\tau\tau} = 0$. We also perform symmetry realization of those textures of M_D, M_R and M_S which leads to viable one-zero textures of m_ν. We consider the Z_7 Abelian symmetry group for realization of the viable textures with an extension of the Standard Model to include a few scalar fields.

This chapter is organised as follows: Section 2.2 deals with a brief review on Minimal Extended Seesaw (MES) mechanism. In Section 2.3, we present S_3 transformations of the fermion mass matrices and their invariance under MES formalism. Section 2.4 presents all phenomenologically viable one-zero textures of $m_\nu^{3\times 3}$. Subsections 2.4.1 and 2.4.2 deal with zero textures of M_D, M_R and M_S under the $(4+4)$ and $(5+3)$ schemes along with their respective correlations obtained in each case. In Section 2.5, we check the consistency of the

correlations obtained by each set of the fermion mass matrices in context of current neutrino oscillation data. In Section 2.6 Z_N group symmetry realization of all the viable textures are presented. And finally we conclude in Section 2.7.

2.2 Minimal extended seesaw (MES) mechanism

Minimal Extended Seesaw mechanism [67] is an extension of the type-I seesaw mechanism wherein the SM is extended with four additional singlets - three right-handed neutrinos and one gauge singlet chiral field 'S'. In this scenario, an eV scale sterile neutrino appears naturally, without the need of any fine tuning to mass term for ν_s. A detailed analysis of MES mechanism have been presented in Chapter 1, but for ready reference, we discuss it briefly here.

The Lagrangian representing Dirac and Majorana mass terms with sterile neutrino mass term is of the following form

$$-\mathscr{L}_m = \bar{\nu}_L M_D \nu_R + \bar{S}^c M_S \nu_R + \frac{1}{2}\bar{\nu}_R^c M_R \nu_R + h.c.. \tag{2.1}$$

Here M_S is a (1×3) row matrix which couples the singlet field 'S' and the three right-handed neutrinos. In the context of MES mechanism, the light neutrino mass matrix $m_\nu^{3\times3}$ gets modified to the following form

$$m_\nu^{3\times3} \backsimeq M_D M_R^{-1} M_S^T (M_S M_R^{-1} M_S^T)^{-1} M_S (M_R^{-1})^T M_D^T - M_D M_R^{-1} M_D^T, \tag{2.2}$$

with

$$m_s \backsimeq -M_S M_R^{-1} M_S^T . \tag{2.3}$$

Here m_s is the sterile neutrino mass term. The strength of active-sterile mixing represented by the fourth column of the mixing matrix is given by

$$R_{3\times1} = M_D M_R^{-1} M_S^T (M_S M_R^{-1} M_S^T)^{-1} = (V_{e4}, V_{\mu4}, V_{\tau4})^T. \tag{2.4}$$

In our work we try to realize the one-zero textures of $m_\nu^{3\times3}$ (Table 2.1) in the MES mechanism (Eq. (2.2)). To proceed we consider the zero textures of M_D, M_R and M_S for predictive scenario : (4+4) scheme, (5+3) scheme and (6+2) scheme, where in a pair within the bracket, the first digit represents the number of zeros of M_D and the second digit represents the number of zeros of M_R. On implementation of MES mechanism, these zeros propagate as zeros to $m_\nu^{3\times3}$.

2.3 S_3 invariance of $m_\nu^{3\times3}$

We find that there exist a number of combinations of zero textures of M_D, M_R and M_S which map into the same m_ν of Eq. (2.2). This correspondence is due to S_3 group transformations among the different Dirac neutrino mass matrices M_D, among different right-handed Majorana neutrino mass matrices M_R, among different M_S. Of course, the author of Ref. [82] used this technique in his work for finding out all possible zeros of M_D and M_R to realize a particular zero texture of m_ν.

S_3 is the smallest non-Abelian discrete group. A group S_N is said to be non-Abelian if $ab \neq ba$, for all elements a,b of the group. A permutation group is formed by all possible permutation among N objects x_i $(i = 1,2,3,.....N)$, that is, $(x_1, x_2, ..., x_N) \to (x_{i_1}, x_{i_2}, ..., x_{i_N})$. Such a group with N elements is denoted by S_N and is called the symmetry group with order $N!$. For $N = 3$, the order of the permutation group S_3 is $3! = 6$. The six elements of S_3 can be represented by 3×3 matrices as

$$E=\begin{pmatrix}1&0&0\\0&1&0\\0&0&1\end{pmatrix},\quad A=\begin{pmatrix}0&1&0\\1&0&0\\0&0&1\end{pmatrix},\quad B=\begin{pmatrix}0&0&1\\0&1&0\\1&0&0\end{pmatrix},$$
$$BA=\begin{pmatrix}0&0&1\\1&0&0\\0&1&0\end{pmatrix},\quad AB=\begin{pmatrix}0&1&0\\0&0&1\\1&0&0\end{pmatrix},\quad ABA=\begin{pmatrix}1&0&0\\0&0&1\\0&1&0\end{pmatrix}. \tag{2.5}$$

Denoting $A=a$ and $BA=b$, we obtain $a^2=b^3=E$, where E is the identity element. Also, it is to be noted that $BAB=ABA$. The element A and BA can generate the whole group and hence they are the generators of the group ($a=A,b=BA,ab=ABA,ba=B,aba=AB$).

The following S_3 transformations of M_D,M_R and M_S keep m_ν invariant:

$$M_D\to M_DZ,\quad M_R\to Z^TM_RZ,\quad M_S\to M_SZ. \tag{2.6}$$

[1] with

$$Z\in S_3=(A,A^2,B,AB,BA,ABA). \tag{2.7}$$

2.4 One-zero textures of $m_\nu^{3\times3}$

All experimentally viable one-zero textures of $m_\nu^{3\times3}$ for three active neutrinos are presented in the Table 2.1. The m_ν having elements either $m_{ee}=0$ or $m_{\mu\tau}=0$ is not permitted by current neutrino data. The remaining four textures $m_{e\mu}=0,m_{e\tau}=0,m_{\mu\mu}=0,m_{\tau\tau}=0$ are allowed [80]. It is interesting to note that all experimentally allowed one-zero textures of m_ν

[1] m_ν, M_R and $M_S^TM_S$ are symmetric and hence they entail permutations of both rows and columns

have mass eigenvalues in inverted hierarchical (IH) mass ordering i.e., $m_1 \simeq m_2 >> m_3$ and no normal hierarchical one-zero texture of $m_\nu^{3\times3}$ is allowed.

Table 2.1 All possible one-zero textures in $m_\nu^{3\times3}$

$m_{ee}=0$	$m_{e\mu}=0$	$m_{e\tau}=0$
$\begin{pmatrix} 0 & X & X \\ X & X & X \\ X & X & X \end{pmatrix}$	$\begin{pmatrix} X & 0 & X \\ 0 & X & X \\ X & X & X \end{pmatrix}$	$\begin{pmatrix} X & X & 0 \\ X & X & X \\ 0 & X & X \end{pmatrix}$
$m_{\mu\mu}=0$	$m_{\mu\tau}=0$	$m_{\tau\tau}=0$
$\begin{pmatrix} X & X & X \\ X & 0 & X \\ X & X & X \end{pmatrix}$	$\begin{pmatrix} X & X & X \\ X & X & 0 \\ X & 0 & X \end{pmatrix}$	$\begin{pmatrix} X & X & X \\ X & X & X \\ X & X & 0 \end{pmatrix}$

It is again point to ponder over in two-zero textures: our detailed investigation shows that no two-zero textures are phenomenologically viable in presence of sterile neutrino i.e., (3+1) models, although they are allowed in 3-active neutrino mass models without sterile neutrino states. Thus $m_\nu^{3\times3}$ in MES are allowed for one-zero textures of inverted hierarchical mass ordering only.

2.4.1 4 zeros in M_D and 4 zeros in M_R

There are ${}^9C_4 = 126$ number of possible 4-zero textures of M_D and ${}^6C_4 = 15$ number of possible 4-zero textures of M_R. Current neutrino data do not permit those M_D consisting of row-zero or block-zero, because the row-zero textures are uninteresting since they yield one massless, decoupled neutrino. Again block-zero textures may also be neglected because they lead to scaling i.e., the neutrino mass matrix has a right eigen vector with one zero entry corresponding to the eigenvalue zero. This implies that the PMNS matrix has one zero matrix element which contradicts experiments [82]. Again, MES mechanism requires M_D and M_R to be singular. Therefore, all row-zero, block-zero and column-zero forms of M_D and M_R are

uninteresting in our study. There are 18 row-zero, 18 column-zero and 9 block-zero textures of M_D, hence the number of viable 4-zero textures of M_D are 81. Again out of 15 four-zero textures of M_R, the following are non-singular which is a mandatory requirement for seesaw mechanism:

$$M_R^a = \begin{pmatrix} 0 & B & 0 \\ B & 0 & 0 \\ 0 & 0 & F \end{pmatrix}, \quad M_R^b = \begin{pmatrix} 0 & 0 & C \\ 0 & D & 0 \\ C & 0 & 0 \end{pmatrix}, \quad M_R^c = \begin{pmatrix} A & 0 & 0 \\ 0 & 0 & E \\ 0 & E & 0 \end{pmatrix} \tag{2.8}$$

S_3 transformations according to Eq. (2.6) lead us to only one basic texture of $M_R = M_R^c$, where the other two textures can be obtained from S_3 transformations of M_R^c. These transformations connect different texture zeros of M_D, M_R and M_S to produce zero in the same location of the neutrino mass matrix m_ν. In our work, only one-zero textures of M_S are allowed as follows:

$$M_S^{(1)} = (0 \quad s_2 \quad s_3), \quad M_S^{(2)} = (s_1 \quad 0 \quad s_3) \quad \text{and} \quad M_S^{(3)} = (s_1 \quad s_2 \quad 0). \tag{2.9}$$

Now the following cases of one-zero textures have been realized in MES formalism:

Case I: realization of $m_{\tau\tau=0}$

It can be realized by the choice of three sets of M_D, M_R and M_S for $m_{\tau\tau} = 0$ in the neutrino mass matrix resulting three correlations.

Case I(a):

$$M_R = M_R^c, \qquad M_D^{(2)} = \begin{pmatrix} 0 & b & c \\ d & e & 0 \\ 0 & 0 & i \end{pmatrix}, \qquad M_S^{(2)} = (s_1 \quad 0 \quad s_3). \tag{2.10}$$

$$m_{e\mu} = -V_{e4}V_{\mu4}m_s + \frac{m_{\mu\tau}(V_{e4}^2 m_s + m_{ee})}{2m_{e\tau}}. \tag{2.11}$$

$$\frac{V_{\mu4}}{V_{e4}} = \frac{m_{\mu\tau}}{m_{e\tau}} + \frac{d}{V_{e4}s_1}. \tag{2.12}$$

CaseI(b):

$$M_R = M_R^c, \qquad M_D^{(3)} = \begin{pmatrix} 0 & b & 0 \\ d & e & f \\ 0 & 0 & i \end{pmatrix}, \qquad M_S^{(2)} = (s_1 \quad 0 \quad s_3), \tag{2.13}$$

$$m_{ee} = -V_{e4}^2 m_s. \tag{2.14}$$

$$\frac{V_{\mu4}}{V_{e4}} = \frac{m_{\mu\tau}}{m_{e\tau}} + \frac{d}{V_{e4}s_1}. \tag{2.15}$$

Case I(c):

$$M_R = M_R^c, \qquad M_D^{(1)} = \begin{pmatrix} a & b & 0 \\ d & e & 0 \\ 0 & 0 & i \end{pmatrix}, \qquad M_S^{(2)} = (s_1 \quad 0 \quad s_3), \tag{2.16}$$

$$m_{\mu\mu} = -V_{\mu4}^2 m_s + \frac{V_{e4}V_{\mu4}m_s + m_{e\mu}^2}{V_{e4}^2 m_s + m_{ee}}, \tag{2.17}$$

$$\frac{V_{\mu4}}{V_{e4}} = \frac{ds_1E + es_3A}{as_1E + bs_3A}. \tag{2.18}$$

Each of these three basic cases of Eq. (2.10), (2.13), (2.16) gives a number of suitable combinations of M_D, M_R and M_S via Eq. (2.6) which leading to the same $m_{\tau\tau} = 0$ are presented in Table 2.3, 2.4 and 2.5.

Case II: realization of $m_{e\tau=0}$

$m_{e\tau}$ can be generated by following set of M_R,M_D and M_S

$$M_R = M_R^c, \qquad M_D^{(4)} = \begin{pmatrix} 0 & b & c \\ d & 0 & f \\ g & 0 & 0 \end{pmatrix}, \qquad M_S^{(1)} = (0 \quad s_2 \quad s_3). \tag{2.19}$$

The correlation on enforcement of zero for $m_{e\tau}$ is

$$m_{\mu\mu} = -V_{\mu4}^2 m_s + \frac{m_{\mu\tau}^2}{m_{\tau\tau}}, \tag{2.20}$$

$$\frac{V_{e4}}{V_{\mu4}} = \frac{e}{f} - \frac{b}{2V_{\mu4}s_2}. \tag{2.21}$$

2.4.2 5 zeros in M_D and 3 zeros in M_R

There are ${}^9C_5 = 126$ number of possible 5-zero textures of M_D, out of which only 36 textures are non-singular. For 3-zero textures of M_R, we have ${}^6C_3 = 20$ possible zero textures, out of which, 14 are non-singular. These non-singular M_R have been presented in the Table 2.2.

The S_3 transformations according to the Eq. (2.6) lead to only the following four basic 3-zero textures of M_R which are need to be studied and other textures are the results of S_3

Table 2.2 All possible three zero textures of M_R.

$M_R^{(1)}$	$M_R^{(2)}$	$M_R^{(3)}$	$M_R^{(4)}$	$M_R^{(5)}$
$\begin{pmatrix} 0 & B & C \\ B & 0 & E \\ C & E & 0 \end{pmatrix}$	$\begin{pmatrix} 0 & 0 & C \\ 0 & D & E \\ C & E & 0 \end{pmatrix}$	$\begin{pmatrix} 0 & B & 0 \\ B & 0 & E \\ 0 & E & F \end{pmatrix}$	$\begin{pmatrix} 0 & 0 & C \\ 0 & D & 0 \\ C & 0 & F \end{pmatrix}$	$\begin{pmatrix} A & 0 & C \\ 0 & 0 & E \\ C & E & 0 \end{pmatrix}$
$M_R^{(6)}$	$M_R^{(7)}$	$M_R^{(8)}$	$M_R^{(9)}$	$M_R^{(10)}$
$\begin{pmatrix} A & 0 & 0 \\ 0 & 0 & E \\ 0 & E & F \end{pmatrix}$	$\begin{pmatrix} A & 0 & 0 \\ 0 & D & 0 \\ 0 & 0 & F \end{pmatrix}$	$\begin{pmatrix} A & 0 & 0 \\ 0 & D & E \\ 0 & E & 0 \end{pmatrix}$	$\begin{pmatrix} A & B & 0 \\ B & 0 & E \\ 0 & E & 0 \end{pmatrix}$	$\begin{pmatrix} A & B & 0 \\ B & 0 & 0 \\ 0 & 0 & F \end{pmatrix}$
$M_R^{(11)}$	$M_R^{(12)}$	$M_R^{(13)}$	$M_R^{(14)}$	-
$\begin{pmatrix} 0 & B & C \\ B & 0 & 0 \\ C & 0 & F \end{pmatrix}$	$\begin{pmatrix} 0 & B & C \\ B & D & 0 \\ C & 0 & 0 \end{pmatrix}$	$\begin{pmatrix} 0 & B & 0 \\ B & D & 0 \\ 0 & 0 & F \end{pmatrix}$	$\begin{pmatrix} A & 0 & C \\ 0 & D & 0 \\ C & 0 & 0 \end{pmatrix}$	-

transformations keeping m_ν invariant:

$$M_R^{(1)} = \begin{pmatrix} 0 & B & C \\ B & 0 & E \\ C & E & 0 \end{pmatrix}, \quad M_R^{(7)} = \begin{pmatrix} A & 0 & 0 \\ 0 & D & 0 \\ 0 & 0 & F \end{pmatrix}, \quad M_R^{(9)} = \begin{pmatrix} A & B & 0 \\ B & 0 & E \\ 0 & E & 0 \end{pmatrix}, \quad M_R^{(10)} = \begin{pmatrix} A & B & 0 \\ B & 0 & 0 \\ 0 & 0 & F \end{pmatrix}. \tag{2.22}$$

In our study, we have seen that $M_R^{(1)}$ can never generate zero texture of m_ν whatever the choice of M_D may be. Hence the rest 13 textures of M_R shall be effective for our work. Again the diagonal $M_R^{(7)}$ in combination with 5-zero M_D has been used by the authors in the Ref. [97] for study. Therefore, we do not present the results for this case because it shall be mere a repetition only.

Case III : realization of $m_{\tau\tau=0}$

Case III(a):The following combination

$$M_R = M_R^{(10)}, \qquad M_D^{(5)} = \begin{pmatrix} 0 & b & 0 \\ 0 & e & f \\ g & 0 & 0 \end{pmatrix}, \qquad M_S^{(2)} = (s_1 \quad 0 \quad s_3), \tag{2.23}$$

leads to $m_{\tau\tau=0}$ with the correlation

$$m_{e\mu} = -V_{e4}V_{\mu4}m_s + \frac{m_{\mu\tau}(V_{e4}^2 m_s + m_{ee})}{m_{e\tau}}, \tag{2.24}$$

$$\frac{V_{\mu4}}{V_{e4}} = \frac{m_{\mu\tau}}{m_{e\tau}} + \frac{f}{V_{e4}s_3}. \tag{2.25}$$

Again S_3 transformations enable us to find another five combinations of M_D, M_R and M_S giving $m_{\tau\tau=0}$ with the same correlations presented in Table 2.6.

Case III(b):

$$M_R = M_R^{(9)}, \qquad M_D^{(6)} = \begin{pmatrix} 0 & 0 & c \\ d & 0 & f \\ 0 & h & 0 \end{pmatrix}, \qquad M_S^{(3)} = (s_1 \quad s_2 \quad 0), \tag{2.26}$$

leads to $m_{\tau\tau=0}$. Implementing S_3 transformations, we have another five combinations giving $m_{\tau\tau=0}$ with the same following correlation presented in the Table 2.7.

$$m_{\mu\mu} = -V_{\mu4}^2 m_s + \frac{V_{e4}V_{\mu4}m_s + m_{e\mu}^2}{V_{e4}^2 m_s + m_{ee}}, \tag{2.27}$$

$$\frac{V_{\mu4}}{V_{e4}} = \frac{m_{\mu\tau}}{m_{e\tau}} + \frac{d}{V_{e4}.s_1}. \tag{2.28}$$

Case IV: realization of $m_{e\tau=0}$

It can be generated with the following combination

$$M_R = M_R^{(10)}, \qquad M_D^{(7)} = \begin{pmatrix} 0 & b & 0 \\ d & 0 & f \\ 0 & 0 & i \end{pmatrix}, \qquad M_S^{(3)} = (s_1 \quad s_2 \quad 0). \tag{2.29}$$

It leads to the correlation

$$m_{\mu\mu} = -V_{\mu4}^2 m_s + \frac{m_{\mu\tau}^2}{m_{\tau\tau}}, \tag{2.30}$$

$$\frac{V_{e4}}{V_{\mu4}} = \frac{s_1 b}{s_2 d} - \frac{Ab}{Bd}. \tag{2.31}$$

Through S_3 transformations one can have another five combinations of M_D, M_R and M_S yielding the same correlations.

Case V: realization of $m_{\mu\mu=0}$

It can be generated with

$$M_R = M_R^{(10)}, \qquad M_D^{(8)} = \begin{pmatrix} 0 & b & c \\ d & 0 & 0 \\ 0 & h & 0 \end{pmatrix}, \qquad M_S = (0 \quad 0 \quad s_3). \tag{2.32}$$

S_3 transformations lead to another combinations of M_D, M_R and M_S which gives the following correlation

$$\frac{m_{ee}}{m_{e\mu}} = \frac{m_{e\tau}}{m_{\mu\tau}}. \tag{2.33}$$

2.5 Viability of such texture zeros of m_ν under current neutrino data

Since one-zero textures of m_ν are inverted hierarchical models, so the expressions for their matrix elements in terms of neutrino parameters i.e., experimental observables with setting approximately $m_3 = 0$ are given by-

$$\begin{aligned}
m_{ee} &= m_1 c_{12}^2 c_{13}^2 + m_2 e^{2i\alpha} s_{12}^2 c_{13}^2 \\
m_{e\mu} &= m_1 c_{12} c_{13}(-s_{12}c_{23} - c_{12}s_{13}s_{23}e^{i\delta}) + m_2 e^{2i\alpha} s_{12}c_{13}(c_{12}c_{23} - s_{12}s_{13}s_{23}e^{i\delta}), \\
m_{e\tau} &= m_1 c_{12} c_{13}(s_{12}s_{23} - c_{12}s_{13}c_{23}e^{i\delta}) + m_2 e^{2i\alpha} s_{12}c_{13}(-c_{12}s_{23} - s_{12}s_{13}c_{23}e^{i\delta}), \\
m_{\mu\mu} &= m_1(-s_{12}c_{23} - c_{12}s_{13}s_{23}e^{i\delta})^2 + m_2 e^{2i\alpha}(c_{12}c_{23} - s_{12}s_{13}s_{23}e^{i\delta})^2, \\
m_{\mu\tau} &= m_1(-s_{12}c_{23} - c_{12}s_{13}s_{23}e^{i\delta})(s_{12}s_{23} - c_{12}s_{13}c_{23}e^{i\delta}) \\
&\quad + m_2 e^{2i\alpha}(c_{12}c_{23} - s_{12}s_{13}s_{23}e^{i\delta})(-c_{12}s_{23} - s_{12}s_{13}c_{23}e^{i\delta}), \\
m_{\tau\tau} &= m_1(s_{12}s_{23} - c_{12}s_{13}c_{23}e^{i\delta})^2 + m_2 e^{2i\alpha}(-c_{12}s_{23} - s_{12}s_{13}c_{23}e^{i\delta})^2,
\end{aligned} \tag{2.34}$$

where $c_{ij} = \cos\theta_{ij}$ and $s_{ij} = \sin\theta_{ij}$

δ and α are the Dirac CP phase and Majorana phase respectively.

2.5.1 Zero textures in (4+4) scenario

We now examine the different cases presented in the preceding Section 2.4.1 under the current neutrino data:

Case I(a):

The set of the following matrices

$$M_D^{(2)} = \begin{pmatrix} 0 & b & c \\ d & e & 0 \\ 0 & 0 & i \end{pmatrix}, \qquad M_s = (s_1 \quad 0 \quad s_3), \qquad M_R = M_R^c = \begin{pmatrix} A & 0 & 0 \\ 0 & 0 & E \\ 0 & E & 0 \end{pmatrix}, \tag{2.35}$$

are put in Eq. (2.2) and we get the following low energy neutrino mass matrix, sterile neutrino mass and the active-sterile neutrino mixing as

$$m_\nu^{3\times 3} = \begin{pmatrix} \frac{b^2 s_3^2 A}{E^2 s_1^2} - \frac{2bc}{E} & \frac{bds_3}{Es_1} + \frac{beAs_3^2}{E^2 s_1^2} - \frac{ce}{E} & -\frac{bi}{E} \\ \frac{bds_3}{Es_1} + \frac{beAs_3^2}{E^2 s_1^2} - \frac{ce}{E} & \frac{e^2 s_3^2 A}{s_1^2 E^2} + \frac{2des_3}{Es_1} & -\frac{ei}{E} \\ -\frac{bi}{E} & -\frac{ei}{E} & 0 \end{pmatrix}, \tag{2.36}$$

with

$$m_s = -\frac{s_1^2}{A}, \qquad R = \begin{pmatrix} \frac{bs_3 A}{Es_1^2} \\ \frac{ds_1 E + eAs_3}{Es_1^2} \\ 0 \end{pmatrix} = \begin{pmatrix} V_{e4} \\ V_{\mu 4} \\ 0 \end{pmatrix}, \tag{2.37}$$

Eq. (2.36) and (2.37) provide the following correlation

$$m_{e\mu} = -V_{e4} V_{\mu 4} m_s + \frac{m_{\mu\tau}(V_{e4}^2 m_s + m_{ee})}{2m_{e\tau}}, \tag{2.38}$$

and

$$\frac{V_{\mu 4}}{V_{e4}} = \frac{m_{\mu\tau}}{m_{e\tau}} + \frac{d}{V_{e4} s_1}. \tag{2.39}$$

The above texture becomes experimentally viable if both the correlations in Eqs. (2.38) and (2.39) are consistent with current neutrino data presented in section 1.7 of Chapter 1. Using 3σ values of the parameters and the values of $\alpha(80\,\text{deg} < \alpha < 110\,\text{deg})$ and

$\delta(140\,\text{deg} < \delta < 220\,\text{deg})$ as already predicted for $m_{\tau\tau} = 0$ in Ref. [97], we plot $m_{e\mu}$ vs m_s from Eq. (2.38), and $\frac{V_{\mu4}}{V_{e4}}$ vs m_s from Eq. (2.39) as shown in Fig. 2.1 and 2.2 respectively.

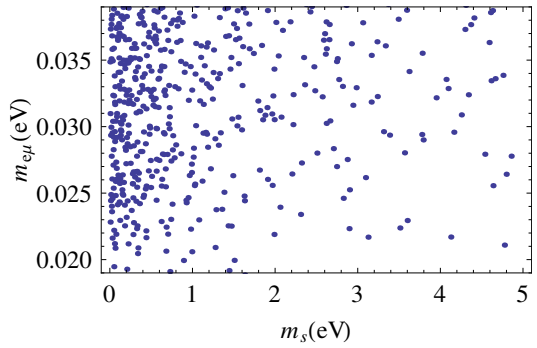

Fig. 2.1 Sterile neutrino mass (m_s) as predicted by Eq. (2.38) for case I(a).

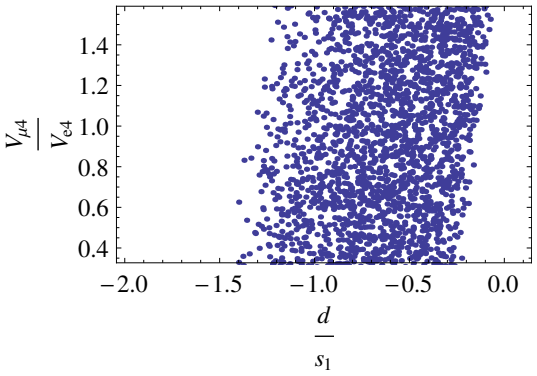

Fig. 2.2 Allowed range for the ratio $(\frac{d}{s_1})$ as predicted by Eq. (2.39) for case I(a).

From Fig. 2.1 it is evident that for the allowed range of $m_{e\mu}$ (0.01912-0.03910)eV, m_s ranges from sub eV scale to few eV scale but favorable domain belongs to less than 1 eV which is fairly consistent with the upper bound, that is, 1.5 eV as predicted by global analysis of 3+1 neutrino oscillation data.

The relation in Eq. (2.39) is experimentally allowed for the choice of the parameters in the ratio $(\frac{d}{s_1})$ lying between $(-1.5 < (\frac{d}{s_1}) < -0.1)$ (Fig. 2.2).

Transformations under S_3 give a number of cases being capable of producing $m_{\tau\tau} = 0$ with the same correlations listed in the Table 2.3.

Case I(b):

Table 2.3 Allowed zero textures of M_D, M_R and M_S leading to $m_{\tau\tau} = 0$ (Case I(a)).

M_D	M_R	M_S	*Correlation* $\frac{V_{\mu 4}}{V_{e4}} = \frac{m_{\mu\tau}}{m_{e\tau}} + \frac{M_{D_{(ij)}}}{V_{e4} M_{s_{(1j)}}}$ $m_{e\mu} = -V_{e4}V_{\mu 4} m_s + \frac{m_{\mu\tau}}{m_{e\tau}}[\frac{1}{2}(V_{e4}^2 m_s + m_{ee})]$
$\begin{pmatrix} a & b & 0 \\ d & 0 & f \\ 0 & h & 0 \end{pmatrix}$	M_R^a	$M_S^{(1)}$	$(i = j = 3)$
$\begin{pmatrix} a & b & 0 \\ 0 & e & f \\ g & 0 & 0 \end{pmatrix}$	M_R^a	$M_S^{(2)}$	$(i = j = 3)$
$\begin{pmatrix} a & 0 & c \\ d & e & 0 \\ 0 & 0 & i \end{pmatrix}$	M_R^b	$M_S^{(1)}$	$(i = j = 2)$
$\begin{pmatrix} a & 0 & c \\ 0 & e & f \\ g & 0 & 0 \end{pmatrix}$	M_R^b	$M_S^{(3)}$	$(i = j = 2)$
$\begin{pmatrix} 0 & b & c \\ d & 0 & f \\ 0 & h & 0 \end{pmatrix}$	M_R^c	$M_S^{(3)}$	$(i = j = 1)$

We consider the following matrices:

$$M_D^{(3)} = \begin{pmatrix} 0 & b & 0 \\ d & e & f \\ 0 & 0 & i \end{pmatrix}, \qquad M_s = (s_1 \quad 0 \quad s_3), \qquad M_R = M_R^c = \begin{pmatrix} A & 0 & 0 \\ 0 & 0 & E \\ 0 & E & 0 \end{pmatrix}. \tag{2.40}$$

Employing these matrices in Eq. (2.2) we have

$$m_\nu^{3\times 3} = \begin{pmatrix} \frac{b^2 s_3^2 A^2}{E^2 s_1^2} & \frac{bds_3}{Es_1} + \frac{beAs_3^2}{E^2 s_1^2} - \frac{bf}{E} & -\frac{bi}{E} \\ \frac{bds_3}{Es_1} + \frac{beAs_3^2}{E^2 s_1^2} - \frac{bf}{E} & \frac{e^2 s_3^2 A}{s_1^2 E^2} + \frac{2des_3 A}{Es_1} - \frac{2ef}{E} & -\frac{ei}{E} \\ -\frac{bi}{E} & -\frac{ei}{E} & 0 \end{pmatrix}, \tag{2.41}$$

$$m_s = -\frac{s_1^2}{A}, \qquad R = \begin{pmatrix} \frac{Abs_3}{Es_1^2} \\ \frac{d}{s_1} + \frac{Aes_3}{Es_1^2} \\ 0 \end{pmatrix} = \begin{pmatrix} V_{e4} \\ V_{\mu 4} \\ 0 \end{pmatrix}, \tag{2.42}$$

with the following correlation

$$m_{ee} = -V_{e4}^2 m_s, \tag{2.43}$$

and

$$\frac{V_{\mu 4}}{V_{e4}} = \frac{m_{\mu\tau}}{m_{\tau\tau}} + \frac{d}{V_{e4}s_1}. \tag{2.44}$$

As seen from Fig. 2.3, for allowed range of $|m_{ee}| \approx (0.014 - 0.018)$eV, the above texture

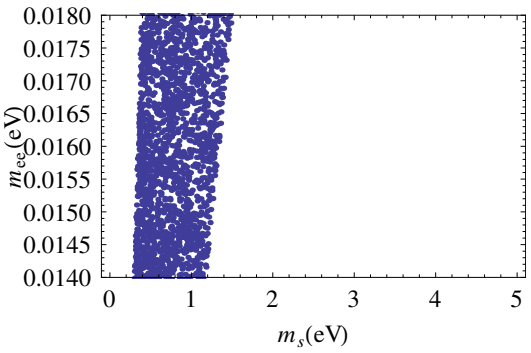

Fig. 2.3 Allowed range of m_s as predicted by Eq. (2.43) for case I(b).

predicts $(0.2 < m_s < 1.5)$eV, which is in fair agreement with the global analysis data. For Eq. (2.44), the condition for $(\frac{d}{s_1})$ is the same as in case I(a) (Fig. 2.2). Again S_3 transformations lead to a number of cases producing $m_{\tau\tau} = 0$ with the same correlations presented in Table 2.4.

Case I(c): We consider $m_{\tau\tau} = 0$

Table 2.4 Allowed zero textures of M_D, M_R and M_S leading to $m_{\tau\tau} = 0$ (Case I(b))

M_D	M_R	M_S	*Correlation* $\frac{V_{\mu 4}}{V_{e4}} = \frac{m_{\mu\tau}}{m_{e\tau}} + \frac{M_{D_{(ij)}}}{V_{e4} M_{s_{(1j)}}}$ $m_{ee} = -V_{e4}^2 m_S$
$\begin{pmatrix} a & 0 & 0 \\ d & e & f \\ 0 & h & 0 \end{pmatrix}$	M_R^a	$M_S^{(1)}$	$(i = j = 3)$
$\begin{pmatrix} 0 & b & 0 \\ d & e & f \\ g & 0 & 0 \end{pmatrix}$	M_R^a	$M_S^{(2)}$	$(i = j = 3)$
$\begin{pmatrix} 0 & 0 & c \\ d & e & f \\ g & 0 & 0 \end{pmatrix}$	M_R^b	$M_S^{(3)}$	$(i = j = 1)$
$\begin{pmatrix} 0 & 0 & c \\ d & e & f \\ 0 & h & 0 \end{pmatrix}$	M_R^c	$M_S^{(3)}$	$(i = j = 1)$
$\begin{pmatrix} a & 0 & 0 \\ d & e & f \\ 0 & 0 & i \end{pmatrix}$	M_R^b	$M_S^{(1)}$	$(i = j = 1)$

$$M_D^{(1)} = \begin{pmatrix} a & b & 0 \\ d & e & 0 \\ 0 & 0 & i \end{pmatrix}, \qquad M_s = (s_1 \quad 0 \quad s_3), \qquad M_R = M_R^c = \begin{pmatrix} A & 0 & 0 \\ 0 & 0 & E \\ 0 & E & 0 \end{pmatrix}, \tag{2.45}$$

and using it in Eq. (2.2) we have the light (3×3) neutrino mass matrix, sterile neutrino mass and active-sterile mixing matrix as

$$m_\nu^{3\times 3} = \begin{pmatrix} \frac{b^2 s_3^2 A}{E^2 s_1^2} + \frac{2abs_3}{Es_1} & \frac{(ae+bd)s_3}{Es_1} + \frac{beAs_3^2}{E^2 s_1^2} & -\frac{bi}{E} \\ \frac{(ae+bd)s_3}{Es_1} + \frac{beAs_3^2}{E^2 s_1^2} & \frac{e^2 s_3^2 A}{s_1^2 E^2} + \frac{2des_3}{Es_1} & -\frac{ei}{E} \\ -\frac{bi}{E} & -\frac{ei}{E} & 0 \end{pmatrix}, \tag{2.46}$$

$$m_s = -\frac{s_1^2}{A}, \qquad R = \begin{pmatrix} \frac{as_1E+bs_3A}{Es_1^2} \\ \frac{ds_1E+eAs_3}{Es_1^2} \\ 0 \end{pmatrix} = \begin{pmatrix} V_{e4} \\ V_{\mu4} \\ 0 \end{pmatrix}, \qquad \frac{V_{e4}}{V_{\mu4}} = \frac{as_1E+bs_3A}{ds_1E+es_3A}. \tag{2.47}$$

From Eq. (2.46) and (2.47) we get the following relations:-

$$m_{\mu\mu} = -V_{\mu4}^2 m_s + \frac{(V_{e4}V_{\mu4}m_s + m_{e\mu})^2}{V_{e4}^2 m_s + m_{ee}}, \tag{2.48}$$

and

$$\frac{V_{\mu4}}{V_{e4}} = \frac{ds_1E+es_3A}{as_1E+bs_3A}. \tag{2.49}$$

Plotting $m_{\mu\mu}$ vs m_s from Eq. (2.48), it is seen from Fig 2.4, that for allowed range of

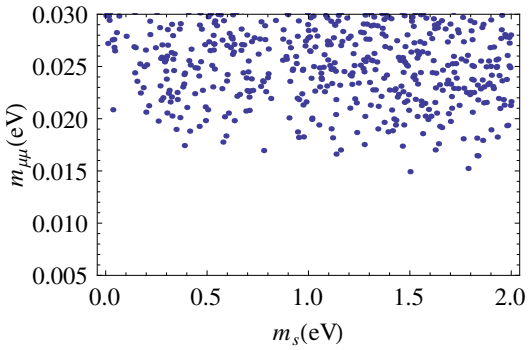

Fig. 2.4 Range of m_s as predicted by Eq. (2.48).

$m_{\mu\mu} \approx (.005 - .03)eV$, m_s have its value well below the upper bound ≈ 1.5 eV. However Eq. (2.49) has a large number of parameters involved and hence gives ample scope for adjusting the parameters as required. S_3 transformations give a number of cases which lead to $m_{\tau\tau} = 0$ with the same correlation as Eq. (2.48) and (2.49) as shown in the Table 2.5.

Table 2.5 Allowed zero textures of M_D, M_R and M_S leading to $m_{\tau\tau} = 0$ (Case I(c))

M_D	M_R	M_S	*Correlation* $\frac{V_{\mu 4}}{V_{e4}} = \frac{(M_D)_{ij}(M_R)_{jk}s^T_{kp}+(M_D)_{il}(M_R)_{lm}s^T_{mi}}{(M_D)_{nj}(M_R)_{jk}s^T_{kp}+(M_D)_{nl}(M_R)_{lm}s^T_{mi}}$ $m_{\mu\mu} = -V^2_{\mu 4}m_s + \frac{(V_{e4}V_{\mu 4}m_s+m_{e\mu})^2}{V^2_{e4}m_s+m_{ee}}$
$\begin{pmatrix} a & b & 0 \\ d & e & 0 \\ 0 & 0 & i \end{pmatrix}$	M^b_R	$M^{(1)}_S$	$(i=1, j=1, p=1, k=2, l=1, m=3, n=2)$
$\begin{pmatrix} a & 0 & c \\ d & 0 & f \\ 0 & h & 0 \end{pmatrix}$	M^c_R	$M^{(3)}_S$	$(i=1, j=1, p=1, k=2, l=3, m=3, n=2)$
$\begin{pmatrix} a & 0 & c \\ d & 0 & f \\ 0 & h & 0 \end{pmatrix}$	M^a_R	$M^{(1)}_S$	$(i=1, j=1, p=1, k=2, l=3, m=3, n=2)$
$\begin{pmatrix} 0 & b & c \\ 0 & e & f \\ g & 0 & 0 \end{pmatrix}$	M^b_R	$M^{(3)}_S$	$(i=1, j=3, p=1, k=1, l=2, m=2, n=2)$
$\begin{pmatrix} 0 & b & c \\ 0 & e & f \\ g & 0 & 0 \end{pmatrix}$	M^a_R	$M^{(2)}_S$	$(i=1, j=3, p=1, k=3, l=2, m=1, n=2)$

Case II: We consider $m_{e\tau} = 0$.

$$M^{(4)}_D = \begin{pmatrix} 0 & b & c \\ d & 0 & f \\ g & 0 & 0 \end{pmatrix}, \qquad M_s = (0 \quad s_2 \quad s_3) \quad \text{and} \quad M_R = M^c_R = \begin{pmatrix} A & 0 & 0 \\ 0 & 0 & E \\ 0 & E & 0 \end{pmatrix}. \tag{2.50}$$

The above set of matrices applied in Eq. (2.2) gives

$$m^{3\times 3}_\nu = \begin{pmatrix} \frac{b^2s_3^2+c^2s_2^2}{2Es_2s_3} - \frac{bc}{E} & \frac{-bf}{2E} + \frac{cfs_2}{2Es_3} & 0 \\ \frac{-bf}{2E} + \frac{cfs_2}{2Es_3} & -\frac{d^2}{A} + \frac{f^2s_2}{2Es_3} & -\frac{dg}{A} \\ 0 & -\frac{dg}{A} & -\frac{g^2}{A} \end{pmatrix}, \tag{2.51}$$

$$m_s = -\frac{2s_2s_3}{E}, \qquad R = \begin{pmatrix} \frac{c}{2s_3} + \frac{b}{2s_2} \\ \frac{f}{2s_3} \\ 0 \end{pmatrix} = \begin{pmatrix} V_{e4} \\ V_{\mu 4} \\ 0 \end{pmatrix}. \tag{2.52}$$

From Eq. (2.51) and (2.52) we get the following correlation:

$$m_{\mu\mu} = -V_{\mu 4}^2 m_s + \frac{m_{\mu\tau}^2}{m_{\tau\tau}}, \tag{2.53}$$

and

$$\frac{V_{e4}}{V_{\mu 4}} = \frac{c}{f} + \frac{b}{2V_{\mu 4}s_2}. \tag{2.54}$$

$m_{\mu\mu}$ vs m_s from Eq. (2.53) gives a plot as shown in Fig. 2.5 below. From the figure, it is

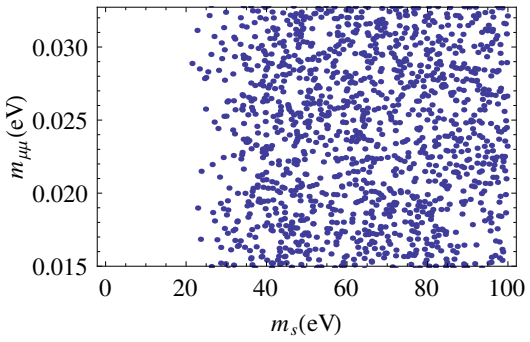

Fig. 2.5 Predicted range of sterile mass m_s from Eq. (2.53) for case II.

evident that the above texture predicts the value of m_s which is not compatible with current oscillation data. Thus this texture is ruled out.

2.5.2 Zero textures in (5+3) scenario

Case III(a): Now we consider the case for $m_{\tau\tau} = 0$.

$$M_D^{(5)} = \begin{pmatrix} 0 & b & 0 \\ 0 & e & f \\ g & 0 & 0 \end{pmatrix} \quad M_s = \begin{pmatrix} s_1 & 0 & s_3 \end{pmatrix} \quad \text{and} \quad M_R = M_R^{(10)} = \begin{pmatrix} A & B & 0 \\ B & 0 & 0 \\ 0 & 0 & F \end{pmatrix}. \tag{2.55}$$

Putting these in Eq. (2.2) gives

$$m_\nu^{3\times3} = \begin{pmatrix} \frac{Ab^2}{B^2} + \frac{b^2Fs_1^2}{B^2s_3^2} & \frac{Abe}{B^2} + \frac{bes_1^2F}{B^2s_3^2} + \frac{bfs_1}{Bs_3} & -\frac{bg}{B} \\ \frac{Abe}{B^2} + \frac{bes_1^2F}{B^2s_3^2} + \frac{bfs_1}{Bs_3} & \frac{Ae^2}{B^2} + \frac{e^2s_1^2F}{B^2s_3^2} + \frac{2efs_1}{Bs_3} & -\frac{eg}{B} \\ -\frac{bg}{B} & -\frac{eg}{B} & 0 \end{pmatrix}, \tag{2.56}$$

$$m_s = -\frac{s_3^2}{F}, \qquad R = \begin{pmatrix} \frac{bFs_1}{Bs_3^2} \\ \frac{eFs_1}{Bs_3^2} + \frac{f}{s_3} \\ 0 \end{pmatrix} = \begin{pmatrix} V_{e4} \\ V_{\mu4} \\ 0 \end{pmatrix}. \tag{2.57}$$

Eq. (2.56) and (2.57) gives

$$m_{e\mu} = -V_{e4}V_{\mu4}m_s + \frac{m_{\mu\tau}}{m_{e\tau}}[V_{e4}^2 m_s + m_{ee}], \tag{2.58}$$

and

$$\frac{V_{\mu4}}{V_{e4}} = \frac{m_{\mu\tau}}{m_{e\tau}} + \frac{f}{V_{e4}s_3}. \tag{2.59}$$

From Fig. 2.6 it is seen that for allowed range of $m_{e\mu} \approx (0.02 - 0.04)$eV, m_s as predicted by

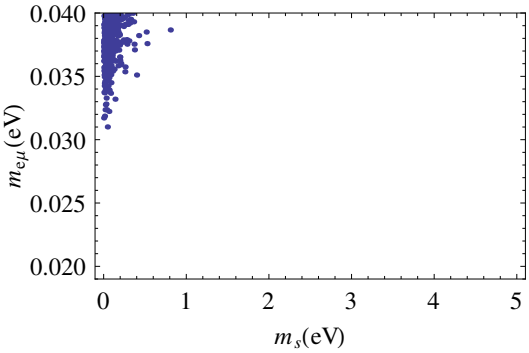

Fig. 2.6 Sterile neutrino mass m_s from Eq. (2.58).

the above texture have a small range of value $\approx (0.00 - 0.06)eV$ which falls under the upper bound by global analysis data but in tension. For the small range of m_s this texture may be considered as viable. Under S_3 permutation it gives a number of cases leading to $m_{\tau\tau} = 0$

with the same correlation shown in the Table 2.6.

Table 2.6 Allowed zero textures of M_D, M_R and M_S leading to $m_{\tau\tau}=0$ in the (5+3) picture (Case III(a)).

M_D	M_R	M_S	*Correlation*
$\begin{pmatrix}0&b&0\\d&e&0\\0&0&i\end{pmatrix}$	$M_R^{(6)}$	$M_S^{(2)}$	$m_{e\mu}=-V_{e4}V_{\mu4}m_s+\frac{m_{\mu\tau}}{m_{e\tau}}[V_{e4}^2m_s+m_{ee}]$
$\begin{pmatrix}0&0&c\\d&0&f\\0&h&0\end{pmatrix}$	$M_R^{(8)}$	$M_S^{(3)}$	–do–
$\begin{pmatrix}0&0&c\\0&e&f\\g&0&0\end{pmatrix}$	$M_R^{(14)}$	$M_S^{(3)}$	–do–
$\begin{pmatrix}a&0&0\\d&e&0\\0&0&i\end{pmatrix}$	$M_R^{(4)}$	$M_S^{(1)}$	–do–
$\begin{pmatrix}a&0&0\\d&0&f\\0&h&0\end{pmatrix}$	$M_R^{(13)}$	$M_S^{(1)}$	–do–

Case III(b): We consider the case for $m_{\tau\tau}=0$

$$M_D^{(6)}=\begin{pmatrix}0&0&c\\d&0&f\\0&h&0\end{pmatrix},\quad M_s=\begin{pmatrix}s_1&s_2&0\end{pmatrix}\quad\text{and}\quad M_R=M_R^{(9)}=\begin{pmatrix}A&B&0\\B&0&E\\0&E&0\end{pmatrix}. \tag{2.60}$$

Putting in Eq. (2.2) gives

$$m_\nu^{3\times3}=\begin{pmatrix}\frac{Ac^2s_2^2}{E^2s_1^2}-\frac{2Bc^2s_2}{E^2s_1}&-\frac{2Bcfs_2}{E^2s_1}+\frac{cds_2}{Es_1}+\frac{Acfs_2^2}{E^2s_1^2}&-\frac{ch}{E}\\-\frac{2Bcfs_2}{E^2s_1}+\frac{cds_2}{Es_1}+\frac{Acfs_2^2}{E^2s_1^2}&\frac{2ds_2f}{Es_1}-\frac{2Bs_2f^2}{E^2s_1}+\frac{As_2^2f^2}{E^2s_1^2}&-\frac{fh}{E}\\-\frac{ch}{E}&-\frac{fh}{E}&0\end{pmatrix}, \tag{2.61}$$

$$m_s = -\frac{s_1^2}{A}, \qquad R = \begin{pmatrix} \frac{c(As_2 - Bs_1)}{Es_1^2} \\ \frac{d}{s_1} + \frac{f(As_2 - Bs_1)}{Es_1^2} \\ 0 \end{pmatrix} = \begin{pmatrix} V_{e4} \\ V_{\mu 4} \\ 0 \end{pmatrix}. \tag{2.62}$$

From Eq. (2.61) and (2.62) we get the following relations:-

$$m_{\mu\mu} = -V_{\mu 4}^2 m_s + \frac{(V_{e4}V_{\mu 4}m_s + m_{e\mu})^2}{V_{e4}^2 m_s + m_{ee}}, \tag{2.63}$$

$$\frac{V_{\mu 4}}{V_{e4}} = \frac{m_{\mu\tau}}{m_{e\tau}} + \frac{d}{V_{e4}s_1}. \tag{2.64}$$

The correlation (2.63) is same as that for case I(c),whereby m_s has its value well below the predicted upper bound. Eq. (2.64) on the other hand have the same interpretation as the above cases for Eq. (2.39). Thus this texture is allowed by neutrino oscillation data.

Table 2.7 Allowed zero textures of M_D,M_R and M_S leading to $m_{\tau\tau} = 0$ in the (5+3) picture (Case III(b)).

M_D	M_R	M_S	*Correlation* $\frac{V_{\mu 4}}{V_{e4}} = \frac{m_{\mu\tau}}{m_{e\tau}} + \frac{M_{D_{(ij)}}}{V_{e4}M_{s_{(1j)}}}$ $m_{\mu\mu} = -V_{\mu 4}^2 m_s + \frac{(V_{e4}V_{\mu 4}m_s + m_{e\mu})^2}{V_{e4}^2 m_s + m_{ee}}$
$\begin{pmatrix} a & 0 & 0 \\ d & e & 0 \\ 0 & 0 & i \end{pmatrix}$	$M_R^{(2)}$	$M_S^{(1)}$	$(i = j = 2)$
$\begin{pmatrix} a & 0 & 0 \\ d & 0 & f \\ 0 & h & 0 \end{pmatrix}$	$M_R^{(3)}$	$M_S^{(1)}$	$(i = j = 3)$
$\begin{pmatrix} 0 & b & 0 \\ d & e & 0 \\ 0 & 0 & i \end{pmatrix}$	$M_R^{(5)}$	$M_S^{(2)}$	$(i = j = 3)$
$\begin{pmatrix} 0 & b & 0 \\ 0 & e & f \\ g & 0 & 0 \end{pmatrix}$	$M_R^{(11)}$	$M_S^{(2)}$	$(i = j = 3)$
$\begin{pmatrix} 0 & 0 & c \\ 0 & e & f \\ g & 0 & 0 \end{pmatrix}$	$M_R^{(12)}$	$M_S^{(3)}$	$(i = j = 2)$

Case IV: For $m_{e\tau}=0$, we take

$$M_D^{(7)}=\begin{pmatrix}0 & b & 0\\ d & 0 & f\\ 0 & 0 & i\end{pmatrix},\quad M_s=(s_1\quad s_2\quad 0),\qquad M_R=M_R^{(10)}=\begin{pmatrix}A & B & 0\\ B & 0 & 0\\ 0 & 0 & F\end{pmatrix}. \tag{2.65}$$

Eq. (2.2) gives

$$m_\nu^{3\times3}=\begin{pmatrix}\frac{b^2s_1^2}{(2Bs_1s_2-As_2^2)} & \frac{bds_1}{As_2-2Bs_1} & 0\\ \frac{bds_1}{As_2-2Bs_1} & -\frac{f^2}{F}+\frac{d^2s_2}{2Bs_1-As_2} & -\frac{fi}{F}\\ 0 & -\frac{fi}{F} & -\frac{i^2}{F}\end{pmatrix}, \tag{2.66}$$

$$m_s=-\frac{s_1^2}{A},\qquad R=\begin{pmatrix}\frac{b(B-A)}{2s_1B}+\frac{b(As_2-s_1)}{As_2^2}\\ \frac{d}{2s_1}-\frac{Bd}{As_2}\\ 0\end{pmatrix}=\begin{pmatrix}V_{e4}\\ V_{\mu4}\\ 0\end{pmatrix}. \tag{2.67}$$

The above equations yield the following correlation-

$$m_{\mu\mu}=-V_{\mu4}^2m_s+\frac{m_{\mu\tau}^2}{m_{\tau\tau}}, \tag{2.68}$$

and

$$\frac{V_{e4}}{V_{\mu4}}=\frac{s_1b}{s_2d}-\frac{Ab}{Bd}. \tag{2.69}$$

Eq. (2.68) and (2.53) being the same has the same prediction for m_s, which is not allowed by current neutrino oscillation data. Thus for both the cases of (4+4) and (5+3), $m_{e\tau}=0$ textures are ruled out.

Case V: For $m_{\mu\mu}=0$, the set of matrices is

$$M_D^{(8)}=\begin{pmatrix}0 & b & c\\ d & 0 & 0\\ 0 & h & 0\end{pmatrix},\quad M_s=(0\quad 0\quad s_3)\quad\text{and}\quad M_R=M_R^{(10)}=\begin{pmatrix}A & B & 0\\ B & 0 & 0\\ 0 & 0 & F\end{pmatrix}. \tag{2.70}$$

Then Eq. (2.2) gives

$$m_\nu^{3\times 3}=\begin{pmatrix}\frac{Ab^2}{B^2} & -\frac{bd}{B} & \frac{Abh}{B^2}\\ -\frac{bd}{B} & 0 & -\frac{dh}{B}\\ \frac{Abh}{B^2} & -\frac{dh}{B} & \frac{Ah^2}{B^2}\end{pmatrix}, \tag{2.71}$$

which yields

$$m_s=-\frac{s_3^2}{F},\qquad R=\begin{pmatrix}\frac{c}{s_3}\\ 0\\ 0\end{pmatrix}=\begin{pmatrix}V_{e4}\\ 0\\ 0\end{pmatrix}. \tag{2.72}$$

The above equation gives the following correlations-

$$\frac{m_{ee}}{m_{e\mu}}=\frac{m_{e\tau}}{m_{\mu\tau}}. \tag{2.73}$$

The current neutrino data do not match with this correlation and hence this set of matrices is ruled out. S_3 invariance gives a number of cases with the same correlation as Eq. (2.73) which are also ruled out. Thus $m_{\mu\mu}=0$ is not a possible zero in presence of sterile neutrino.

2.6 Symmetry realization

It is observed that for every set of fermion mass matrices with texture zeros in arbitrary entries, a scalar sector exists. Such texture zeros can be imposed by an Abelian discrete symmetry group Z_n. The procedure of implementation of zero in the entry of the neutrino mass matrices in the method-2 of Ref. [100] is followed here to enforce zeros of our viable

structures only. We consider a diagonal M_l which amounts to six-zeros in this matrix used in the seesaw mechanism. There are a number of papers where zero textures are realized via an extended scalar sector under Abelian symmetry group. In this work, we concentrate on the smallest possible Z_n cyclic group. But smaller groups like Z_3, Z_4 etc. are not sufficient to arrive at our intended textures. We consider the next possible Z_7 symmetry group.

$$Z_7 = (1, \omega, \omega^2, \omega^3, \omega^4, \omega^5, \omega^6)$$

where $\omega = e^{i\frac{2\pi}{7}}$ is the generator of the group. For the case I(a) under Z_7 we consider the leptonic fields to transform as-

$$\begin{aligned} \bar{D}_{e_L} \to \omega^5 \bar{D}_{e_L}, \qquad e_R \to \omega^2 e_R, \qquad \nu_{e_R} \to \nu_{e_R} \\ \bar{D}_{\mu_L} \to \bar{D}_{\mu_L}, \qquad \mu_R \to \mu_R, \qquad \nu_{\mu_R} \to \omega \nu_{\mu_R}. \\ \bar{D}_{\tau_L} \to \omega^3 \bar{D}_{\tau_L}, \qquad \tau_R \to \omega^5 \tau_R, \qquad \nu_{\tau_R} \to \omega^3 \nu_{\tau_R} \end{aligned} \tag{2.74}$$

Here $\bar{D}_{j_L}$,l_R and ν_{k_R} are the $SU(2)_L$ doublets, the RH $SU(2)_L$ singlets and the RH neutrino singlets respectively. The bilinears $\bar{D}_{j_L} l_R, \bar{D}_{j_L} \nu_{k_R}, \nu_{k_R}^T C^{-1} \nu_{j_R}$ relevant for M_l ,M_D and M_R respectively transforms as-

$$\bar{D}_{k_L} l_{j_R} = \begin{pmatrix} 1 & \omega^5 & \omega^3 \\ \omega^2 & 1 & \omega^5 \\ \omega^5 & \omega^3 & \omega \end{pmatrix}, \quad \bar{D}_{k_L} \nu_{j_R} = \begin{pmatrix} \omega^5 & \omega^6 & \omega \\ 1 & \omega & \omega^3 \\ \omega^3 & \omega^4 & \omega^6 \end{pmatrix}, \quad \nu_{k_R}^T C^{-1} \nu_{j_R} = \begin{pmatrix} 1 & \omega & \omega^3 \\ \omega & \omega^2 & \omega^4 \\ \omega^3 & \omega^4 & \omega^6 \end{pmatrix}. \tag{2.75}$$

We introduce three $SU(2)_L$ doublet Higgs (Φ_1, Φ_2, Φ_3) transforming under Z_7 as-

$$\Phi_1 \to \Phi_1, \qquad \Phi_2 \to \omega \Phi_2, \qquad \Phi_3 \to \omega^6 \Phi_3. \tag{2.76}$$

The Z_7 invariant Yukawa Lagrangian becomes

$$-\mathscr{L} = Y^l_{11}\bar{D}_{e_L}\Phi_1 e_R + Y^l_{22}\bar{D}_{\mu_L}\Phi_1\mu_R + Y^l_{33}\bar{D}_{\tau_L}\Phi_3\tau_R + Y^D_{12}\bar{D}_{e_L}\tilde{\Phi}_2\nu_{\mu_R} + Y^D_{13}\bar{D}_{e_L}\tilde{\Phi}_3\nu_{\tau_R} + Y^D_{21}\bar{D}_{\mu_L}\tilde{\Phi}_1\nu_{e_R} + Y^D_{22}\bar{D}_{\mu_L}\tilde{\Phi}_3\nu_{\mu_R} + Y^D_{33}\bar{D}_{\tau_L}\tilde{\Phi}_2\nu_{\tau_R} + h.c \quad (2.77)$$

The Higgs field after acquiring a vacuum expectation value gives the following form of M_l and M_D-

$$M_l = \begin{pmatrix} m_e & 0 & 0 \\ 0 & m_\mu & 0 \\ 0 & 0 & m_\tau \end{pmatrix}, \qquad M_D = \begin{pmatrix} 0 & b & c \\ d & e & 0 \\ 0 & 0 & i \end{pmatrix}. \quad (2.78)$$

We also introduce a scalar singlet χ for M_R transforming as-

$$\chi \to \omega^3\chi_1. \quad (2.79)$$

To prevent mass term of the form $\bar{S^c}S$ as demanded by MES model, we transform the singlet field 'S' as -

$$S \to \omega S. \quad (2.80)$$

In addition we consider two scalar singlets λ_1, λ_2 for M_S where

$$\lambda_1 \to \lambda_1, \qquad \lambda_2 \to \omega^4\lambda_2. \quad (2.81)$$

This leads to the following form of M_R and M_S

$$M_R = \begin{pmatrix} A & 0 & 0 \\ 0 & 0 & E \\ 0 & E & 0 \end{pmatrix}, \qquad M_S = \begin{pmatrix} s_1 & 0 & s_3 \end{pmatrix}, \quad (2.82)$$

which are the required zero textures for case I(a) leading to $m_{\tau\tau} = 0$. Interestingly we find that realization of all the other set of matrices as listed in Table 2.3, follows a typical pattern. The first set of matrices of Table 2.3, follows Eq. (2.6) with the element "BA" of the S_3 group, where

$$BA = \begin{pmatrix} 0 & 0 & 1 \\ 1 & 0 & 0 \\ 0 & 1 & 0 \end{pmatrix}. \tag{2.83}$$

The matrix in Eq. (2.83) refers to the interchange of the third with the first column, second with the third and first with the second column. It is found that if we follow the similar pattern and exchange the transformations of $\nu_{e_R} \to \nu_{\tau_R}$, $\nu_{\tau_R} \to \nu_{\mu_R}$ and $\nu_{\mu_R} \to \nu_{e_R}$ of the representative case(case I(a)) of Eq.(2.74), at the same time keeping the transformation of $\bar{D}_{j_L}$,l_R,Φ,χ,S and λ of Eq. (2.74), (2.76), (2.79), (2.80) and (2.81) respectively the same, then this gives us the first set of matrices of Table 2.3. Similarly the second set of matrices being generated by the the element "B" of S_3, requires only the interchange in the transformation of $\nu_{e_R} \Leftrightarrow \nu_{\tau_R}$ of Eq. (2.74) and so on. Thus all the textures presented in Table 2.3, 2.4, 2.5, 2.6 and 2.7 can be realized from their respective transformations of the basic texture in each case I(a), I(b), I(c), III(a) and III(b) by simply interchanging the transformations of the RH neutrino singlets, keeping all other field transformations the same for each case.

Symmetry realization of all the basic texture zeros are listed in Table 2.8.

Table 2.8 Z_7 Symmetry Realization of all the allowed basic cases.

Scheme	M_D, M_R, M_S	$\bar{\mathtt{D}}_{\mathtt{e_L}}, \bar{\mathtt{D}}_{\mu_\mathtt{L}}, \bar{\mathtt{D}}_{\tau_\mathtt{L}}$	$\mathtt{e_R}, \mu_\mathtt{R}, \tau_\mathtt{R}$	$\nu_{\mathtt{e_R}}, \nu_{\mu_\mathtt{R}}, \nu_{\tau_\mathtt{R}}$	$\chi'\mathtt{s}$	$\Phi'\mathtt{s}$	S	$\lambda' s$
(4+4)	$(1)(c)(2)$	$1, \omega, \omega^4$	$1, \omega^4, \omega^3$	$1, \omega, \omega^3$	ω^3	$1, \omega^2, \omega$	ω	$1, \omega^4$
	$(3)(c)(2)$	$\omega^6, 1, \omega^4$	$\omega, \omega^6, \omega^3$	$1, \omega, \omega^3$	ω^3	$1, \omega^3, \omega$	ω	$1, \omega^4$
(5+3)	$(5)(10)(2)$	$\omega, \omega^3, 1$	$\omega^4, \omega, 1$	$1, \omega^4, \omega^2$	ω^3	$1, \omega^5$	ω	$1, \omega^5$
	$(6)(9)(3)$	$\omega^3, \omega^5, \omega^2$	$\omega^6, \omega^2, \omega^5$	$1, \omega^2, \omega^5$	ω^2	$1, \omega^6$	ω	$1, \omega^2$

2.7 Conclusion

We have systematically explored the texture zeros of three active neutrino sector of neutrino mass matrices in the minimal extended type-I seesaw (MES) mechanism with one sterile neutrino (gauge singlet) of 1eV scale. The phenomenologically predictive cases of such scenario in conformity with current neutrino data dictate that the sum of zeros of M_D and M_R is eight irrespective of zeros in M_S. With this hypothesis we have considered three schemes like (6+2), (5+3) and (4+4) where the paired numbers represent the number of zeros in M_D and M_R respectively. It has been seen that there is no viable structure of the type (6+2) at all. The (5+3) and (4+4) schemes are productive because these can generate one-zero texture of m_ν like $m_{e\tau} = 0$, $m_{\tau\tau} = 0$ and (5+3) can additionally give $m_{\mu\mu} = 0$. On enforcement of zeros, some constraint relations termed as correlations have been obtained which are then scanned under the current available neutrino data of 3σ range. The current neutrino data do not support $m_{\mu\mu} = 0$ and $m_{e\tau} = 0$ but there are some allowed cases for $m_{\tau\tau} = 0$. We have found that there are different set of M_D, M_R and M_S corresponding to a given viable set of such matrices under the transformations S_3 in Eq. (2.6) and the results have been presented in Table 2.3-2.7. Interestingly no two-zero texture survives in presence of sterile neutrino, otherwise there is a number of phenomenologically viable structures studied in literature.

We have implemented Z_7 Abelian symmetry to realize the viable structures of M_D and M_R which require 1 scalar singlet (χ) and 3 Higgs' doublets (Φ) in case of (4+4) scheme. One of Higgs' doublets is SM Higgs' doublet which transforms trivially and the rest are extended sector. Again in case of (5+3) scheme, we require 1 scalar singlet and 2 Higgs' doublets one of which is SM doublet and the other belongs to extended sector. Also two singlets are needed for zeros in sterile mass matrix M_S. We presented the detail procedure of implementing Z_7 symmetry for case I(a) as a representative case only. We have also exhibited how other set of matrices obtained by permutation with the elements of S_3 can be realized by Z_7 by simply interchanging the transformations of the RH neutrino singlets from their

respective basic cases.The symmetry realizations of the basic sets of M_D, M_R and M_S are shown in Table 2.8 for (4+4) and (5+3) schemes.

3

Understanding of 2-zero textures of MES $m_\nu^{4\times4}$ and Z_9 symmetry realization

3.1 Introduction

This chapter is based on our work presented in Ref. [99]. In Chapter 2, we have explored the zero textures of 3×3 neutrino mass matrix $m_\nu^{3\times3}$ and found that no two-zero textures of $m_\nu^{3\times3}$ survives in the context of MES mechanism under predictive scenario, that is (4+4),

(5+3), (6+2) scheme, where digits in the pair represents the number of zeros of M_D and M_R respectively.

In this chapter, we are motivated to relook into the two-zero textures of neutrino mass matrix m_ν in its (4×4) form in the context of MES mechanism. For realization of the two-zero textures of $m_\nu^{4\times4}$ via MES mechanism we shall concentrate on the predictive scenario of (4+4) scheme, that is, equal contribution of zeros of M_D and M_R respectively, along with suitable zero textures of M_S.

The compatibility scenario of texture zeros with recent experimental data are quite different in (3×3) and (4×4) form of neutrino mass matrix m_ν. With three active neutrinos, out of 15 possible two-zero textures only 7 textures are allowed [78] by experimental data. Whereas in (3+1) paradigm, all the 15 two-zero textures of $m_\nu^{4\times4}$ are found to be compatible [96] with experiments, provided zeros are in the active sector of $m_\nu^{4\times4}$. Zeros in the sterile sector, that is, fourth row and fourth column of $m_\nu^{4\times4}$ is not allowed by experimental constraints.

Again, the determinant of $m_\nu^{4\times4}$ in MES mechanism [67] vanishes and as such it cannot be a matrix of rank 4. Out of 15 possible two-zero textures of $m_\nu^{4\times4}$, 12 textures $(A_1, A_2, B_3, B_4, C, D_1, D_2, E_1, E_2, F_1, F_2, F_3)$ are of rank 3, while the other three textures (B_1, B_2 and E_3) are of rank 4. We shall therefore concentrate only on the 12 two-zero textures of $m_\nu^{4\times4}$ which are of rank 3. In our work, we find that all the 12 two-zero textures can be realized under the (4+4) scheme in MES mechanism. Implementation of zeros in $m_\nu^{4\times4}$ leads to a number of correlations whereby different mass matrix elements are related to each other. We check the viability of each of the textures by examining their respective correlations under recent neutrino oscillation data by keeping the Dirac and Majorana CP phases with or without restricting to certain values. We observe that there is an inter-play of the CP phases on determining the dynamics of a texture.

There are a large number of combinations of M_D, M_R and M_S with diagonal charged lepton mass matrices M_l under the (4+4) scheme which lead to the desired two-zero textures in $m_\nu^{4\times4}$. However, S_3 group permutation between the fermion mass matrices under MES mechanism leads us to a minimum number of basic combination which generates the desired zero textures in the 4×4 neutrino mass matrix. In our work, the prospective textures of M_D, M_R and M_S for generating two-zero textures in m_ν are realized with Z_9 cyclic group symmetry. For this realization we extend the SM with few scalar singlets and doublets.

The chapter is organised as follows: Section 3.2 includes a brief discussion on the MES mechanism for convenience. In section 3.3 we review the viable two-zero textures of $m_\nu^{4\times4}$. Section 3.4 includes a brief review on the four-zero textures of M_D and M_R along with zero textures of M_S, followed by the S_3 invariance of fermion mass matrices in the MES formalism. In section 3.5, the two-zero textures are realized in the context of MES mechanism. Also we present the correlations for each texture under the (4+4) scheme. In section 3.6, we check the viability of each texture under recent neutrino oscillation data for both unconstrained and constrained CP phases. In section 3.7 symmetry realization of the allowed textures are presented. Finally we conclude in section 3.8.

3.2 Minimal extended seesaw (MES) mechanism

In MES mechanism, the Standard Model is extended with four additional singlets - three right-handed neutrinos and one gauge singlet chiral field 'S'. This leads to a (7×7) form of neutrino mass matrix m_ν which on applying seesaw approximation $M_R >> M_S > M_D$ reduces to

$$m_\nu^{4\times4} = -\begin{pmatrix} M_D M_R^{-1} M_D^T & M_D M_R^{-1} M_S^T \\ M_S (M_R^{-1})^T M_D^T & M_S M_R^{-1} M_S^T \end{pmatrix} \tag{3.1}$$

$m_\nu^{4\times4}$ is a square matrix of rank three and hence one of the active neutrino mass states remains as massless. The mass matrix $m_\nu^{4\times4}$ can have at most rank 3 since

$$\begin{aligned}\det(m_\nu^{4\times4}) &= \det(M_D M_R^{-1} M_D^T)\det[-M_S M_R^{-1} M_S^T \\ &\quad + M_S M_R^{-1} M_D^T (M_D M_R^{-1} M_D^T)^{-1} M_D M_R^{-1} M_S^T] \\ &= \det(M_D M_R^{-1} M_D^T)\det[M_S(M_R^{-1} - M_R^{-1}) M_S^T] \\ &= 0\end{aligned} \tag{3.2}$$

where both M_D and M_R are considered to be non-singular. Thus at least one of the active neutrino mass states remains as massless.

Block diagonalization of Eq. (3.1) leads to the mass of the sterile neutrino as

$$m_s \sim -M_S M_R^{-1} M_S^T \tag{3.3}$$

3.3 Two-zero textures of $m_\nu^{4\times4}$

Table 3.1 Viable two-zero textures [96] of rank 3. Here 'X' indicates the elements with non-zero entries.

A_1	A_2	B_3	B_4
$\begin{pmatrix} 0 & 0 & X & X \\ 0 & X & X & X \\ X & X & X & X \\ X & X & X & X \end{pmatrix}$	$\begin{pmatrix} 0 & X & 0 & X \\ X & X & X & X \\ 0 & X & X & X \\ X & X & X & X \end{pmatrix}$	$\begin{pmatrix} X & 0 & X & X \\ 0 & 0 & X & X \\ X & X & X & X \\ X & X & X & X \end{pmatrix}$	$\begin{pmatrix} X & X & 0 & X \\ X & X & X & X \\ 0 & X & 0 & X \\ X & X & X & X \end{pmatrix}$
C	D_1	D_2	E_1
$\begin{pmatrix} X & X & X & X \\ X & 0 & X & X \\ X & X & 0 & X \\ X & X & X & X \end{pmatrix}$	$\begin{pmatrix} X & X & X & X \\ X & 0 & 0 & X \\ X & 0 & X & X \\ X & X & X & X \end{pmatrix}$	$\begin{pmatrix} X & X & X & X \\ X & X & 0 & X \\ X & 0 & 0 & X \\ X & X & X & X \end{pmatrix}$	$\begin{pmatrix} 0 & X & X & X \\ X & 0 & X & X \\ X & X & X & X \\ X & X & X & X \end{pmatrix}$
E_2	F_1	F_2	F_3
$\begin{pmatrix} 0 & X & X & X \\ X & X & X & X \\ X & X & 0 & X \\ X & X & X & X \end{pmatrix}$	$\begin{pmatrix} X & 0 & 0 & X \\ 0 & X & X & X \\ 0 & X & X & X \\ X & X & X & X \end{pmatrix}$	$\begin{pmatrix} X & 0 & X & X \\ 0 & X & 0 & X \\ X & 0 & X & X \\ X & X & X & X \end{pmatrix}$	$\begin{pmatrix} X & X & 0 & X \\ X & X & 0 & X \\ 0 & 0 & X & X \\ X & X & X & X \end{pmatrix}$

We consider only those two-zero textures of $m_\nu^{4\times4}$ of rank 3 which are listed in Table 3.1.

There exist a $P_{\mu\tau}$ symmetry [96] between the textures $A_1 - A_2$, $B_3 - B_4$, $D_1 - D_2$, $E_1 - E_2$, $F_2 - F_3$ of the form

$$A_2 = P_{\mu\tau}^T A_1 P_{\mu\tau}, \tag{3.4}$$

where

$$P_{\mu\tau} = \begin{pmatrix} 1 & 0 & 0 & 0 \\ 0 & 0 & 1 & 0 \\ 0 & 1 & 0 & 0 \\ 0 & 0 & 0 & 1 \end{pmatrix}. \tag{3.5}$$

However, no such symmetry exists for the texture C and F_1.

In this work we consider the $m_\nu^{4\times4}$ form of MES mechanism (Eq. (3.1)) to realize the two-zero textures of m_ν in Table 3.1.

3.4 (4+4) Scheme and S_3 invariance

Four-zero textures of M_D:

There are ${}^9C_4 = 126$ possible 4 zero textures of M_D. However, the requirement of non singular M_D as demanded by the condition in Eq. (3.2) rules out those textures of M_D which are either of row zero, column zero or block zero. The row-zero or block-zero structures of M_D are also not useful as they lead to one neutrino massless and decoupled from others, and zero entry in PMNS matrix respectively [82]. Barring these forbidden textures, the rest 81 four-zero textures of M_D on amalgamating with 4 zero textures of M_R and one/two zero textures of M_S can produce the two zero textures of $m_\nu^{4\times4}$.

Four-zero textures of M_R:

Similarly, out of 15 four-zero textures of M_R only three remains non-singular.

$$M_R^a = \begin{pmatrix} 0 & B & 0 \\ B & 0 & 0 \\ 0 & 0 & F \end{pmatrix}, \quad M_R^b = \begin{pmatrix} 0 & 0 & C \\ 0 & D & 0 \\ C & 0 & 0 \end{pmatrix}, \quad M_R^c = \begin{pmatrix} A & 0 & 0 \\ 0 & 0 & E \\ 0 & E & 0 \end{pmatrix} \tag{3.6}$$

S_3 invariance according to Eq. (3.8) leads to one basic form of $M_R = M_R^c$. The other two forms are obtained by S_3 permutation of M_R^c.

Zero textures of M_S:

Since the sterile sector of $m_\nu^{4\times4}$ involves the active sterile mixing matrix M_S, we consider the zero textures of M_S in such a way that non-zero terms appears in the fourth row and column of the mass matrix. We find that under the (4+4) scheme, two-zero texture of M_S is not allowed. Only one-zero texture of M_S can lead to non-vanishing entries in the sterile sector. Possible one-zero texture of M_S are given by Eq. (3.7).

$$M_S^{(1)} = (0 \quad s_2 \quad s_3), \quad M_S^{(2)} = (s_1 \quad 0 \quad s_3) \quad \text{and} \quad M_S^{(3)} = (s_1 \quad s_2 \quad 0). \tag{3.7}$$

The non-singular textures of M_R, one-zero textures of M_S and all the 81 textures of M_D are mapped together in order to achieve the two-zero textures of $m_\nu^{4\times4}$ (Table 3.1). Furthermore, different combination of M_D, M_R and M_S produces zeros in the same location of $m_\nu^{4\times4}$ due to their interconvertability nature according to Eq. (3.8).

S_3 invariance under (4+4) scheme:

We find that under (4+4) scheme, there exists S_3 permutation[1] between different combinations of M_D, M_R and M_S which keeps $m_\nu^{4\times4}$ invariant.

[1]For details, refer to section 2.3, Chapter 2

Under the S_3 permutation group M_D, M_R and M_S transform as:

$$M_D \to M_D Z, \quad M_R \to Z^T M_R Z, \quad M_S \to M_S Z. \tag{3.8}$$

This reduces the voluminous work of exploring a large number of combinations of M_D, M_R and M_S and eases our job thereby making it more economic as only a few zero textures of M_D and M_R are required to deal with.

3.5 Realization of two-zero textures in (4+4) scheme

Under (4+4) scheme, the viable two-zero textures of m_ν can be realized from some basic combinations of M_D, M_R and M_S along with certain correlations among the neutrino parameters. Corresponding to each such combination, there exist another five combinations of M_D, M_R and M_S obtainable via S_3 transformations in Eq. (3.8) leading to the same textures and correlations as the basic combination yields. In our study, we find a total of 24 textures of M_D (Table 3.2) which can generate the two-zero textures of $m_\nu^{4\times4}$ along with their respective M_R^c and M_S (Eq. (3.7)).

Class A

Class A consists of two textures A_1 and A_2 that allow only NH mass ordering. There are three basic combinations of M_D, M_R and M_S for each of the texture A_1 and A_2. Using $M_R = M_R^c$ in Eq. (3.6), the particular four-zero textures of M_D (Table 3.2) and one-zero textures of M_S in Eq. (3.7), we can construct the textures A_1 and A_2 with different correlations:

Texture A_1: The following combination of M_D and M_S

$$(a): \quad M_D = M_D^{(1)}, \qquad M_S = M_S^{(2)}. \tag{3.9}$$

Table 3.2 Four-zero textures of M_D.

$M_D^{(1)}$	$M_D^{(2)}$	$M_D^{(3)}$	$M_D^{(4)}$	$M_D^{(5)}$	$M_D^{(6)}$
$\begin{pmatrix} 0 & b & 0 \\ d & e & 0 \\ g & 0 & l \end{pmatrix}$	$\begin{pmatrix} 0 & b & 0 \\ d & 0 & f \\ g & h & 0 \end{pmatrix}$	$\begin{pmatrix} 0 & b & 0 \\ d & e & 0 \\ 0 & h & l \end{pmatrix}$	$\begin{pmatrix} 0 & b & 0 \\ 0 & e & f \\ g & h & 0 \end{pmatrix}$	$\begin{pmatrix} 0 & b & 0 \\ d & 0 & 0 \\ g & h & l \end{pmatrix}$	$\begin{pmatrix} 0 & b & 0 \\ d & e & f \\ g & 0 & 0 \end{pmatrix}$
$M_D^{(7)}$	$M_D^{(8)}$	$M_D^{(9)}$	$M_D^{(10)}$	$M_D^{(11)}$	$M_D^{(12)}$
$\begin{pmatrix} a & b & 0 \\ 0 & e & 0 \\ g & 0 & l \end{pmatrix}$	$\begin{pmatrix} a & b & 0 \\ d & 0 & f \\ 0 & h & 0 \end{pmatrix}$	$\begin{pmatrix} a & b & 0 \\ 0 & e & 0 \\ 0 & h & l \end{pmatrix}$	$\begin{pmatrix} a & b & 0 \\ 0 & e & f \\ 0 & h & 0 \end{pmatrix}$	$\begin{pmatrix} a & 0 & 0 \\ 0 & e & 0 \\ g & h & l \end{pmatrix}$	$\begin{pmatrix} a & 0 & 0 \\ d & e & f \\ 0 & h & 0 \end{pmatrix}$
$M_D^{(13)}$	$M_D^{(14)}$	$M_D^{(15)}$	$M_D^{(16)}$	$M_D^{(17)}$	$M_D^{(18)}$
$\begin{pmatrix} a & b & c \\ 0 & e & 0 \\ g & 0 & 0 \end{pmatrix}$	$\begin{pmatrix} a & b & c \\ d & 0 & 0 \\ 0 & h & 0 \end{pmatrix}$	$\begin{pmatrix} a & b & 0 \\ 0 & 0 & f \\ g & 0 & l \end{pmatrix}$	$\begin{pmatrix} a & b & 0 \\ d & 0 & f \\ 0 & 0 & l \end{pmatrix}$	$\begin{pmatrix} 0 & b & c \\ 0 & e & 0 \\ g & h & 0 \end{pmatrix}$	$\begin{pmatrix} 0 & b & c \\ d & e & 0 \\ 0 & h & 0 \end{pmatrix}$
$M_D^{(19)}$	$M_D^{(20)}$	$M_D^{(21)}$	$M_D^{(22)}$	$M_D^{(23)}$	$M_D^{(24)}$
$\begin{pmatrix} 0 & b & 0 \\ 0 & 0 & f \\ g & h & l \end{pmatrix}$	$\begin{pmatrix} 0 & b & 0 \\ d & e & f \\ 0 & 0 & l \end{pmatrix}$	$\begin{pmatrix} 0 & b & c \\ d & 0 & 0 \\ 0 & h & l \end{pmatrix}$	$\begin{pmatrix} 0 & b & c \\ 0 & e & f \\ g & 0 & 0 \end{pmatrix}$	$\begin{pmatrix} a & b & c \\ 0 & e & 0 \\ 0 & 0 & l \end{pmatrix}$	$\begin{pmatrix} a & 0 & 0 \\ 0 & e & f \\ 0 & h & l \end{pmatrix}$

in Eq. (3.1) gives the following correlations

$$m_{\tau\tau} m_{ss} = m_{\tau s}^2, \tag{3.10}$$

$$\frac{m_{\mu s}}{m_{\tau s}} = \sqrt{\frac{m_{\mu\mu}}{m_{\tau\tau}}} + \frac{eAs_3}{gEs_1}. \tag{3.11}$$

$$(b): \quad M_D = M_D^{(3)}, \qquad M_S = M_S^{(2)}. \tag{3.12}$$

Eq. (3.1) yields

$$\frac{m_{\tau\tau}}{m_{\tau s}} = 2\left(\frac{m_{e\tau}}{m_{es}}\right), \tag{3.13}$$

$$\frac{m_{\mu s}}{m_{es}} = \frac{m_{\mu\tau}}{m_{e\tau}} + \frac{dEs_1}{bAs_3}. \tag{3.14}$$

$$(c): \quad M_D = M_D^{(5)}, \qquad M_S = M_S^{(2)}. \tag{3.15}$$

Eq. (3.1) yields

$$m_{\mu\mu}m_{ss} = m_{\mu s}^2, \tag{3.16}$$

$$\frac{m_{\tau s}}{m_{\mu s}} = \frac{m_{\mu\tau}}{m_{\mu\mu}} + \frac{hAs_3}{dEs_1}. \tag{3.17}$$

Equations of the form (3.11), (3.14) and (3.17) enlighten us with the idea of the allowed range of the parameter values of $\frac{es_3A}{gEs_1}$, $\frac{dEs_1}{bAs_3}$ and $\frac{hAs_3}{dEs_1}$ respectively. A particular texture leads to a number of such correlations which give the allowed range of the ratio of the elements of M_D, M_R and M_S. However, such correlations do not guarantee the viability of a texture.

Texture A_2: For the texture A_2 we present below the combinations of M_D and M_S and their respective correlations from Eq. (3.1).

$$(a): \quad M_D = M_D^{(2)}, \qquad M_S = M_S^{(2)}. \tag{3.18}$$

$$m_{\mu\mu}m_{ss} = m_{\mu s}^2, \qquad \frac{m_{\tau s}}{m_{\mu s}} = \sqrt{\frac{m_{\tau\tau}}{m_{\mu\mu}}} + \frac{hAs_3}{dEs_1}. \tag{3.19}$$

$$(b): \quad M_D = M_D^{(4)}, \qquad M_S = M_S^{(2)}. \tag{3.20}$$

$$\frac{m_{\mu\mu}}{m_{\mu s}} = 2\left(\frac{m_{e\mu}}{m_{es}}\right), \qquad \frac{m_{\tau s}}{m_{es}} = \frac{m_{\mu\tau}}{m_{e\mu}} + \frac{gs_1E}{bs_3A}. \tag{3.21}$$

$$(c): \quad M_D = M_D^{(6)}, \qquad M_S = M_S^{(2)}. \tag{3.22}$$

$$m_{\tau\tau}m_{ss} = m_{\tau s}^2, \qquad \frac{m_{\mu s}}{m_{\tau s}} = \frac{m_{\mu\tau}}{m_{\tau\tau}} + \frac{es_3A}{gEs_1}. \tag{3.23}$$

The $\mu - \tau$ exchange symmetry between the textures are evident from Eq. (3.10)-(3.19), Eq. (3.13)-(3.21), Eq. (3.16)-(3.23).

Class B:

Each of the textures B_3 and B_4 has three basic combinations of M_R, M_D and M_S. With $M_R = M_R^c$ the combinations and their correlations are given below:

Texture B_3:

$$(a): \quad M_D = M_D^{(7)}, \qquad M_S = M_S^{(1)}. \tag{3.24}$$

$$\frac{m_{ss}}{m_{\tau s}} = 2\left(\frac{m_{\mu s}}{m_{\mu\tau}}\right), \qquad \frac{m_{e\tau}}{m_{\tau\tau}} = \sqrt{\frac{m_{ee}}{m_{\tau\tau}}} + \frac{blA}{Eg^2}. \tag{3.25}$$

$$(b): \quad M_D = M_D^{(9)}, \qquad M_S = M_S^{(1)}. \tag{3.26}$$

$$\frac{m_{e\tau}}{m_{es}} = \frac{m_{\mu\tau}}{m_{\mu s}}, \qquad 2\left(\frac{m_{\tau s}}{m_{ss}}\right) - \frac{m_{e\tau}}{m_{es}} = \frac{m_{\tau\tau}m_{es}}{m_{ss}m_{e\tau}}. \tag{3.27}$$

$$(c): \quad M_D = M_D^{(11)}, \qquad M_S = M_S^{(2)}. \tag{3.28}$$

$$m_{ee}m_{ss} = m_{es}^2, \qquad \frac{m_{\tau s}}{m_{es}} = \frac{m_{e\tau}}{m_{ee}} + \frac{hs_3A}{as_1E}. \tag{3.29}$$

Texture B_4: The combinations of M_D, M_S which generates the texture B_4 are (a) $M_D^{(8)}, M_S^{(1)}$ (b) $M_D^{(10)}, M_S^{(1)}$ and (c) $M_D^{(12)}, M_S^{(2)}$ with correlations which are $\mu-\tau$ exchange symmetric to the correlations in Eq. (3.25), (3.27) and (3.29) respectively.

Class C:

There is only one basic combination that generates the texture C.

$$M_R = M_R^c, \qquad M_D = M_D^{(23)}, \qquad M_S = M_S^{(1)}. \tag{3.30}$$

$$\frac{m_{ss}}{m_{\tau s}} = 2\left(\frac{m_{\mu s}}{m_{\mu\tau}}\right), \qquad \frac{m_{ee}}{m_{e\mu}} = 2\left(\frac{m_{e\tau}}{m_{\mu\tau}}\right) + \frac{a^2E}{ceA}. \tag{3.31}$$

Class D:

Texture D_1 and D_2 consists of three basic combination of M_D, M_R^c and M_S.

Texture D_1:

$$(a): \quad M_D = M_D^{(13)}, \qquad M_S = M_S^{(2)}. \tag{3.32}$$

$$m_{\tau\tau} m_{ss} = m_{\tau s}^2, \qquad \frac{m_{es}}{m_{ss}} = \frac{m_{e\tau}}{m_{\tau s}} + \frac{bAs_3}{Es_1^2}. \tag{3.33}$$

$$(b): \quad M_D = M_D^{(15)}, \qquad M_S = M_S^{(1)}. \tag{3.34}$$

$$\frac{m_{e\mu}}{m_{es}} = 2\left(\frac{m_{\mu s}}{m_{ss}}\right), \qquad \frac{m_{e\tau}}{m_{e\mu}} = \frac{m_{\tau s}}{m_{\mu s}} + \frac{agE}{bfA}. \tag{3.35}$$

$$(c): \quad M_D = M_D^{(17)}, \qquad M_S = M_S^{(2)}. \tag{3.36}$$

$$\frac{m_{ee}}{m_{e\mu}} = 2\left(\frac{m_{es}}{m_{\mu s}}\right), \qquad \frac{m_{\tau s}}{m_{\mu s}} = \frac{m_{e\tau}}{m_{e\mu}} + \frac{gs_1 E}{es_3 A}. \tag{3.37}$$

Texture D_2: The combination (a) $M_D^{(14)}, M_S^{(2)}$ (b) $M_D^{(16)}, M_S^{(1)}$ (c) $M_D^{(18)}, M_S^{(2)}$ generate the texture D_2 with correlations which are $\mu - \tau$ exchange symmetric to Eq. (3.33), (3.35) and (3.37) respectively.

Class E:

Each of the texture E_1 and E_2 has one basic combination of M_D, M_R and M_S.

Texture E_1:

$$M_R = M_R^c, \qquad M_D = M_D^{(19)}, \qquad M_S = M_S^{(1)}. \tag{3.38}$$

$$\frac{m_{e\mu}}{m_{es}} = 2\left(\frac{m_{\mu s}}{m_{ss}}\right), \qquad m_{\tau s} m_{e\mu} - m_{e\tau} m_{\mu s} = m_{\mu\tau} m_{es}. \tag{3.39}$$

Texture E_2: With $M_D^{(20)}, M_S^{(1)}$ we arrive at the correlations which are $\mu-\tau$ exchange symmetric to Eq. (3.39).

Class F:

Each of the textures F_1, F_2 and F_3 posses one basic combination of M_D, M_R and M_S.

Texture F_1:

$$M_R = M_R^c, \qquad M_D = M_D^{(24)}, \qquad M_S = M_S^{(3)}. \tag{3.40}$$

$$m_{ee}m_{ss} = m_{es}^2, \qquad 2\left(\frac{m_{\mu\tau}}{m_{\tau s}}\right) - \frac{m_{\mu\mu}}{m_{\mu s}} = \frac{m_{\mu s}m_{\tau\tau}}{m_{\tau s}^2}. \tag{3.41}$$

Texture F_2:

$$M_R = M_R^c, \qquad M_D = M_D^{(21)}, \qquad M_S = M_S^{(2)}. \tag{3.42}$$

$$m_{\mu\mu}m_{ss} = m_{\mu s}^2, \qquad 2\left(\frac{m_{e\tau}}{m_{es}}\right) - \frac{m_{\tau\tau}}{m_{\tau s}} = \frac{m_{ee}m_{\tau s}}{m_{es}^2}. \tag{3.43}$$

Texture F_3: The combination $M_R^c, M_D^{(22)}, M_S^{(3)}$ generates the texture F_3 with correlations which are $\mu-\tau$ exchange symmetric to Eq. (3.43).

3.6 Experimental compatibility of the textures with current neutrino data

We shall consider a texture to be viable if the correlations corresponding to the texture show the consistency with the current neutrino data. The numerical procedure of consistency check of a given correlation is as follows: we first calculate the respective ranges of values of neutrino mass matrix elements m_{ij} with $(i,j = e,\mu,\tau,s)$ from their respective expressions given in the Appendix A, using 3σ values of masses and mixing angles of the recent neutrino oscillation data [Refer section 1.7, chapter 1] with and without constraining CP phases.

Also we calculate the allowed ranges of values for the expression involving m_{ij} in lhs and rhs of a given correlation while plotting them against $\sin\theta_{34}$ which is constrained from an upper bound < 0.4 [109]. In our analysis, we have taken its lower limit as 0. Under such condition if the two plots (lhs of the correlation vs $\sin\theta_{34}$ and rhs of the correlation vs $\sin\theta_{34}$) overlap in a considerable range, then the given correlation is taken as consistent. Again for those textures whose correlations are not significantly different in respect of their phenomenologies, only the correlations of one of them as a representative case are plotted against $\sin\theta_{34}$ taking the range from $(0-0.4)$ for both the mass order: normal hierarchy (NH) and inverted hierarchy (IH). As the plots are made with or without constraining the Dirac and Majorana CP phases, for convenience, we have classified the textures into (i) CP phase dependent textures, of which the correlations are sensitive to the variation of CP phases and (ii) CP phase independent textures, of which, the correlations do not respond to the variation of the CP phases. Constrained CP phases mean that we pick up smaller ranges of values of unknown CP phases from the complete range $(0-2\pi)$ at our own choice as a representative case and plot the correlations to check the consistency.

3.6.1 Class A

CP phase dependent textures:

Texture A_1 and A_2 has $ee = 0, e\mu = 0$ and $ee = 0, e\tau = 0$ respectively in its 4×4 form (Table 3.1). Class A allows only normal hierarchy (NH) spectrum in the 3+1 scenario [96] . Therefore, we present only the normal hierarchical case for class A.

Case I:

The basic combinations in Eq. (3.9) and Eq. (3.22) for texture A_1 and A_2 respectively lead to the correlation of the form as in Eq. (3.10). On plotting the lhs and rhs of this correlation $m_{\tau\tau}m_{ss}$ and $m_{\tau s}^2$ against $\sin\theta_{34}$ with the CP phases running unconstrained from 0 to 2π, we

see that there is overlapping of the two graphs for $\sin\theta_{34} > 0.08$ in Fig. 3.1 (left plot). Thus, the textures are experimentally allowed for $\sin\theta_{34} > 0.08$ that puts a lower limit on $\sin\theta_{34}$ for these textures.

It is interesting to note that there is strong interplay of CP phases as the choice of $\gamma = \delta_{13} = (0-30^0), \beta = \delta_{24} = (0-45^0), \delta_{14} = (180^0-225^0), \alpha = (315^0-360^0)$, the overlapping appears only for values of $\sin\theta_{34} > 0.12$. The allowed range with CP unconstrained are now squeezed when CP is constrained to the ranges under consideration. Of course this particular choice of constrained CP phases are in no way unique. The survey of constraining phases shows that these textures are never allowed for the lower values of the mixing angles θ_{34}. Thus this puts a constraint on the lower limit of θ_{34}. Fig. 3.1 shows the scatter plots of the correlation in Eq. (3.10) under both the cases of with or without constraining CP phases.

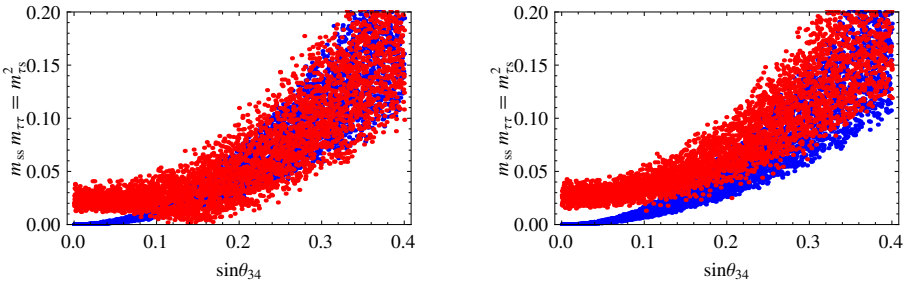

Fig. 3.1 Scatter plots for Eq. (3.10) where : ■ $m_{\tau\tau}m_{ss}$ and ■ $m_{\tau s}^2$. The left plot is for unconstrained CP phases while the right plot is for constrained ranges of CP phases: $\gamma = \delta_{13} = (0-30^0), \beta = \delta_{24} = (0-45^0), \delta_{14} = (180^0-225^0), \alpha = (315^0-360^0)$ (Texture A_1, A_2).

These particular combinations in Eq. (3.9) and Eq. (3.22) also yield a number of correlations involving the parameters of their respective M_D, M_R and M_S. From these equations one can determine the allowed range of the ratio of the parameter values. One such equation for each texture is given in Eq. (3.11) and (3.19) (second correlation) for texture A_1 and A_2 respectively. As a representative case we plot the Eq. (3.11) in Fig. 3.2. Similar evaluation of the values of the ratio of the parameters of M_D, M_R and M_S can be obtained from the scatter plots for all the textures. The values of the parameters $\frac{es_3A}{gEs_1}$ in Eq. (3.11) remain almost the same for both unconstrained and constrained ranges of CP phases (Fig. 3.2). From Fig. 3.1, it

is seen that the texture is allowed for values of $\sin\theta_{34} > 0.08$ without constraining CP phases, while $\sin\theta_{34} > 0.12$ with constrained CP phases. Therefore, the value of $\frac{es_3A}{gEs_1} < 1.8$ for unconstrained CP phases (left plot of Fig. 3.2) and $\frac{es_3A}{gEs_1} < 1$ when CP values are constrained to $\gamma = \delta_{13} = (0-30^0), \beta = \delta_{24} = (0-45^0), \delta_{14} = (180^0-225^0), \alpha = (315^0-360^0)$ (right plot of Fig. 3.2).

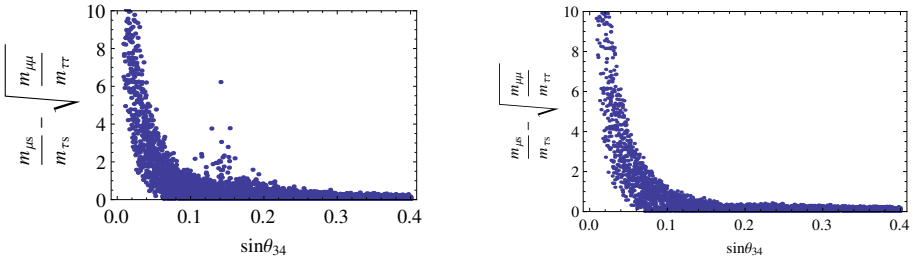

Fig. 3.2 Scatter plots for Eq. (3.11) for unconstrained (left plot) and constrained CP values (right plot) ($\gamma = \delta_{13} = (0-30^0), \beta = \delta_{24} = (0-45^0), \delta_{14} = (180^0-225^0), \alpha = (315^0-360^0)$ (Texture A_1).

Case II:

The basic combinations in Eq. (3.12) and (3.20) of texture A_1 and A_2 respectively yields correlation in Eq. (3.13) and Eq. (3.21) which possess $\mu-\tau$ symmetry. Both the equations behave differently under recent neutrino oscillation data. This is evident from Fig. 3.3 and Fig. 3.4 below.

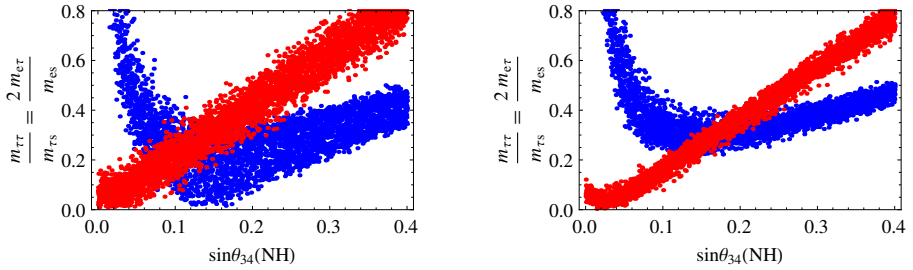

Fig. 3.3 Scatter plots for Eq. (3.13) where : ■ $\frac{m_{\tau\tau}}{m_{\tau s}}$ and ■ $2\left(\frac{m_{e\tau}}{m_{es}}\right)$. The left plot is for unconstrained CP phases. The right plot is for constrained ranges : $\gamma = (0-30^0), \delta_{14} = (0-10^0), \beta = (0-30^0), \delta_{13} = (150^0-180^0), \alpha = (0-90^0), \delta_{24} = (0-180^0)$ (Texture A_1).

The left plot of Fig. 3.3 shows that when CP phases are not constrained, the texture is allowed only for values of $\sin\theta_{34} \approx (0.06 - 0.2)$. For other values of $\sin\theta_{34}$ there exists no overlapping between lhs and rhs of Eq. (3.13) and hence the texture is disallowed for those ranges.

A fair interplay of the CP phases has also been witnessed in the right plot of Fig. 3.3. When CP phases are constrained to $\gamma = (0 - 30^0), \delta_{14} = (0 - 10^0), \beta = (0 - 30^0), \delta_{13} = (150^0 - 180^0), \alpha = (0 - 90^0), \delta_{24} = (0 - 180^0)$, the texture becomes viable in the range $\sin\theta_{34} = (0.12 - 0.22)$. However, we also find that the texture withstands for any choice of the ranges of the CP phases.

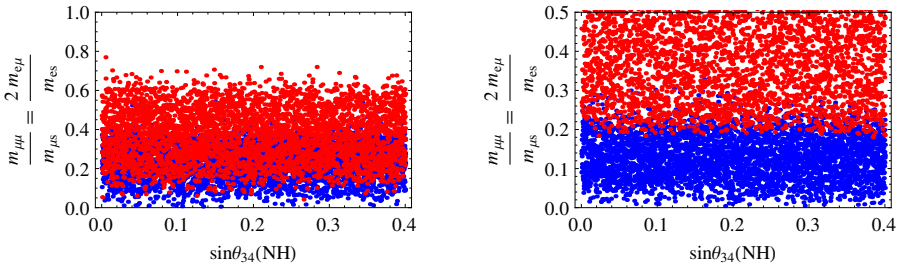

Fig. 3.4 Scatter plots for Eq. (3.21) where : ■ $\frac{m_{\mu\mu}}{m_{\mu s}}$ and ■ $2\left(\frac{m_{e\mu}}{m_{es}}\right)$. Left plot is for unconstrained CP phases and right plot for $\gamma, \beta, \delta_{24} = (0 - 5^0)$ and $\delta_{14} = \alpha = (145^0 - 170^0), \delta_{13} = (70^0 - 90^0)$ (Texture A_2).

On the other hand for the texture A_2 we find that there exists a clear overlapping between the lhs and rhs of the correlation (3.21) for all values of $\sin\theta_{34} = (0 - 0.4)$ without restricting CP phases to a particular range. This shows that the texture is allowed for all ranges of $\sin\theta_{34}$. However, the texture is not viable when CP values are constrained to small values like $\gamma, \beta, \delta_{24} = (0 - 5^0)$ and $\delta_{14} = \alpha = (145^0 - 170^0), \delta_{13} = (70^0 - 90^0)$. This becomes visible in Fig. 3.4 as lhs and rhs are separated leading to inconsistency of the correlation.

CP phase independent textures

There exist some combinations of M_D, M_R and M_S leading to certain correlations which remain consistent with the current neutrino data with or without constraining CP phases. Such combinations are discussed below.

Case III:

The basic combination in Eq. (3.15) and (3.18) for texture A_1 and A_2 respectively, leads to the correlation in Eq. (3.16). We find that there exists a fair overlapping between both sides of Eq. (3.16) for unconstrained CP phases. Again CP phases have been restricted to different segments of the values, still the correlation remains unaffected. Even on putting zero values for all the CP phases, the texture continues to survive within 3σ range of oscillation data. Fig. 3.5 shows the scatter plot of the correlation (3.16) for unconstrained CP phases while Fig. 3.6 demonstrates its insensitivity to the variation of the CP phases.

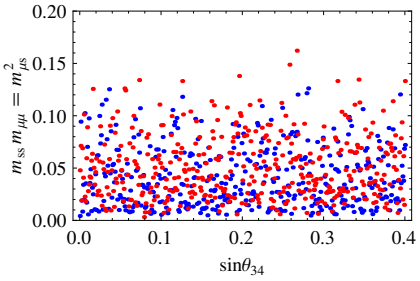

Fig. 3.5 Scatter plots for Eq. (3.16) for unconstrained CP phases where : ■ $m_{\mu\mu}m_{ss}$ and ■ $m^2_{\mu s}$ (Texture A_1, A_2).

3.6.2 Class B

Out of four textures B_1, B_2, B_3, B_4 in class B, only two of them B_3, B_4 are of rank 3. B_3 has zeros in its $e-\mu$ and $\mu-\mu$ entries of the $m_\nu^{4\times4}$, and B_4 is having zeros in $e-\tau$ and $\tau-\tau$ entries. Class B allows all the three mass patterns: normal hierarchy (NH), inverted hierarchy (IH) and quasi degenerate (QD). However, MES mechanism requires one of the

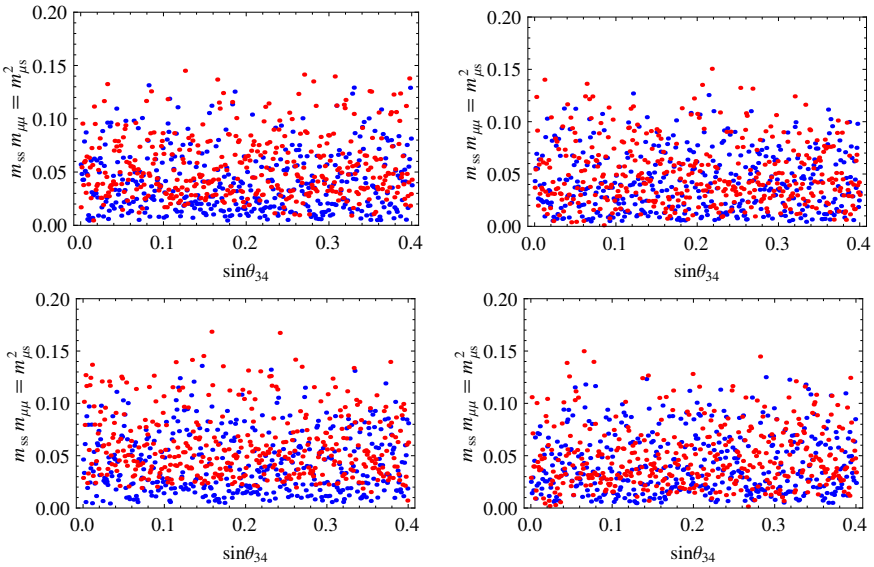

Fig. 3.6 Scatter plots for Eq. (3.16) for different ranges of CP phases. The upper left plot is for $\gamma = \alpha = \delta_{24} = (0-30^0), \delta_{13} = (0-90^0), \beta = (0-60^0)$. The upper right plot is for $\gamma = \delta_{14} = (225^0-270^0), \alpha = (180^0-225^0), \delta_{13} = \delta_{24} = (90^0-135^0), \beta = (0-45^0)$. The lower left plot is for $\gamma = (90^0-135^0), \alpha = (0-90^0), \delta_{24} = (315^0-360^0), \delta_{13} = (225^0-270^0), \beta = (0-45^0), \delta_{14} = (180^0-225^0)$. The lower right plot is for $\gamma = (30^0-90^0), \alpha = \delta_{24} = \delta_{13} = (0-90^0), \beta = (135^0-180^0), \delta_{14} = (90^0-135^0)$ (Texture A_1, A_2).

active neutrinos to be massless and hence QD spectrum is ruled out. Therefore, in our analysis we shall consider only the NH and IH patterns of the textures B_3 and B_4.

CP phase dependent textures

Out of the three basic combinations of M_D, M_R and M_S for B_3 and B_4, two combinations show CP phase dependence when their correlations are plotted for different ranges of CP values.

Case I:

The combination in Eq. (3.24) of B_3 and case (a) of B_4 lead to the same correlation in Eq. (3.25) due to $\mu\tau$ symmetry.

Scatter plots for NH spectrum in Fig. 3.7 for correlation in Eq. (3.25) shows that when CP phases are unconstrained, the texture is allowed excluding only for a narrow range of $\approx (0-0.02)$ of $\sin\theta_{34}$. However, when CP phases are constrained to: $\gamma = \delta_{14} = \delta_{13} =$

$(0-45^0), \beta = (180^0-225^0), \delta_{24} = \alpha = (0-30^0)$, the texture is allowed only for the range $\approx (0.02-0.16)$ of $\sin\theta_{34}$. The overlapping of the correlation disappears beyond the above range of $\sin\theta_{34}$, and hence the texture is disfavoured for this range. This shows the CP phase dependencies of the texture. Similar phenomenology has been observed for IH spectrum.

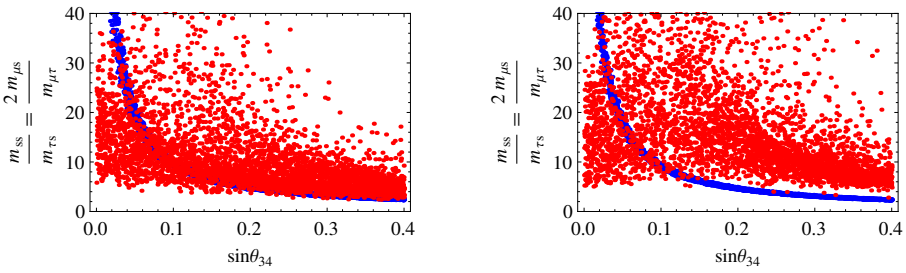

Fig. 3.7 Scatter plots for Eq. (3.25) where : ■ $\frac{m_{ss}}{m_{\tau s}}$ and ■ $2(\frac{m_{\mu s}}{m_{\mu\tau}})$. The left plot is for unconstrained and right plot for constrained CP phases $(\gamma = \delta_{14} = \delta_{13} = (0-45^0), \beta = (180^0-225^0), \delta_{24} = \alpha = (0-30^0))$ for NH spectrum (Texture B_3 and B_4).

Case II:

Scatter plots for correlation in Eq. (3.27) (texture B_3) and its $\mu-\tau$ counterpart for case (b) (texture B_4) are plotted in Fig. 3.8 - Fig. 3.10 for NH and IH.

Texture B_3:

Normal Hierarchy: From the Fig. 3.8 it is seen that the plot for Eq. (3.27)(second correlation) disallows the range $\approx (0-0.08)$ when CP phases are kept unconstrained (left plot). When CP phases are constrained to the ranges $\gamma = \beta = (45^0-90^0), \alpha = \delta_{14} = \delta_{24} = (0-30^0), \delta_{13} = (180^0-225^0)$, the overlapping of lhs and rhs disappears and hence the texture is forbidden for the range under consideration. The first correlation shows similar phenomenology whereby the texture is allowed for the range of $\sin\theta_{34} > 0.02$ when CP phases are unconstrained. For similar ranges of constrained CP phases, the first correlation is also not allowed. This shows that the texture depends on the CP phases.

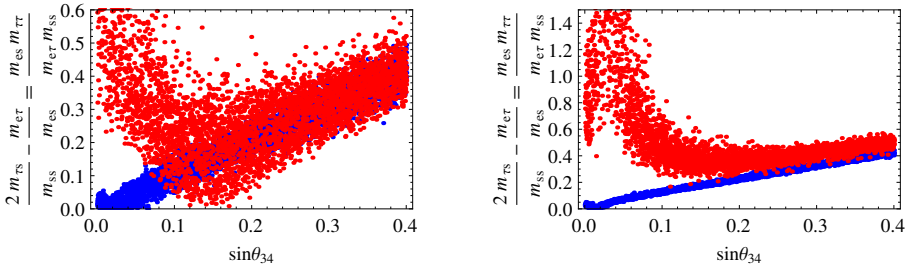

Fig. 3.8 Scatter plots for Eq. (3.27) (second correlation) where : ■ $2\left(\frac{m_{\tau s}}{m_{ss}}\right) - \frac{m_{e\tau}}{m_{es}}$ and ■ $\frac{m_{\tau\tau}m_{es}}{m_{ss}m_{e\tau}}$. The left plot is for unconstrained CP phases and right plot for constrained ranges of CP phases : $\gamma = \beta = (45^0 - 90^0), \alpha = \delta_{14} = \delta_{24} = (0 - 30^0), \delta_{13} = (180^0 - 225^0)$ for NH spectrum (Texture B_3).

Inverted Hierarchy: For IH case, we find that for unconstrained CP phases both the correlations are allowed for all ranges of $\sin\theta_{34}$. Fig. 3.9 shows the scatter plot for the first correlation against $\sin\theta_{34}$. However, the overlapping vanishes for the first correlation when phases are constrained to $\gamma = \alpha = \delta_{13} = (180^0 - 225^0), \delta_{14} = \beta = (225^0 - 270^0), \delta_{24} = (180^0 - 210^0)$ and thus the texture is disallowed.

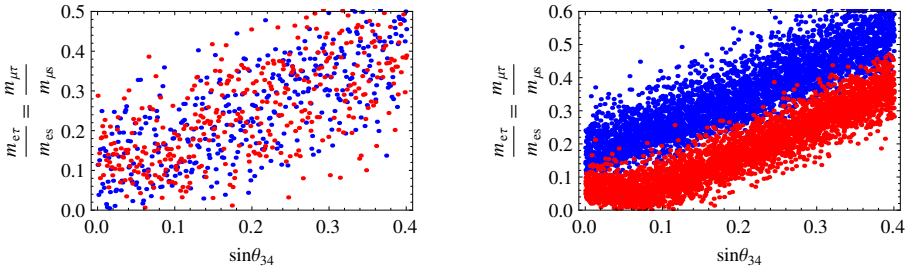

Fig. 3.9 Scatter plots for Eq. (3.27) where : ■ $\frac{m_{e\tau}}{m_{es}}$ and ■ $\frac{m_{\mu\tau}}{m_{\mu s}}$. The left and right plot is for unconstrained and constrained ranges ($\gamma = \alpha = \delta_{13} = (180^0 - 225^0), \delta_{14} = \beta = (225^0 - 270^0), \delta_{24} = (180^0 - 210^0)$) of CP phases respectively for IH spectrum (Texture B_3).

Texture B_4:

Normal Hierarchy: For the texture B_4, when CP phases are unconstrained, the second correlation is allowed for all ranges of the experimentally permissible range of $\sin\theta_{34}$ (left plot of Fig. 3.10). However, when CP phases are constrained to $\gamma = \beta = (320^0 - 360^0), \delta_{14} = (0 - 20^0), \delta_{13} = \alpha = (340^0 - 360^0), \delta_{24} = (180^0 - 200^0)$, the texture is not allowed (right

plot). For the first correlation we find that the allowed range of $\sin\theta_{34} > 0.02$ and $\sin\theta_{34} > 0.06$ respectively for unconstrained and constrained ranges of CP phases.

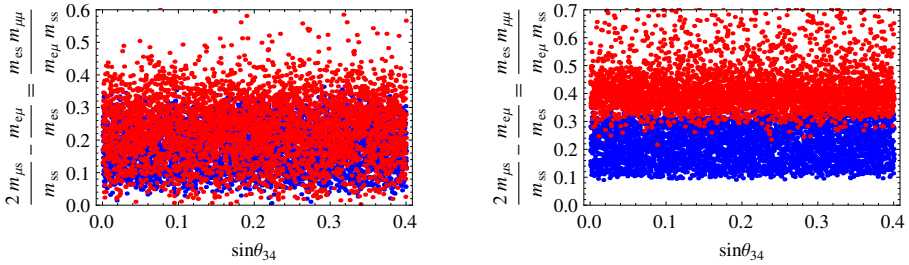

Fig. 3.10 Scatter plots for correlation in case (b) for unconstrained (left plot) and constrained (right plot) CP phases: $\gamma = \beta = (320^0 - 360^0), \delta_{14} = (0 - 20^0), \delta_{13} = \alpha = (340^0 - 360^0), \delta_{24} = (180^0 - 200^0)$ for NH spectrum where : ■ $2\left(\frac{m_{\mu s}}{m_{ss}}\right) - \frac{m_{e\mu}}{m_{es}}$, ■ $\frac{m_{\mu\mu}m_{es}}{m_{ss}m_{e\mu}}$ (Texture B_4).

Inverted Hierarchy: For IH it has been observed that the texture is allowed for values of $\sin\theta_{34} > 0.02$ (first correlation) and all values of $\sin\theta_{34} = (0 - 0.4)$ (second correlation) when CP phases are not constrained. When CP phases are constrained to $\gamma = (270^0 - 360^0), \delta_{14} = \delta_{24} = (0 - 30^0), \beta = \alpha = (315^0 - 360^0), \delta_{13} = (180^0 - 225^0)$, overlapping disappears for second correlation and the texture is not allowed. The phenomenology is similar to NH case, however, with different ranges of CP phases.

CP phase independent textures

Case III:

Scatter plots of the correlation in Eq. (3.29) generated by the combination in Eq. (3.28) (texture B_3) and case (c) (texture B_4) for both NH and IH are presented in Fig. 3.11. The correlation remains consistent for unconstrained CP phases as well as when CP phases are constrained to different ranges.

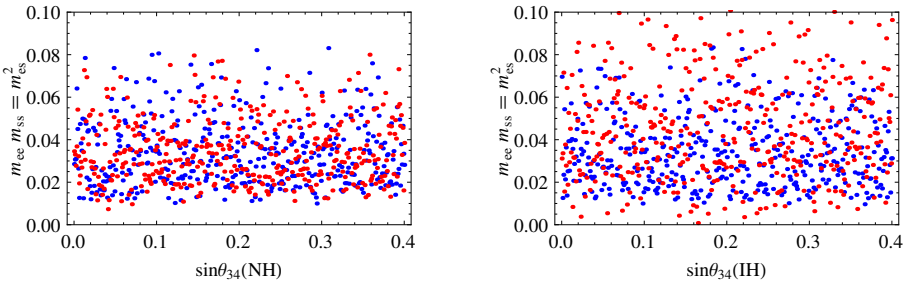

Fig. 3.11 Scatter plots of Eq. (3.29) for unconstrained CP phases for NH(left plot) and IH (right plot). Here ■ $m_{ee}m_{ss}$, ■ m_{es}^2 (Texture B_3 and B_4).

3.6.3 Class C

The class C consists of only one member, the texture C itself. It doesnot exhibit $P_{\mu\tau}$ symmetry with any other texture. The texture C has zeros in its $\mu\mu$ and $\tau\tau$ entry of the mass matrix. In (4+4) scheme of MES m_ν, there are a total of 6 combinations of M_D, M_R and M_S which can generate the texture C. There is one basic combination of M_D, M_R and M_S which can be transformed to the other five combinations via S_3 group symmetry in Eq. (3.8). The basic combination is presented in Eq. (3.30) that yields the correlation in Eq. (3.31) which is similar to the correlation in Eq. (3.25) for texture B_3. Hence the scatter plots for unconstrained and constrained CP phases are the same as shown in Fig. 3.7. The texture C, therefore, is allowed for all values of $\sin\theta_{34} > 0.02$ for unconstrained CP phases. If CP phases are constrained to $\gamma = \delta_{14} = \delta_{13} = (0 - 45^0), \beta = (180^0 - 225^0), \delta_{24} = \alpha = (0 - 30^0)$, the texture is allowed only for a small range of $\sin\theta_{34} \approx (0.02 - 0.16)$. This is the same for both NH and IH cases.

3.6.4 Class D

The class D consists of two textures D_1 and D_2 with zeros in their respective $\mu\mu, \mu\tau$, and $\mu\tau, \tau\tau$ entries. Both NH and IH are favored by these textures. Also D_1 and D_2 possess $P_{\mu\tau}$ symmetry according to Eq. (3.4). There are three basic combinations for each texture with respective correlation which behaves differently under unconstrained as well as constrained CP phases.

CP phase dependent textures

Case I:

The correlation $m_{\tau\tau}m_{ss} = m_{\tau s}^2$ in Eq. (3.33) for texture D_1 is similar to Eq. (3.10) and (3.23) for texture A_1 and A_2 respectively. The scatter plots for NH spectrum is therefore similar to Fig. 3.1. Similar phenomenology has been observed for IH case, the texture is not viable for the range of $\sin\theta_{34} \approx (0-0.06)$, when CP phases are unconstrained. But when the CP phases are restricted to the values of $\gamma = \delta_{14} = \beta = \alpha = (0-30^0), \delta_{13} = \delta_{24} = (0-45^0)$, the texture is allowed only for the range of $\sin\theta_{34} \approx (0.12-0.4)$.

Case II:

The basic combination in Eq. (3.34) (texture D_1) leads to the correlation in Eq. (3.35) and case (b) (texture D_2) leads to correlation which is $\mu-\tau$ symmetric to Eq. (3.35). Scatter plots are presented in Fig. 3.12 and 3.13.

Texture D_1:

Normal Hierarchy: The NH spectrum of the texture D_1 with the correlation in Eq. (3.35) is allowed for all ranges of $\sin\theta_{34}$ with or without constraining the CP phases and hence is CP phase independent texture.

Inverted Hierarchy: Fig. 3.12 shows that for unconstrained CP phases, the texture is allowed for all values of $\sin\theta_{34}$. However, the correlation is not consistent for small ranges of $\gamma = \delta_{24} = (0-10^0), \delta_{13} = \delta_{14} = (0-30^0), \alpha = (0-20^0)$ and β=unconstrained.

Texture D_2:

Normal Hierarchy: In the NH case, overlapping of the lhs and rhs of the correlation ceases for unconstrained CP phases and hence the texture is forbidden (Fig. 3.13, left plot).

Inverted Hierarchy: For IH the texture is allowed for $\sin\theta_{34} \approx (0-0.2)$ when CP phases are unconstrained (Fig. 3.13, right plot). However, the texture is not allowed when CP values

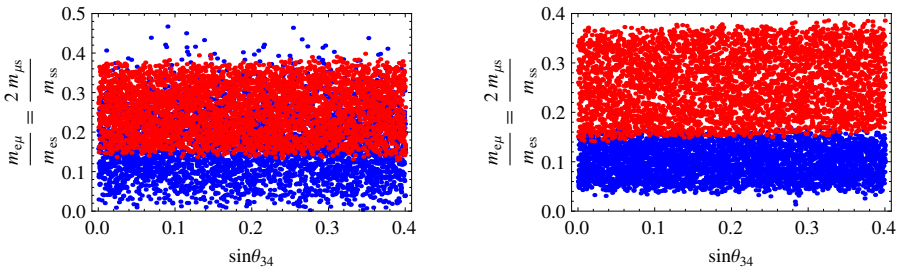

Fig. 3.12 Scatter plots for Eq. (3.35) with unconstrained (left) and constrained (right) CP phases :($\gamma = \delta_{24} = (0-10^0), \delta_{13} = \delta_{14} = (0-30^0), \alpha = (0-20^0)$, β=unconstrained) for IH spectrum. Here : $\frac{m_{e\mu}}{m_{es}}$, $2\left(\frac{m_{\mu s}}{m_{ss}}\right)$ (Texture D_1).

.

are constrained as $\gamma = \delta_{14} = (90^0 - 130^0), \alpha = \beta = \delta_{24} = (0-30^0), \delta_{13} = (45^0 - 90^0)$.

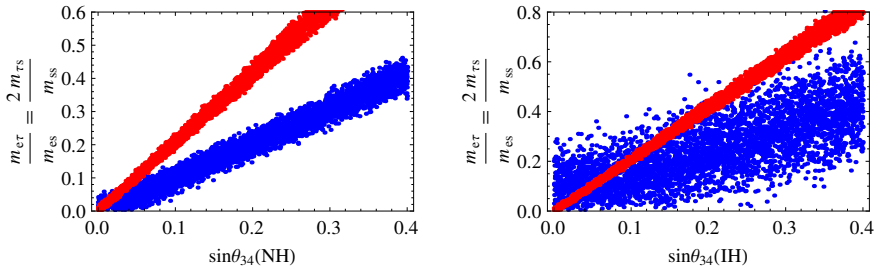

Fig. 3.13 Scatter plots for correlation in case (b) with unconstrained CP phases. The left and right plot is for NH and IH respectively. Here: $\frac{m_{e\tau}}{m_{es}}$, $2\left(\frac{m_{\tau s}}{m_{ss}}\right)$ (Texture D_2).

Case III:

The basic combination in case (c) for texture D_2 leads to the correlation which is $\mu - \tau$ symmetric to Eq. (3.37).

Normal Hierarchy: For NH case, the texture is not allowed as the overlapping between the left-hand side and right-hand side vanishes even when CP phases are kept unconstrained.

Inverted Hierarchy: For IH, it has been observed that for unconstrained CP phase the texture is allowed for $\sin\theta_{34} > 0.02$ in Fig. 3.14. But when constrained to different ranges of CP values $\gamma = \beta = (135^0 - 180^0), \delta_{14} = (315^0 - 360^0), \delta_{13} = (0-90^0), \alpha = (270^0 - 315^0), \delta_{24} = (180^0 - 225^0)$ the texture is not allowed.

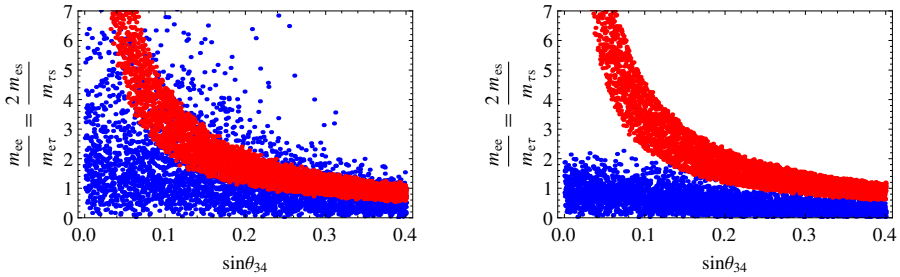

Fig. 3.14 Scatter plots for case (c) with unconstrained (left) and constrained CP phases (right) ($\gamma = \beta = (135^0 - 180^0), \delta_{14} = (315^0 - 360^0), \delta_{13} = (0 - 90^0), \alpha = (270^0 - 315^0), \delta_{24} = (180^0 - 225^0)$) for IH spectrum. Here: ■ $\frac{m_{ee}}{m_{e\tau}}$, ■ $2\left(\frac{m_{es}}{m_{\tau s}}\right)$ (Texture D_2).

CP phase independent textures

Case IV:

The correlation $m_{\mu\mu}m_{ss} = m_{\mu s}^2$ generated by the basic combination in case (a) for texture D_2 is similar to the correlation in Eq. (3.16) and (3.19) for the texture A_1,A_2 respectively. The correlation plots for NH are therefore similar to Fig. 3.5. For IH, the correlation plot shows similar phenomenology, whereby the texture remains as an allowed texture for any ranges of CP phases. The texture, therefore, is CP phase independent.

Case V:

The combination in Eq. (3.36) for the texture D_1 gives the correlation in Eq. (3.37). In this case also, we have seen that the texture is allowed for all ranges of CP values.

3.6.5 Class E

The first correlation in Eq. (3.39) for texture E_1 being similar to Eq. (3.35) exhibits CP phase independence. However, when the CP phases are unconstrained, the lhs and rhs of the second correlation for texture E_1 show very poor coincidence within 3σ range of experimental data (Fig. 3.15, right plot) . Thus, texture E_1 may be ruled out.

Similarly, for texture E_2, the second correlation shows poor overlapping (Fig. 3.15, left plot) and on the other hand the first correlation being similar to that of case (b) for texture D_2 is not consistent for NH spectrum. Thus, texture E_2 is also ruled out.

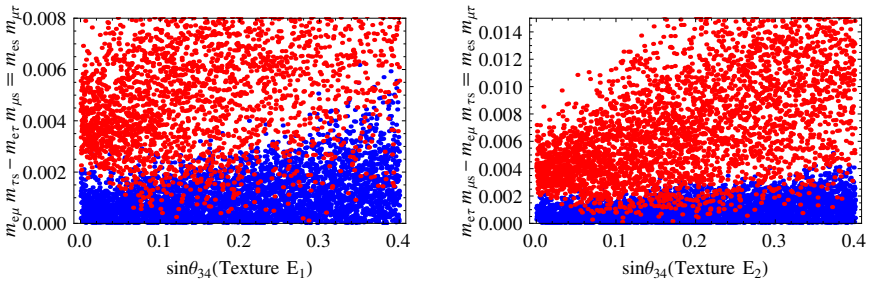

Fig. 3.15 Scatter plots for Eq. (3.39) with unconstrained CP phases. Here: ■ $m_{\tau s}m_{e\mu} - m_{e\tau}m_{\mu s}$, ■ $m_{\mu\tau}m_{es}$ (Texture E_1, left plot); ■ $m_{\mu s}m_{e\tau} - m_{e\mu}m_{\tau s}$, ■ $m_{\mu\tau}m_{es}$ (Texture E_2, right plot).

3.6.6 Class F

The class F consists of three textures F_1, F_2 and F_3 which can fit NH, IH and quasi-degenerate (QD) spectrum. However, MES mechanism restricts only to NH and IH spectrum. Also the textures F_2 and F_3 possess $P_{\mu\tau}$ symmetry between them. There exists one basic combination of M_D, M_R and M_S for each texture which leads to their specific correlations. The consistency of the correlations is verified in the same procedure:

Texture F_1: The correlation $m_{ee}m_{ss} = m_{es}^2$ in Eq. (3.41) is similar to Eq. (3.29) for texture B_3 which shows no variation to CP phases (Fig. 3.11). The second correlation in Eq. (3.41) shows variations with CP phases. This can be seen in Fig. 3.16.

Texture F_2: The combination in Eq. (3.42) leads to two correlations in Eq. (3.43). Phenomenology of the first correlation has already been presented in Fig. 3.5. The correlation is CP phase independent for both NH and IH spectrum. Scatter plots for the second correlation

are presented in Fig. 3.17.

Texture F_3: The first correlation of texture F_3 is similar to Eq. (3.10) which has already been plotted in Fig. 3.1. The second correlation remains unaffected with variation in CP phases which depicts that this texture is independent of CP phases.

For the textures F_1, F_2, F_3 one correlation shows CP dependency while the other is CP independent. Thus the textures shows hybrid nature of CP dependence

CP phase dependent textures

Texture F_1:

For both NH and IH spectrum, the texture is allowed for the range of $\sin\theta_{34} > 0.02$ when CP phases are unconstrained. However, when constrained to range $\gamma = \delta_{24} = (130^0 - 180^0), \delta_{14} = \beta = \delta_{13} = \alpha = (0 - 30^0)$ the texture is allowed for two ranges of $\sin\theta_{34} \approx (0 - 0.04)$ and $\approx (0.3 - 0.4)$ for NH case. Similarly for the constrained ranges: $\gamma = (210^0 - 225^0), \delta_{14} = (0 - 30^0), \beta = (120^0 - 150^0), \delta_{13} = (140^0 - 180^0), \alpha = \delta_{24} = (340^0 - 360^0)$ the texture is allowed for two ranges of $\sin\theta_{34} \approx (0.02 - 0.1)$ and $\approx (0.35 - 0.4)$ for IH case. Scatter plots for NH spectrum of texture F_1 are presented in Fig. 3.16.

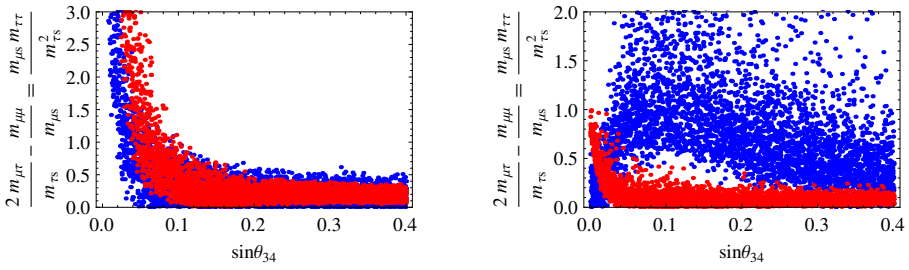

Fig. 3.16 Scatter plots for Eq. (3.41) (second correlation) with unconstrained (left) and constrained CP phases (right) ($\gamma = \delta_{24} = (130^0 - 180^0), \delta_{14} = \beta = \delta_{13} = \alpha = (0 - 30^0)$) for NH spectrum. Here: ■ $2\left(\frac{m_{\mu\tau}}{m_{\tau s}}\right) - \frac{m_{\mu\mu}}{m_{\mu s}}$, ■ $\frac{m_{\mu s}m_{\tau\tau}}{m_{\tau s}^2}$ (Texture F_1).

Texture F_2:

For NH spectrum with unconstrained CP phases, texture is not allowed for the range $\sin\theta_{34} \approx$

$(0-0.08)$. When CP phases are constrained to $\gamma = (315^0 - 360^0), \delta_{14} = (0-30^0), \beta = (270^0 - 315^0), \delta_{13} = (120^0 - 180^0), \alpha = (0-45^0), \delta_{24}$ =unconstrained, the overlapping ceases and the texture is not allowed.

Similar phenomenology has been observed for IH spectrum. When CP phases are unconstrained the texture is allowed through out the range $\sin\theta_{34} = (0-0.4)$. Again the texture is not viable when CP phases are constrained to the ranges of choice: $\gamma = (0-100^0), \delta_{14} = (0-30^0), \alpha = (0-60^0), \delta_{13} = \delta_{24} = \beta$ =unconstrained for IH spectrum. We present the scatter plots for NH in Fig. 3.17.

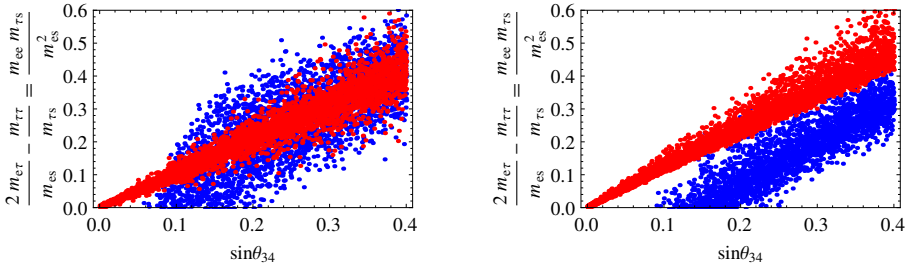

Fig. 3.17 Scatter plots for Eq. (3.43)(second correlation) with unconstrained(left) and constrained CP phases(right) $(\gamma = (315^0 - 360^0), \delta_{14} = (0-30^0), \beta = (270^0 - 315^0), \delta_{13} = (120^0 - 180^0), \alpha = (0-45^0), \delta_{24}$=unconstrained) for NH spectrum. Here: ■ $2\left(\frac{m_{e\tau}}{m_{es}}\right) - \frac{m_{\tau\tau}}{m_{\tau s}}$, ■ $\frac{m_{ee}m_{\tau s}}{m_{es}^2}$ (Texture F_2).

CP phase independent textures

The first correlation in Eq. (3.41)(Texture F_1), Eq. (3.43) (Texture F_2) and second correlation of texture F_3 doesnot respond to CP variations.

For convenience the results are summarized in Table 3.3 where we have presented the allowed range of $\sin\theta_{34}$ for each texture for both unconstrained and constrained CP phases. The constrained CP phases mentioned here are those values of CP phases for which the scatter plots for each textures are obtained. Texture B_3 with $M_D^{(9)}, M_S^{(1)}$; B_4 with $M_D^{(10)}, M_S^{(1)}$; E_1, E_2, F_1, F_2 and F_3 have 2 correlations each and thereby have two allowed ranges of $\sin\theta_{34}$.

Table 3.3 Results: Textures with different combinations of M_D, M_R, M_S allowed in the range of $\sin\theta_{34}$ are presented. Second column represents the basic combination of M_D and M_S ($M_R = M_R^c$ for all the cases). Textures not allowed by constrained CP phases are labelled as '*NA*'. Textures allowed for all values of $\sin\theta_{34}$ are labelled as '*All*'.

Texture	M_D, M_S	*No. of* correlations	Range of $\sin\theta_{34}$ when CP phases are			
			Unconstrained		Constrained	
			NH	IH	NH	IH
A_1	(1),(2)	1	> 0.08	-	> 0.12	-
	(3),(2)	1	$(0.06 - 0.2)$	-	$(0.12 - 0.22)$	-
	(5),(2)	1	*All*	-	*All*	-
A_2	(2),(2)	1	> 0.08	-	> 0.12	-
	(4),(2)	1	*All*	-	*NA*	-
	(6),(2)	1	*All*	-	*All*	-
B_3	(7),(1)	1	> 0.02	> 0.02	$(0.02 - 0.16)$	$(0.02 - 0.16)$
	(9),(1)	2	> 0.02	*All*	*NA*	*NA*
			> 0.08	*All*	*NA*	> 0.08
	(11),(2)	1	*All*	*All*	*All*	*All*
B_4	(8),(1)	1	> 0.02	> 0.02	$(0.02 - 0.16)$	$(0.02 - 0.16)$
	(10),(1)	2	> 0.04	> 0.02	> 0.02	> 0.04
			All	*All*	*NA*	*NA*
	(12),(2)	1	*All*	*All*	*All*	*All*
C	(23),(1)	1	> 0.02	> 0.02	$(0.02 - 0.16)$	$(0.02 - 0.16)$
D_1	(13),(2)	1	> 0.08	> 0.06	> 0.12	> 0.12
	(15),(1)	1	*All*	*All*	*All*	*NA*
	(17),(2)	1	*All*	*All*	*All*	*All*
D_2	(14),(2)	1	*All*	*All*	*All*	*All*
	(16),(1)	1	$(0 - 0.06)$	$(0 - 0.22)$	*NA*	$(0 - 0.02)$
	(18),(2)	1	*All*	> 0.02	*NA*	*NA*
E_1	(19),(1)	2	*All*	-	*All*	-
			> 0.04	-	*NA*	-
E_2	(20),(1)	2	$(0 - 0.06)$	-	*NA*	-
			> 0.04	-	*NA*	-
F_1	(24),(3)	2	*All*	*All*	*All*	*All*
			> 0.02	> 0.02	$(0 - 0.04)$	$(0.02 - 0.1)$
					$(0.3 - 0.4)$	$(0.35 - 0.4)$
F_2	(21),(3)	2	*All*	*All*	*All*	*All*
			> 0.08	*All*	*NA*	*NA*
F_3	(22),(3)	2	> 0.08	> 0.06	> 0.12	> 0.12
			All	*All*	*All*	*All*

The second correlation for texture F_1 allows two values of $\sin\theta_{34}$ viz. $(0-0.04),(0.3-0.4)$ for NH and $(0.02-0.1),(0.35-0.4)$ for IH (Constrained CP phases).

Phenomenologically allowed two-zero textures of ($A_1, A_2, B_1, B_2, B_3, B_4$ and C) in 3 active neutrino scenario [78] as well as in the 3+1 picture along with sterile sector [96] have been realized in MES with the corresponding consistent correlations excluding the textures B_1 and B_2 in the $m_\nu^{4\times4}$ not being matrices of rank 3. Again the two-zero textures ($D_1, D_2, E_1, E_2, F_1, F_2$ and F_3) which are phenomenologically allowed in $(3+1)$ picture but not in 3 active neutrino case, have also been realized in MES with consistent correlations.

3.7 Symmetry realization

Zeros of the fermion mass matrices which propagate as zeros of m_ν can be realized by an Abelian flavor symmetry Z_n with an extended scalar sector. The paper [100] employed the Abelian symmetries in the context of type-I seesaw mechanism to generate the zeros in the arbitrary entries of the fermion mass matrices. For symmetry realization of the viable textures in the context of MES mechanism under consideration, we adopt the method-2 of Ref. [100]. We are considering the charged lepton mass matrix M_l to be diagonal through out the chapter. We have found the Z_9 symmetry group suitable for realization of the textures. The Z_9 symmetry group consists of the elements $(1, \omega, \omega^2, \omega^3, \omega^4, \omega^5, \omega^6, \omega^7, \omega^8)$ with $\omega = e^{i\frac{2\pi}{9}}$ being the generator of the group. We present a representative case of the symmetry realization for texture A_1 case(a).

The transformations of the leptonic fields under Z_9 are considered as-

$$\begin{aligned}
\bar{D}_{e_L} &\to \omega^7 \bar{D}_{e_L}, \qquad e_R \to \omega^5 e_R, \qquad \nu_{e_R} \to \omega \nu_{e_R} \\
\bar{D}_{\mu_L} &\to \omega^5 \bar{D}_{\mu_L}, \qquad \mu_R \to \omega^4 \mu_R, \qquad \nu_{\mu_R} \to \omega^4 \nu_{\mu_R}. \\
\bar{D}_{\tau_L} &\to \omega \bar{D}_{\tau_L}, \qquad \tau_R \to \omega^6 \tau_R, \qquad \nu_{\tau_R} \to \omega^5 \nu_{\tau_R}
\end{aligned} \tag{3.44}$$

$\bar{D}_{j_L}$, l_R and ν_{k_R} represent the $SU(2)_L$ doublets, the RH $SU(2)_L$ singlets and the RH neutrino singlets respectively. The bilinears $\bar{D}_{j_L} l_R, \bar{D}_{j_L} \nu_{k_R}, \nu_{k_R}^T C^{-1} \nu_{j_R}$ are respectively relevant for M_l ,M_D and M_R and they transform as-

$$\bar{D}_{k_L} l_{j_R} = \begin{pmatrix} \omega^3 & \omega^2 & \omega^4 \\ \omega & 1 & \omega^2 \\ \omega^6 & \omega^5 & \omega^7 \end{pmatrix}, \quad \bar{D}_{k_L} \nu_{j_R} = \begin{pmatrix} \omega^8 & \omega^2 & \omega^3 \\ \omega^6 & 1 & \omega \\ \omega^2 & \omega^5 & \omega^6 \end{pmatrix}, \quad \nu_{k_R}^T C^{-1} \nu_{j_R} = \begin{pmatrix} \omega^2 & \omega^5 & \omega^6 \\ \omega^5 & \omega^8 & 1 \\ \omega^6 & 1 & \omega \end{pmatrix}. \tag{3.45}$$

We introduce three $SU(2)_L$ doublet Higgs (Φ_1, Φ_2, Φ_3) transforming under Z_9 as-

$$\Phi_1 \to \Phi_1\,, \qquad \Phi_2 \to \omega^6 \Phi_2\,, \qquad \Phi_3 \to \omega^2 \Phi_3. \tag{3.46}$$

The Z_9 invariant Yukawa Lagrangian becomes

$$\begin{aligned} -\mathscr{L} = Y_{11}^l \bar{D}_{e_L} \Phi_2 e_R + Y_{22}^l \bar{D}_{\mu_L} \Phi_1 \mu_R + Y_{33}^l \bar{D}_{\tau_L} \Phi_3 \tau_R + Y_{12}^D \bar{D}_{e_L} \tilde{\Phi}_3 \nu_{\mu_R} \\ + Y_{21}^D \bar{D}_{\mu_L} \tilde{\Phi}_2 \nu_{e_R} + Y_{22}^D \bar{D}_{\mu_L} \tilde{\Phi}_1 \nu_{\mu_R} + Y_{31}^D \bar{D}_{\tau_L} \tilde{\Phi}_3 \nu_{e_R} + Y_{33}^D \bar{D}_{\tau_L} \tilde{\Phi}_2 \nu_{\tau_R} + h.c.. \end{aligned} \tag{3.47}$$

The Higgs field after acquiring a vacuum expectation value gives the following form of M_l and M_D-

$$M_l = \begin{pmatrix} m_e & 0 & 0 \\ 0 & m_\mu & 0 \\ 0 & 0 & m_\tau \end{pmatrix}, \qquad M_D = \begin{pmatrix} 0 & b & 0 \\ d & e & 0 \\ g & 0 & l \end{pmatrix}. \tag{3.48}$$

We also introduce a scalar singlet χ for M_R transforming as-

$$\chi \to \omega^7 \chi_1, \tag{3.49}$$

which leads to the following form of M_R

$$M_R = \begin{pmatrix} A & 0 & 0 \\ 0 & 0 & E \\ 0 & E & 0 \end{pmatrix}. \tag{3.50}$$

To prevent bare mass term of the form $\bar{S^c}S$ as demanded by MES model, we transform the singlet field 'S' as -

$$S \to \omega S. \tag{3.51}$$

Two scalar singlets λ_1, λ_2 transforming as

$$\lambda_1 \to \omega^7 \lambda_1, \quad \lambda_2 \to \omega^3 \lambda_2, \tag{3.52}$$

leads to the following form of M_S

$$M_S = \begin{pmatrix} s_1 & 0 & s_3 \end{pmatrix}, \tag{3.53}$$

which are the required zero textures in Eq. (3.9) for texture A_1.

Symmetry realization of all the other S_3 symmetric textures follows a definite pattern. We take the element "A"of the S_3 group[2]

$$A = \begin{pmatrix} 0 & 1 & 0 \\ 1 & 0 & 0 \\ 0 & 0 & 1 \end{pmatrix}, \tag{3.54}$$

[2]Refer sec. 2.3 for details.

whereby there exist an interchange of the first and second column of the matrix "A". Following the similar pattern if we interchange the Z_9 transformation of the RH ν singlets of the basic combination in Eq. (3.44), that is, exchanging $\nu_{e_R} \Leftrightarrow \nu_{\mu_R}$ or

$$\nu_{e_R} \to \omega^4 \nu_{e_R}, \quad \nu_{\mu_R} \to \omega \nu_{\mu_R}, \tag{3.55}$$

meanwhile keeping the transformation of ν_{τ_R} as well as that of $\bar{D}_{j_L}$,l_R,Φ,χ and λ the same as that for the basic case in Eq. (3.44), (3.46), (3.49), (3.51) and (3.52) we arrive at the following set of matrices

$$M_D = \begin{pmatrix} a & 0 & 0 \\ d & e & 0 \\ 0 & h & l \end{pmatrix}, \quad M_R = M_R^a, \quad M_s = \begin{pmatrix} 0 & s_2 & s_3 \end{pmatrix}. \tag{3.56}$$

The above set of matrices in Eq.(3.56) are simply the transformations of the basic set of matrices in Eq.(3.48) and Eq.(3.50) by the element "A" of the S_3 group.

Similarly one can arrive at the symmetry realization of the other textures by simply interchanging the transformations of the RH neutrino singlets according to the interchange of the columns of the respective elements of S_3 group for each set of combinations of M_D, M_R and M_S, meanwhile keeping all other field transformations the same as the basic texture for each case.

Symmetry realization of all the basic combinations for each texture are listed in Table 3.4. For all the basic combinations the right handed Majorana neutrino mass matrix is the same, $M_R = M_R^c$. Therefore, in our work we keep the transformation of the right handed neutrino singlets ν_{k_R} to be the same as Eq. (3.44) for each basic texture. The transformations of the left handed $SU(2)_L$ doublets $\bar{D}_{j_L}$, right handed $SU(2)_L$ singlets l_R, Higgs doublets $\phi's$, singlet field 'S' and scalar singlets $\lambda's$ are presented in Table 3.4.

Table 3.4 Z_9 Symmetry realization of all the basic cases.

Texture	M_D, M_S	$\bar{\mathtt{D}}_{\mathtt{e}_L}, \bar{\mathtt{D}}_{\mu_L}, \bar{\mathtt{D}}_{\tau_L}$	$\mathtt{e}_R, \mu_R, \tau_R$	$\Phi'\mathtt{s}$	S	$\lambda' s$
$A_1(ii)$	$(3)(2)$	$\omega^5, \omega^7, \omega^4$	$\omega^4, 1, \omega^6$	$1, \omega^2, \omega^8$	ω	ω^7, ω^3
(iii)	$(5)(2)$	$\omega^2, 1, \omega^5$	$\omega, \omega^8, \omega^4$	$1, \omega^6, \omega$	ω	ω^7, ω^3
$A_2(i)$	$(2)(2)$	$\omega^7, \omega, \omega^5$	$\omega^5, \omega^6, \omega^4$	$1, \omega^6, \omega^2$	ω	ω^7, ω^3
(ii)	$(4)(2)$	$\omega^5, \omega^4, \omega^7$	$\omega^4, \omega^6, 1$	$1, \omega^8, \omega^2$	ω	ω^7, ω^3
(iii)	$(6)(2)$	$\omega^2, \omega^5, 1$	$\omega, \omega^4, \omega^8$	$1, \omega^6, \omega$	ω	ω^7, ω^3
$B_3(i)$	$(7)(1)$	$\omega^5, \omega^7, \omega$	$\omega^4, \omega^5, \omega^6$	$1, \omega^6, \omega^2$	ω^5	$1, \omega^8$
(ii)	$(9)(1)$	$\omega^7, \omega^5, \omega^4$	$1, \omega^4, \omega^6$	$1, \omega^2, \omega^8$	ω^5	$1, \omega^8$
(iii)	$(11)(2)$	$1, \omega^2, \omega^5$	$\omega^8, \omega, \omega^4$	$1, \omega, \omega^6$	ω	ω^7, ω^3
$B_4(i)$	$(8)(1)$	$\omega^5, \omega, \omega^7$	$\omega^4, \omega^6, \omega^5$	$1, \omega^3, \omega^7$	ω^5	$1, \omega^8$
(ii)	$(10)(1)$	$\omega^7, \omega^4, \omega^5$	$1, \omega^6, \omega^4$	$1, \omega^2, \omega^8$	ω^5	$1, \omega^8$
(iii)	$(12)(2)$	$1, \omega^5, \omega^2$	$\omega^8, \omega^4, \omega$	$1, \omega, \omega^6$	ω	ω^7, ω^3
C	$(23)(1)$	$\omega^5, \omega^6, \omega^4$	$\omega^7, \omega^2, \omega^5$	$1, \omega^6, \omega$	ω^5	$1, \omega^8$
$D_1(i)$	$(13)(2)$	$\omega^5, \omega^2, 1$	$\omega^4, \omega, \omega^8$	$1, \omega^6, \omega$	ω	ω^7, ω^3
(ii)	$(15)(1)$	$\omega^5, \omega^4, \omega^8$	$\omega^7, \omega^5, \omega^6$	$1, \omega^6, \omega^4$	ω^5	$1, \omega^8$
(iii)	$(17)(2)$	$\omega^4, \omega^5, \omega^8$	$\omega^6, \omega^4, \omega^7$	$1, \omega^8, \omega^3$	ω	ω^7, ω^3
$D_2(i)$	$(14)(2)$	$\omega^5, 1, \omega^2$	$\omega^4, \omega^8, \omega$	$1, \omega, \omega^6$	ω	ω^7, ω^3
(ii)	$(16)(1)$	$\omega^5, \omega^8, \omega^4$	$\omega^7, \omega^6, \omega^5$	$1, \omega^6, \omega^4$	ω^5	$1, \omega^8$
(iii)	$(18)(2)$	$\omega^4, \omega^8, \omega^5$	$\omega^6, \omega^7, \omega^4$	$1, \omega^8, \omega^3$	ω	ω^7, ω^3
E_1	$(19)(1)$	$\omega^6, \omega^4, \omega^5$	$\omega^2, \omega^5, \omega^7$	$1, \omega, \omega^6$	ω^5	$1, \omega^8$
E_2	$(20)(1)$	$\omega^6, \omega^5, \omega^4$	$\omega^2, \omega^7, \omega^5$	$1, \omega, \omega^6$	ω^5	$1, \omega^8$
F_1	$(24)(3)$	$1, \omega^5, \omega^4$	$1, \omega^3, \omega^6$	$1, \omega, \omega^8$	ω^5	$1, \omega^3$
F_2	$(21)(2)$	$\omega^5, 1, \omega^4$	$\omega^3, 1, \omega^6$	$1, \omega, \omega^8$	ω	ω^7, ω^3
F_3	$(22)(3)$	$\omega^5, \omega^4, 1$	$\omega^3, \omega^6, 1$	$1, \omega, \omega^8$	ω^5	$1, \omega^3$

3.8 Conclusion

In chapter 2, we explored the 3×3 neutrino mass matrix m_ν and found that no two-zero textures can be realized in the context of MES mechanism and predictive scenario. In this chapter we have realized the two-zero textures of (4×4) neutrino mass matrix m_ν in the context of MES mechanism under (4+4) scheme. No two-zero texture of M_S has been useful for realizing the desired textures. As demanded by MES mechanism, we consider only those two-zero textures, which are of rank 3 ($A_1, A_2, B_3, B_4, C, D_1, D_2, E_1, E_2, F_1, F_2, F_3$). On realizing the textures we have arrived at certain correlations for each texture which are then checked under recent neutrino oscillation data. In our analysis, we have considered the values

of $\sin\theta_{34} = (0.0 - 0.40)$. The viability of a texture has been checked under two conditions: (i) unconstrained $(0 - 360^0)$ Dirac and Majorana CP phases and (ii) constraining the CP phases to different segment of values.

In our analysis, it has been observed that when CP phases are unconstrained, recent neutrino oscillation data disfavours both the texture E_1, E_2 of class E, as its correlation remains inconsistent. Similarly, out of three combinations of M_D, M_R and M_S for texture D_2, two combinations in case (b) and case(c) for NH are ruled out. Our results of the numerical study of the textures have been summarised in the Table 3.3.

Under CP phase dependent textures, we have found there are a number of textures which is allowed for some ranges of $\sin\theta_{34}$ when CP remains unconstrained. However, when CP phases are constrained to different ranges the texture requires different ranges of $\sin\theta_{34}$ for its viability. This kind of behaviour have been observed for textures $A_1, A_2, B_3, B_4, C, D_1, D_2, F_1, F_3$ with combinations : $M_D, M_S = (1),(2),(3),(2);\ (2),(2);\ (7),(1);\ (8),(1);\ (23),(1);\ (13),(2);$ $(16),(1)$ (IH); $(24),(3)$ (second correlation) and $(22),(3)$ (first correlation) respectively. These textures are sensitive to CP phases in the sense that the different ranges of CP values demands different ranges of $\sin\theta_{34}$ for its viability (Table. 3.3).

Again for a number of cases it has been found that the texture is allowed for all ranges of $\sin\theta_{34}$ when CP phases are kept unconstrained, but has failed to survive when CP phases are constrained to certain ranges. Such behaviours are seen for texture A_2, B_3, B_4, D_1, F_2 with the combination of $M_D, M_S = (4),(2);\ (9),(1)$ (first correlation, IH); $(10),(1)$ (second correlation); $(15)(1)$ (IH) and $(21),(3)$ (second correlation, IH) respectively.

For certain textures we have seen that for unconstrained CP phases the correlations survived for a small range of $\sin\theta_{34}$. However, for constrained ranges of CP phases, it has been found that the correlations remain inconsistent and the textures are not allowed. This is evident from Table 3.3 for texture B_3, D_2, F_2 for $M_D, M_S = (9),(1)$ (NH); $(16),(1)$(NH) & $(18),(2)$ (IH) and $(21),(3)$ (second correlation, NH) respectively.

Interestingly we have found that there also exists certain textures where presence/absence of CP phases doesnot affect its viability and the texture remains as an allowed texture for all values of $\sin\theta_{34}$. This is evident from Table 3.3 for texture $A_1, A_2, B_3, B_4, D_1, D_2, F_1, F_2$ and F_3 for $M_D, M_S = (5),(2);\ (6),(2);\ (11),(2);\ (12),(2);\ (15),(1)$ (NH) & $(17),(2);\ (14),(2);\ (24),(3)$ (first correlation); $(21),(3)$ (first correlation) and $(22),(3)$ (second correlation) respectively.

The viable textures in our study are finally subjected to symmetry realization, where we have undertaken the Z_9 Abelian symmetry group. On realizing the textures we required : 3 Higgs' doublets (Φ) one of which is the SM Higgs transforming trivially under Z_9, scalar singlet χ for obtaining the four-zero texture of M_R and two singlets λ to realize the one-zero texture of M_S.

4

Phenomenology and group symmetry realization of fermion mass matrices for texture zeros of MES $m_\nu^{4\times4}$

4.1 Introduction

This chapter is based on our work in Ref. [125]. In this chapter, we shall explore the (5+3) and (6+2) predictive cases for realization of two-zero textures of MES $m_\nu^{4\times4}$ along

with one/two-zero textures of M_S. We also discuss the S_3 group permutation between the fermion mass matrices under MES mechanism which leads us to a minimum number of basic combination of M_D, M_R and M_S. $m_\nu^{4\times4}$ being a matrix is of rank 3 demands one of the mass eigenvalues to vanish and hence one has to consider one of the active neutrinos massless as vanishing sterile neutrino mass becomes trivial. Out of 15 viable two-zero textures, only 12 textures are of rank 3. We find that the (5+3) and (6+2) schemes are more constrained than the (4+4) scheme in chapter 3. Out of 12 two-zero textures of rank 3, only 9 textures can be realized within (5+3) scheme. Textures E_1, E_2 which were realizable under (4+4) scheme but ruled out by neutrino oscillation data, cannot be even realized under the (5+3) scheme. Moreover, none of the textures can be realized within the (6+2) scheme. It is to be noted that although there are a number of allowed three-zero [126] and four-zero [127] textures of $m_\nu^{4\times4}$, but they can never be realized in the MES mechanism, as M_D and M_R should remain as non-singular in MES.

Enforcing zeros in $m_\nu^{4\times4}$ under (5+3) gives a number of correlations among the neutrino mass matrix elements m_{ij}. We check the consistency of the correlations of each of the texture by plotting scatter plots with the current neutrino oscillation data. We also present the interplay of Dirac and Majorana CP phases on the viability of the textures. The coveted textures are then realized using Abelian flavor group symmetry Z_8 by extending the scalar sector of the SM.

The chapter is organized as follows: In Section 4.2 we present a brief discussion on MES mechanism. Section 4.3 includes a brief review on five-zero textures of M_D and three-zero textures of M_R along with zero textures of M_S. Also, S_3 permutation of fermion mass matrices under MES mechanism is presented in Sec. 4.3. In Section 4.4 we present the realization of the two-zero textures. In Section 4.5 we check the viability of the textures under recent neutrino oscillation data for both unconstrained and constrained CP phases. Symmetry

realization of the viable textures are presented in Section 4.6. Finally, we conclude in Section 4.7.

4.2 Minimal extended seesaw (MES) mechanism

In MES mechanism, Standard Model (SM) is extended with three right-handed neutrinos and one gauge singlet chiral field 'S' which leads to the full neutrino mass matrix in the basis (ν_L, ν_R^c, S^c) as

$$m_\nu^{7\times 7} = \begin{pmatrix} 0 & M_D & 0 \\ M_D^T & M_R & M_S^T \\ 0 & M_S & 0 \end{pmatrix}. \tag{4.1}$$

Block diagonalizing Eq. (4.1) and considering the hierarchy $M_R \gg M_S > M_D$, leads to the effective neutrino mass matrix in the basis (ν_L, S^c) as

$$m_\nu^{4\times 4} = -\begin{pmatrix} M_D M_R^{-1} M_D^T & M_D M_R^{-1} M_S^T \\ M_S (M_R^{-1})^T M_D^T & M_S M_R^{-1} M_S^T \end{pmatrix}. \tag{4.2}$$

The square matrix in Eq. (4.2) contains four light eigenstates corresponding to three active neutrinos and one sterile neutrino [68]. However, the determinant of the mass matrix $m_\nu^{4\times 4}$ is zero with the condition of M_D and M_R being non-singular. Thus the mass matrix $m_\nu^{4\times 4}$ is a matrix of rank 3. This implies that at least one of the active neutrino mass states remains as massless.

In our work, we shall consider the MES neutrino mass matrix in Eq. (4.2) to realize the two-zero textures of (4×4) neutrino mass matrix m_ν of rank 3. We find that only 9 out of 12 two-zero textures of rank 3 can be realized within the (5+3) scheme. Three textures C, E_1, E_2 under (5+3) scheme and any of the textures under (6+2) scheme cannot be realized in the

context of MES mechanism. In the paper [96] authors found the following: (i) the textures A_1 and A_2 belong to class A, which allow only the normal heirarchical mass patterns, (ii) the textures D_1, D_2 of class D allow both NH and IH mass orderings, (iii) the textures B_3, B_4 of class B and F_1, F_2, F_3 of class F favors all the three mass patterns: normal hierarchy (NH), inverted hierarchy (IH) and quasi degenerate(QD). As one of the mass eigenvalues of the matrix $m_\nu^{4\times4}$ in MES is massless, so the NH and IH mass patterns of the textures are allowed in MES but the QD textures are not allowed. The 9 two-zero textures of rank 3 are presented in Table 4.1.

Also, $P_{\mu\tau}$ symmetry [96] exists between the textures $A_1 - A_2$; $B_3 - B_4$; $D_1 - D_2$ and $F_2 - F_3$ according to Eq. (4.3). However, such a symmetry does not exist for the texture F_1.

$$B_4 = P_{\mu\tau}^T B_3 P_{\mu\tau}, \tag{4.3}$$

where

$$P_{\mu\tau} = \begin{pmatrix} 1 & 0 & 0 & 0 \\ 0 & 0 & 1 & 0 \\ 0 & 1 & 0 & 0 \\ 0 & 0 & 0 & 1 \end{pmatrix}. \tag{4.4}$$

4.3 (5+3) scheme and S_3 permutation group

3-zero textures of M_R:

The right-handed Majorana mass matrix M_R is symmetric with six independent entries and so we have ${}^6C_3 = 20$ possible 3-zero textures, out of which only 14 are non-singular (Table 4.2). However, according to Eq. (4.8) S_3 group permutations permit us to work with

Table 4.1 Viable two-zero textures [96] of rank 3. Here 'X' indicates the elements with non-zero entries.

A_1	A_2	B_3
$\begin{pmatrix} 0 & 0 & X & X \\ 0 & X & X & X \\ X & X & X & X \\ X & X & X & X \end{pmatrix}$	$\begin{pmatrix} 0 & X & 0 & X \\ X & X & X & X \\ 0 & X & X & X \\ X & X & X & X \end{pmatrix}$	$\begin{pmatrix} X & 0 & X & X \\ 0 & 0 & X & X \\ X & X & X & X \\ X & X & X & X \end{pmatrix}$
B_4	D_1	D_2
$\begin{pmatrix} X & X & 0 & X \\ X & X & X & X \\ 0 & X & 0 & X \\ X & X & X & X \end{pmatrix}$	$\begin{pmatrix} X & X & X & X \\ X & 0 & 0 & X \\ X & 0 & X & X \\ X & X & X & X \end{pmatrix}$	$\begin{pmatrix} X & X & X & X \\ X & X & 0 & X \\ X & 0 & 0 & X \\ X & X & X & X \end{pmatrix}$
F_1	F_2	F_3
$\begin{pmatrix} X & 0 & 0 & X \\ 0 & X & X & X \\ 0 & X & X & X \\ X & X & X & X \end{pmatrix}$	$\begin{pmatrix} X & 0 & X & X \\ 0 & X & 0 & X \\ X & 0 & X & X \\ X & X & X & X \end{pmatrix}$	$\begin{pmatrix} X & X & 0 & X \\ X & X & 0 & X \\ 0 & 0 & X & X \\ X & X & X & X \end{pmatrix}$

Table 4.2 All possible non-singular three-zero textures of M_R

$M_R^{(1)}$	$M_R^{(2)}$	$M_R^{(3)}$	$M_R^{(4)}$
$\begin{pmatrix} 0 & B & C \\ B & 0 & E \\ C & E & 0 \end{pmatrix}$	$\begin{pmatrix} 0 & 0 & C \\ 0 & D & E \\ C & E & 0 \end{pmatrix}$	$\begin{pmatrix} 0 & B & 0 \\ B & 0 & E \\ 0 & E & F \end{pmatrix}$	$\begin{pmatrix} 0 & 0 & C \\ 0 & D & 0 \\ C & 0 & F \end{pmatrix}$
$M_R^{(5)}$	$M_R^{(6)}$	$M_R^{(7)}$	$M_R^{(8)}$
$\begin{pmatrix} A & 0 & C \\ 0 & 0 & E \\ C & E & 0 \end{pmatrix}$	$\begin{pmatrix} A & 0 & 0 \\ 0 & 0 & E \\ 0 & E & F \end{pmatrix}$	$\begin{pmatrix} A & 0 & 0 \\ 0 & D & 0 \\ 0 & 0 & F \end{pmatrix}$	$\begin{pmatrix} A & 0 & 0 \\ 0 & D & E \\ 0 & E & 0 \end{pmatrix}$
$M_R^{(9)}$	$M_R^{(10)}$	$M_R^{(11)}$	$M_R^{(12)}$
$\begin{pmatrix} A & B & 0 \\ B & 0 & E \\ 0 & E & 0 \end{pmatrix}$	$\begin{pmatrix} A & B & 0 \\ B & 0 & 0 \\ 0 & 0 & F \end{pmatrix}$	$\begin{pmatrix} 0 & B & C \\ B & 0 & 0 \\ C & 0 & F \end{pmatrix}$	$\begin{pmatrix} 0 & B & C \\ B & D & 0 \\ C & 0 & 0 \end{pmatrix}$
$M_R^{(13)}$	$M_R^{(14)}$	-	-
$\begin{pmatrix} 0 & B & 0 \\ B & D & 0 \\ 0 & 0 & F \end{pmatrix}$	$\begin{pmatrix} A & 0 & C \\ 0 & D & 0 \\ C & 0 & 0 \end{pmatrix}$	-	-

only three basic 3-zero textures $M_R^{(7)}$, $M_R^{(9)}$ and $M_R^{(10)}$ as follows:

$$M_R^{(7)} = \begin{pmatrix} A & 0 & 0 \\ 0 & D & 0 \\ 0 & 0 & F \end{pmatrix}, \quad M_R^{(9)} = \begin{pmatrix} A & B & 0 \\ B & 0 & E \\ 0 & E & 0 \end{pmatrix}, \quad M_R^{(10)} = \begin{pmatrix} A & B & 0 \\ B & 0 & 0 \\ 0 & 0 & F \end{pmatrix}. \tag{4.5}$$

It is noted that $M_R^{(1)}$ is uninteresting as its inverse matrix consists of all entries non-zero. So zeros of m_ν can never be generated whatever the choice of M_D may be.

5-zero textures of M_D:

As the Dirac neutrino mass matrices are non-symmetric with all 9 elements being independent, there might be ${}^9C_5 = 126$ possible 5-zero textures. However, as the MES mechanism demands M_D to be non-singular, 90 such textures of M_D which have either row zero, column zero or block zero are not useful for being singular. The remaining 36 non-singular textures are viable. Again we find that 26 textures of M_D (Table 4.3) out of aforesaid 36 textures play the role in the basic combinations with M_R in Eq. (4.5) and M_S (Eq. (4.6),(4.7)) to reproduce the desired two-zero textures of $m_\nu^{4\times4}$. All other combinations can be obtained via S_3 transformations according to Eq. (4.8).

Zero textures of M_S:

The 1×3 row matrix $M_S = \begin{pmatrix} s_1 & s_2 & s_3 \end{pmatrix}$ can have two possible zero textures:

(1) One-zero textures:

$$M_S^{(1)} = \begin{pmatrix} 0 & s_2 & s_3 \end{pmatrix}, \quad M_S^{(2)} = \begin{pmatrix} s_1 & 0 & s_3 \end{pmatrix}, \quad M_S^{(3)} = \begin{pmatrix} s_1 & s_2 & 0 \end{pmatrix}. \tag{4.6}$$

Table 4.3 5-zero textures of M_D required in basic combinations.

$M_D^{(1)}$	$M_D^{(2)}$	$M_D^{(3)}$	$M_D^{(4)}$
$\begin{pmatrix} a & 0 & 0 \\ 0 & 0 & f \\ 0 & h & l \end{pmatrix}$	$\begin{pmatrix} 0 & b & 0 \\ d & 0 & 0 \\ g & 0 & l \end{pmatrix}$	$\begin{pmatrix} 0 & b & 0 \\ d & e & 0 \\ 0 & 0 & l \end{pmatrix}$	$\begin{pmatrix} 0 & b & 0 \\ d & 0 & 0 \\ 0 & h & l \end{pmatrix}$
$M_D^{(5)}$	$M_D^{(6)}$	$M_D^{(7)}$	$M_D^{(8)}$
$\begin{pmatrix} a & 0 & 0 \\ d & 0 & f \\ 0 & h & 0 \end{pmatrix}$	$\begin{pmatrix} a & 0 & 0 \\ 0 & e & f \\ 0 & 0 & l \end{pmatrix}$	$\begin{pmatrix} a & 0 & 0 \\ 0 & e & 0 \\ g & 0 & h \end{pmatrix}$	$\begin{pmatrix} 0 & b & 0 \\ d & 0 & f \\ g & 0 & 0 \end{pmatrix}$
$M_D^{(9)}$	$M_D^{(10)}$	$M_D^{(11)}$	$M_D^{(12)}$
$\begin{pmatrix} 0 & b & 0 \\ 0 & e & f \\ g & 0 & 0 \end{pmatrix}$	$\begin{pmatrix} 0 & b & 0 \\ 0 & 0 & f \\ g & h & 0 \end{pmatrix}$	$\begin{pmatrix} a & b & 0 \\ 0 & e & 0 \\ 0 & 0 & l \end{pmatrix}$	$\begin{pmatrix} a & 0 & c \\ d & 0 & 0 \\ 0 & h & 0 \end{pmatrix}$
$M_D^{(13)}$	$M_D^{(14)}$	$M_D^{(15)}$	$M_D^{(16)}$
$\begin{pmatrix} a & 0 & 0 \\ 0 & e & 0 \\ 0 & h & l \end{pmatrix}$	$\begin{pmatrix} 0 & 0 & c \\ d & 0 & 0 \\ 0 & h & l \end{pmatrix}$	$\begin{pmatrix} a & b & 0 \\ 0 & 0 & f \\ 0 & h & 0 \end{pmatrix}$	$\begin{pmatrix} a & 0 & c \\ 0 & e & 0 \\ g & 0 & 0 \end{pmatrix}$
$M_D^{(17)}$	$M_D^{(18)}$	$M_D^{(19)}$	$M_D^{(20)}$
$\begin{pmatrix} a & 0 & 0 \\ 0 & e & f \\ 0 & h & 0 \end{pmatrix}$	$\begin{pmatrix} 0 & 0 & c \\ 0 & e & f \\ g & 0 & 0 \end{pmatrix}$	$\begin{pmatrix} 0 & b & c \\ d & 0 & 0 \\ 0 & 0 & l \end{pmatrix}$	$\begin{pmatrix} 0 & b & c \\ 0 & e & 0 \\ g & 0 & 0 \end{pmatrix}$
$M_D^{(21)}$	$M_D^{(22)}$	$M_D^{(23)}$	$M_D^{(24)}$
$\begin{pmatrix} 0 & 0 & c \\ 0 & e & 0 \\ g & h & 0 \end{pmatrix}$	$\begin{pmatrix} 0 & b & c \\ d & 0 & 0 \\ 0 & h & 0 \end{pmatrix}$	$\begin{pmatrix} 0 & b & c \\ 0 & 0 & f \\ g & 0 & 0 \end{pmatrix}$	$\begin{pmatrix} 0 & 0 & c \\ d & e & 0 \\ 0 & h & 0 \end{pmatrix}$
$M_D^{(25)}$	$M_D^{(26)}$	-	-
$\begin{pmatrix} a & b & 0 \\ d & 0 & 0 \\ 0 & 0 & l \end{pmatrix}$	$\begin{pmatrix} a & 0 & 0 \\ d & e & 0 \\ 0 & 0 & l \end{pmatrix}$	-	-

(2) Two-zero textures:

$$M_S^{(4)} = \begin{pmatrix} s_1 & 0 & 0 \end{pmatrix}, \quad M_S^{(5)} = \begin{pmatrix} 0 & s_2 & 0 \end{pmatrix}, \quad M_S^{(6)} = \begin{pmatrix} 0 & 0 & s_3 \end{pmatrix}. \tag{4.7}$$

S_3 invariance under (5+3) scheme

We find that there exists S_3 transformations[1] (Eq. 4.8) between a number of combinations of M_D, M_R and M_S under the (5+3) scheme which keeps $m_\nu^{4\times4}$ in Eq. (4.2) invariant.

$$M_D \to M_D Z, \quad M_R \to Z^T M_R Z, \quad M_S \to M_S Z. \tag{4.8}$$

These transformations reduce the voluminous work of dealing with a large number of possible combinations of M_D, M_R and M_S under the (5+3) scheme to only a few basic combinations.

4.4 Realization of two-zero textures

We have 36 five-zero textures of M_D, 13 three-zero textures of M_R and 6 one and two-zero textures of M_S under (5+3) scheme mentioned in the previous section to realize the two-zero textures of $m_\nu^{4\times4}$ in MES. There exist 210 number of possible choices for the combinations of M_D, M_R and M_S being effective for realization of our desired two-zero textures of $m_\nu^{4\times4}$. Again the complexity of the texture study of these 210 combinations can further be reduced by S_3 transformations to only 42 basic combinations for each of which there are five S_3 transformations. The zeros of M_D, M_R and M_S propagate to $m_\nu^{4\times4}$ through MES formula in Eq.(4.2) which acquires a form of two zero texture. In this process we also obtain the correlations among some of the matrix elements m_{ij} with $i, j = e, \mu, \tau, s$ of $m_\nu^{4\times4}$ as results of the functional relations among the parameters of M_D, M_R and M_S. Again the question of viability of a two-zero texture is addressed by the consistency check of these correlations under the current neutrino data. This analysis shall follow in the next section. Now we present three representative cases out of 42 basic combinations for understanding of the problem:

[1]For details, refer section 2.3, chapter 2

Case I: The following basic combination of

$$M_R = M_R^{(9)}, \qquad M_D = M_D^{(11)}, \qquad M_S = M_S^{(6)}, \tag{4.9}$$

in Eq. (4.5), Table 4.3 and Eq. (4.7) respectively used in Eq. (4.2) leads to the form of $m_\nu^{4\times4}$ as

$$m_\nu^{(4\times4)} = \begin{pmatrix} \frac{a^2}{A} & 0 & \frac{(bA-aB)l}{AE} & \frac{(bA-aB)s_3}{AE} \\ 0 & 0 & \frac{el}{E} & \frac{es_3}{E} \\ \frac{(bA-aB)l}{AE} & \frac{el}{E} & \frac{l^2B^2}{AE^2} & \frac{ls_3B^2}{AE^2} \\ \frac{(bA-aB)s_3}{AE} & \frac{es_3}{E} & \frac{ls_3B^2}{AE^2} & \frac{s_3^2B^2}{AE^2} \end{pmatrix}, \tag{4.10}$$

This is the texture B_3 in Table 4.1 and reproduces the following correlation

$$\frac{m_{e\tau}}{m_{es}} = \frac{m_{\mu\tau}}{m_{\mu s}} = \frac{m_{\tau\tau}}{m_{\tau s}} = \frac{m_{\tau s}}{m_{ss}} = \sqrt{\frac{m_{\tau\tau}}{m_{ss}}}. \tag{4.11}$$

According to Eq. (4.8) S_3 transformations of the basic combination in Eq. (4.9) give a number of cases which generate textures B_3 with the same correlations as in Eq. (4.11). These are presented in Table 4.4.

Case II: Another basic combination of

$$M_R = M_R^{(9)}, \qquad M_D = M_D^{(21)}, \qquad M_S = M_S^{(6)}, \tag{4.12}$$

in Eq. (4.5), Table 4.3 and Eq. (4.7) respectively applied in Eq. (4.2) produces the following m_ν

$$m_\nu^{(4\times4)} = \begin{pmatrix} \frac{c^2B^2}{AE^2} & \frac{ce}{E} & \frac{(hA-gB)c}{AE} & \frac{cs_3AE^2}{B^2} \\ \frac{ce}{E} & 0 & 0 & \frac{es_3}{E} \\ \frac{(hA-gB)c}{AE} & 0 & \frac{g^2}{A} & \frac{(hA-gB)s_3}{AE} \\ \frac{cs_3AE^2}{B^2} & \frac{es_3}{E} & \frac{(hA-gB)s_3}{AE} & \frac{s_3^2B^2}{AE^2} \end{pmatrix}. \tag{4.13}$$

Table 4.4 S_3 symmetric textures of the basic combination in Eq. (4.9).

Case	M_D	M_R	M_S
(a)	$\begin{pmatrix} a & b & 0 \\ d & 0 & 0 \\ 0 & 0 & l \end{pmatrix}$	$M_R^{(12)}$	$M_S^{(6)}$
(b)	$\begin{pmatrix} 0 & b & c \\ 0 & e & 0 \\ g & 0 & 0 \end{pmatrix}$	$M_R^{(3)}$	$M_S^{(4)}$
(c)	$\begin{pmatrix} 0 & b & c \\ 0 & 0 & f \\ g & 0 & 0 \end{pmatrix}$	$M_R^{(2)}$	$M_S^{(5)}$
(d)	$\begin{pmatrix} a & 0 & c \\ d & 0 & 0 \\ 0 & h & 0 \end{pmatrix}$	$M_R^{(11)}$	$M_S^{(4)}$
(e)	$\begin{pmatrix} a & 0 & c \\ 0 & 0 & f \\ 0 & h & 0 \end{pmatrix}$	$M_R^{(5)}$	$M_S^{(4)}$

This is of the texture D_1 in Table 4.1 that leads to the following correlation

$$\frac{m_{ee}}{m_{es}} = \frac{m_{es}}{m_{ss}} = \frac{m_{e\tau}}{m_{\tau s}} = \frac{m_{e\mu}}{m_{\mu s}} = \sqrt{\frac{m_{ee}}{m_{ss}}}. \tag{4.14}$$

In this case also there exist another five combinations of M_D, M_R, M_S which are S_3 symmetric to Eq. (4.12) giving the same correlation as in Eq. (4.14) (Table 4.5).

Case III: The basic combination of

$$M_R^{(9)}, M_D^{(5)}, M_S^{(6)}, \tag{4.15}$$

in Eq. (4.5), Table 4.3 and Eq. (4.7) respectively used in Eq. (4.2) leads to the texture B_4 and it reproduces two correlations:

$$\frac{m_{e\mu}}{m_{\mu s}} = \frac{m_{ee}}{m_{es}}, \tag{4.16}$$

$$m_{ee} m_{ss} = m_{es}^2. \tag{4.17}$$

Table 4.5 S_3 symmetric textures of the basic combination in Eq. (4.12).

Case	M_D	M_R	M_S
(a)	$\begin{pmatrix} 0 & 0 & c \\ d & 0 & 0 \\ g & h & 0 \end{pmatrix}$	$M_R^{(12)}$	$M_S^{(6)}$
(b)	$\begin{pmatrix} a & 0 & 0 \\ 0 & e & 0 \\ 0 & h & l \end{pmatrix}$	$M_R^{(3)}$	$M_S^{(4)}$
(c)	$\begin{pmatrix} a & 0 & 0 \\ 0 & 0 & f \\ 0 & h & l \end{pmatrix}$	$M_R^{(2)}$	$M_S^{(5)}$
(d)	$\begin{pmatrix} 0 & b & 0 \\ d & 0 & 0 \\ g & 0 & l \end{pmatrix}$	$M_R^{(11)}$	$M_S^{(4)}$
(e)	$\begin{pmatrix} 0 & b & 0 \\ 0 & 0 & f \\ g & 0 & l \end{pmatrix}$	$M_R^{(5)}$	$M_S^{(4)}$

However, there exist another five combinations (Table 4.6) which are S_3 symmetric to Eq. (4.15) giving the same correlations as in Eq. (4.16) and (4.17).

The remaining 39 basic combinations of M_D, M_R and M_S along with their correlations are presented in Table 4.7 and 4.8. In our analysis we have found that some combinations are having multiple correlations.

4.5 Analysis of the textures under current neutrino data

In our analysis we calculate the mass matrix elements m_{ij} (Eq. (A.1)-(A.10), Appendix A) where $i, j = (e, \mu, \tau \text{ and } s)$ using the current neutrino data[2]. We have chosen the Dirac and the Majorana CP phases in the ranges $(0 - 2\pi)$. To check the viability of a texture, the left hand side (lhs) and the right hand side (rhs) of the correlation(s) of the texture are plotted against $\sin\theta_{34}$ which is has an upper bound < 0.4 [109]. In our analysis, we have taken its lower limit as 0. If there happens a reasonable overlapping of the plots of lhs and rhs, then

[2]Refer section 1.7, Chapter 1.

Table 4.6 S_3 symmetric textures of the basic combination in Eq. (4.15).

Case	M_D	M_R	M_S
(a)	$\begin{pmatrix} 0 & b & 0 \\ 0 & e & f \\ h & 0 & 0 \end{pmatrix}$	$M_R^{(12)}$	$M_S^{(6)}$
(b)	$\begin{pmatrix} 0 & 0 & c \\ d & 0 & f \\ 0 & h & 0 \end{pmatrix}$	$M_R^{(3)}$	$M_S^{(4)}$
(c)	$\begin{pmatrix} 0 & b & 0 \\ d & e & 0 \\ 0 & 0 & l \end{pmatrix}$	$M_R^{(2)}$	$M_S^{(5)}$
(d)	$\begin{pmatrix} 0 & 0 & c \\ 0 & e & f \\ g & 0 & 0 \end{pmatrix}$	$M_R^{(11)}$	$M_S^{(4)}$
(e)	$\begin{pmatrix} a & 0 & 0 \\ d & e & 0 \\ 0 & 0 & h \end{pmatrix}$	$M_R^{(5)}$	$M_S^{(4)}$

the texture is considered as an allowed texture within the overlapping range of $\sin\theta_{34}$. We also study the viability of the textures when the CP phases are constrained to some random ranges of values within $(0-2\pi)$. In analysis, we categorise them as (i) CP phase dependent textures and (ii) CP phase independent textures.

4.5.1 CP phase dependent textures

This category of textures is viable for unconstrained CP phases within the range $(0-2\pi)$, but there may exist some combinations of segmented ranges of CP phases δ_{13}, δ_{14}, δ_{24}, α, β and γ for which the overlapping of plots of lhs and rhs of the correlations of a texture may partially or completely disappear. Again if there are more than one correlations of a texture and at least one of them shows CP phase dependence, then such texture is also considered under this category. In the analysis, we find that with constrained CP phases, some of the textures are completely ruled out i.e., there are no overlapping of plots of lhs and rhs within the range of $\sin\theta_{34}$, while some of them retain their viability but in the squeezed range of

Table 4.7 Basic combination required for realization of the allowed two-zero textures: A_1, A_2, B_3, B_4 under (5+3) scheme and their respective correlations.

Texture	M_D, M_R, M_S	*Correlations*
$A_1(i)$	(1),(10),(1)	$m_{es}(m_{\tau s}m_{\mu\mu} - m_{\mu\tau}m_{\mu s}) = m_{e\tau}(m_{ss}m_{\mu\mu} - m_{\mu s}^2)$
(ii)	(2),(9),(6)	$(a)\quad \frac{m_{\mu\tau}}{m_{\mu\mu}} = \frac{m_{\tau s}}{m_{\mu s}}\,,\quad (b)\quad m_{\mu\mu}m_{ss} = m_{\mu s}^2$
(iii)	(3),(9),(6)	$\frac{m_{e\tau}}{m_{es}} = \frac{m_{\mu\tau}}{m_{\mu s}} = \frac{m_{\tau\tau}}{m_{\tau s}} = \frac{m_{\tau s}}{m_{ss}} = \sqrt{\frac{m_{\tau\tau}}{m_{ss}}}$
(iv)	(4),(9),(6)	$(a)\quad \frac{m_{e\tau}}{m_{es}} = \frac{m_{\mu\tau}}{m_{\mu s}}\,,\quad (b)\quad m_{\mu\mu}m_{ss} = m_{\mu s}^2$
(v)	(5),(10),(5)	$\frac{m_{e\tau}}{m_{es}} = \frac{m_{\mu\tau}}{m_{\mu s}} = \frac{m_{\tau\tau}}{m_{\tau s}} = \frac{m_{\tau s}}{m_{ss}} = \sqrt{\frac{m_{\tau\tau}}{m_{ss}}}$
$A_2(i)$	(6),(10),(1)	$m_{es}(m_{\mu s}m_{\tau\tau} - m_{\mu\tau}m_{\tau s}) = m_{e\mu}(m_{ss}m_{\tau\tau} - m_{\tau s}^2)$
(ii)	(8),(9),(6)	$(a)\quad \frac{m_{\mu\tau}}{m_{\tau\tau}} = \frac{m_{\mu s}}{m_{\tau s}}\,,\quad (b)\quad m_{\tau\tau}m_{ss} = m_{\tau s}^2$
(iii)	(7),(10),(5)	$\frac{m_{e\mu}}{m_{es}} = \frac{m_{\mu\tau}}{m_{\tau s}} = \frac{m_{\mu\mu}}{m_{\mu s}} = \frac{m_{\mu s}}{m_{ss}} = \sqrt{\frac{m_{\mu\mu}}{m_{ss}}}$
(iv)	(9),(9),(6)	$(a)\quad \frac{m_{e\mu}}{m_{es}} = \frac{m_{\mu\tau}}{m_{\tau s}}\,,\quad (b)\quad m_{\tau\tau}m_{ss} = m_{\tau s}^2$
(v)	(10),(9),(6)	$\frac{m_{e\mu}}{m_{es}} = \frac{m_{\mu\tau}}{m_{\tau s}} = \frac{m_{\mu\mu}}{m_{\mu s}} = \frac{m_{\mu s}}{m_{ss}} = \sqrt{\frac{m_{\mu\mu}}{m_{ss}}}$
$B_3(i)$	(11),(9),(6)	$\frac{m_{e\tau}}{m_{es}} = \frac{m_{\mu\tau}}{m_{\mu s}} = \frac{m_{\tau\tau}}{m_{\tau s}} = \frac{m_{\tau s}}{m_{ss}} = \sqrt{\frac{m_{\tau\tau}}{m_{ss}}}$
(ii)	(12),(10),(5)	$\frac{m_{e\tau}}{m_{es}} = \frac{m_{\mu\tau}}{m_{\mu s}} = \frac{m_{\tau\tau}}{m_{\tau s}} = \frac{m_{\tau s}}{m_{ss}} = \sqrt{\frac{m_{\tau\tau}}{m_{ss}}}$
(iii)	(7),(9),(6)	$(a)\quad \frac{m_{e\tau}}{m_{\tau s}} = \frac{m_{ee}}{m_{es}},\quad (b)\quad m_{ee}m_{ss} = m_{es}^2$
(iv)	(13),(9),(6)	$(a)\quad \frac{m_{e\tau}}{m_{es}} = \frac{m_{\mu\tau}}{m_{\mu s}},\quad (b)\quad m_{ee}m_{ss} = m_{es}^2$
(v)	(14),(10),(1)	$m_{ee}(m_{\tau\tau}m_{\mu s} - m_{\mu\tau}m_{\tau s}) = m_{e\tau}(m_{e\tau}m_{\mu s} - m_{es}m_{\mu\tau})$
$B_4(i)$	(15),(9),(6)	$\frac{m_{e\mu}}{m_{es}} = \frac{m_{\mu\tau}}{m_{\tau s}} = \frac{m_{\mu\mu}}{m_{\mu s}} = \frac{m_{\mu s}}{m_{ss}} = \sqrt{\frac{m_{\mu\mu}}{m_{ss}}}$
(ii)	(16),(10),(5)	$\frac{m_{e\mu}}{m_{es}} = \frac{m_{\mu\tau}}{m_{\tau s}} = \frac{m_{\mu\mu}}{m_{\mu s}} = \frac{m_{\mu s}}{m_{ss}} = \sqrt{\frac{m_{\mu\mu}}{m_{ss}}}$
(iii)	(5),(9),(6)	$(a)\quad \frac{m_{e\mu}}{m_{\mu s}} = \frac{m_{ee}}{m_{es}},\quad (b)\quad m_{ee}m_{ss} = m_{es}^2$
(iv)	(17),(9),(6)	$(a)\quad \frac{m_{e\mu}}{m_{es}} = \frac{m_{\mu\tau}}{m_{\tau s}},\quad (b)\quad m_{ee}m_{ss} = m_{es}^2$
(v)	(18),(10),(1)	$m_{ee}(m_{\mu\mu}m_{\tau s} - m_{\mu s}m_{\mu\tau}) = m_{e\mu}(m_{e\mu}m_{\tau s} - m_{es}m_{\mu\tau})$

$\sin\theta_{34}$. These two categories are referred to as Category (I) and Category (II) below.

Category (I): There is a class of textures which are allowed for some ranges of $\sin\theta_{34}$ when CP phases are unconstrained. However, for some ranges of CP phases, the textures cease to be viable within $\sin\theta_{34} = (0 - 0.4)$. This is illustrated as follows:

We pick up the case of the texture $B_3(i)$ in Table 4.7. Each of 5 expressions in the correlations for $B_3(i)$ in Eq. (4.11) separated by equality sign is plotted against $\sin\theta_{34}$ with

Table 4.8 Basic combination required for realization of the allowed two-zero textures: D_1, D_2, F_1, F_2, F_3 under (5+3) scheme and their respective correlations.

$D_1(i)$	(19),(10),(1)		$\frac{m_{ee}}{m_{e\tau}} - \frac{m_{e\tau}}{m_{\tau\tau}} = \left(\frac{m_{ee}}{m_{\tau\tau}} - \frac{m_{e\tau}^2}{m_{\tau\tau}^2}\right)\frac{l}{c}$
(ii)	(20),(9),(6)	(a)	$\frac{m_{e\mu}}{m_{\mu s}} = \frac{m_{e\tau}}{m_{\tau s}}$, (b) $m_{\tau\tau}m_{ss} = m_{\tau s}^2$
(iii)	(2),(10),(5)		$\frac{m_{e\mu}}{m_{\mu s}} = \frac{m_{e\tau}}{m_{\tau s}} = \sqrt{\frac{m_{ee}}{m_{ss}}}$
(iv)	(21),(9),(6)		$\frac{m_{ee}}{m_{es}} = \frac{m_{es}}{m_{ss}} = \frac{m_{e\tau}}{m_{\tau s}} = \frac{m_{e\mu}}{m_{\mu s}} = \sqrt{\frac{m_{ee}}{m_{ss}}}$
(v)	(16),(9),(6)	(a)	$\frac{m_{e\tau}}{m_{\tau s}} = \frac{m_{es}}{m_{ss}}$, (b) $m_{ee}m_{ss} = m_{es}^2$
$D_2(i)$	(23),(10),(1)		$\frac{m_{ee}}{m_{e\mu}} - \frac{m_{e\mu}}{m_{\mu\mu}} = \left(\frac{m_{ee}}{m_{\mu\mu}} - \frac{m_{e\mu}^2}{m_{\mu\mu}^2}\right)\frac{f}{c}$
(ii)	(22),(9),(6)	(a)	$\frac{m_{e\tau}}{m_{\tau s}} = \frac{m_{e\mu}}{m_{\mu s}}$, (b) $m_{\mu\mu}m_{ss} = m_{\mu s}^2$
(iii)	(8),(10),(5)		$\frac{m_{e\tau}}{m_{\tau s}} = \frac{m_{e\mu}}{m_{\mu s}} = \sqrt{\frac{m_{ee}}{m_{ss}}}$
(iv)	(24),(9),(6)		$\frac{m_{ee}}{m_{es}} = \frac{m_{es}}{m_{ss}} = \frac{m_{e\tau}}{m_{\tau s}} = \frac{m_{e\mu}}{m_{\mu s}} = \sqrt{\frac{m_{ee}}{m_{ss}}}$
(v)	(12),(9),(6)	(a)	$\frac{m_{e\mu}}{m_{\mu s}} = \frac{m_{es}}{m_{ss}}$, (b) $m_{ee}m_{ss} = m_{es}^2$
$F_1(i)$	(24),(10),(2)		$m_{ee}m_{ss} = m_{es}^2$
(ii)	(21),(10),(2)		$m_{ee}m_{ss} = m_{es}^2$
(iii)	(17),(7),(3)		$\frac{m_{\mu\tau}}{m_{\tau\tau}} = \frac{m_{\mu s}}{m_{\tau s}}$
(iv)	(13),(7),(3)		$\frac{m_{\mu\mu}}{m_{\mu\tau}} = \frac{m_{\mu s}}{m_{\tau s}}$
$F_2(i)$	(15),(10),(2)		$m_{\mu\mu}m_{ss} = m_{\mu s}^2$
(ii)	(10),(10),(2)		$m_{\mu\mu}m_{ss} = m_{\mu s}^2$
(iii)	(7),(7),(3)		$\frac{m_{ee}}{m_{es}} = \frac{m_{e\tau}}{m_{\tau s}}$
(iv)	(22),(7),(3)		$\frac{m_{e\tau}}{m_{es}} = \frac{m_{\tau\tau}}{m_{\tau s}}$
$F_3(i)$	(11),(10),(2)		$m_{\tau\tau}m_{ss} = m_{\tau s}^2$
(ii)	(3),(10),(2)		$m_{\tau\tau}m_{ss} = m_{\tau s}^2$
(iii)	(25),(7),(2)		$\frac{m_{ee}}{m_{es}} = \frac{m_{e\mu}}{m_{\mu s}}$
(iv)	(26),(7),(2)		$\frac{m_{e\mu}}{m_{es}} = \frac{m_{\mu\mu}}{m_{\mu s}}$

its range $(0-0.4)$ and using 3σ range of the parameters of neutrino data (Section1.7, Chapter 1) and expressions for m_{ij}, where $i,j = (e,\mu,\tau \text{ and } s)$ in the Appendix. The plots are done first without constraining CP phases i.e., for the whole range $(0-2\pi)$. Fig. 4.1 shows the correlation plot of Eq. (4.11) for Normal hierarchy (NH) case of texture $B_3(i)$.

From Fig. 4.1 it is evident that the correlation in Eq. (4.11) is consistent only for $\sin\theta_{34} > 0.1$. For values of $\sin\theta_{34} < 0.1$ the overlapping of the expressions $\frac{m_{\tau\tau}}{m_{\tau s}}$ and $\sqrt{\frac{m_{\tau\tau}}{m_{ss}}}$

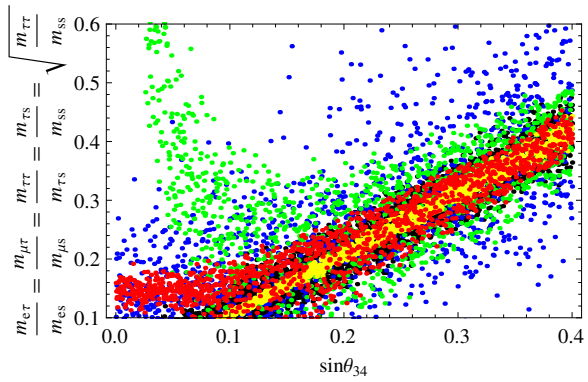

Fig. 4.1 Scatter plot for Eq. (4.11) against $\sin\theta_{34}$ for unconstrained CP phases (Texture $B_3(i)$, NH). ■ $\frac{m_{e\tau}}{m_{es}}$, ■ $\frac{m_{\mu\tau}}{m_{\mu s}}$, ■ $\frac{m_{\tau\tau}}{m_{\tau s}}$, ■ $\frac{m_{\tau s}}{m_{ss}}$, ■ $\sqrt{\frac{m_{\tau\tau}}{m_{ss}}}$.

ceases and the texture is not allowed within that range of $\sin\theta_{34}$. This predicts a lower bound on $\sin\theta_{34}$ to be 0.1.

Interestingly we observe that when CP phases are constrained to the ranges : $\delta_{13} = \delta_{14} = (45^0 - 90^0), \delta_{24} = (180^0 - 225^0), \alpha = (135^0 - 180^0), \beta = \gamma = (0 - 45^0)$, the overlapping completely vanishes and the texture is not allowed for any range of $\sin\theta_{34}$ (Fig. 4.2). This shows the fair play of CP phases in determining the viability of a texture. The constrained ranges of CP phases mentioned above are those ranges for which the texture is not allowed. However, with other choices of the ranges of CP phases, the texture shows different phenomenology and requires some other constrained ranges of $\sin\theta_{34}$ for its viability.

Fig. 4.1 and 4.2 for Eq. (4.11) show the correlation plots for NH pattern. The textures $A_1(iii),(v)$; $B_3(i),(ii)$ (Table 4.7) give the same correlations as in Eq. (4.11) and therefore, they show similar phenomenology. The textures which behave phenomenologically similarly are listed in Table 4.9. We also report their respective constrained ranges of CP phases that are not consistent with the allowed range of $\sin\theta_{34} = (0.0 - 0.4)$.

Category (II): Under this category of textures, they are allowed for a range of values of $\sin\theta_{34}$ without constraining CP phases. The special features of these textures are that they

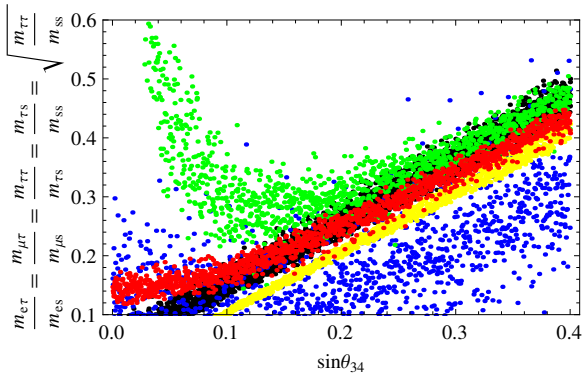

Fig. 4.2 Scatter plot for Eq. (4.11) against $\sin\theta_{34}$ for constrained ranges of CP phases: $\delta_{13}=\delta_{14}=(45^0-90^0), \delta_{24}=(180^0-225^0), \alpha=(135^0-180^0), \beta=\gamma=(0-45^0)$ (Texture $B_3(i)$, NH). ■ $\frac{m_{e\tau}}{m_{es}}$, ■ $\frac{m_{\mu\tau}}{m_{\mu s}}$, ■ $\frac{m_{\tau\tau}}{m_{\tau s}}$, ■ $\frac{m_{\tau s}}{m_{ss}}$, ■ $\sqrt{\frac{m_{\tau\tau}}{m_{ss}}}$.

Table 4.9 Constrained ranges of CP phases for textures under Category (I).

Texture	*Constrained CP phases*
$A_1(iv)(a)$(NH);$B_3(iv)(a)$(NH)	$\delta_{13}=(180^0-225^0)$, $\delta_{14}=\delta_{24}<30^0$, $\alpha=(0-90^0)$, $\beta=(315^0-360^0)$, $\gamma=(270^0-315^0)$.
$B_3(i),(ii)$ (IH)	$\delta_{13}=(45^0-90^0)$, $\delta_{14}=(90^0-135^0)$ $\delta_{24}=(0-45^0)$, $\alpha=(270^0-315^0)$, $\beta=\gamma=(0-30^0)$
$B_3(iii)(a)$(IH)	$\delta_{13}=\gamma=(0-90^0)$, $\delta_{14}=(90^0-130^0)$, $\delta_{24}=\beta=(0-180^0)$, $\alpha=(0-30^0)$.
$B_3(iv)(a)$(NH, IH)	$\gamma=\alpha=\delta_{13}=\gamma=(180^0-225^0)$, $\delta_{14}=\beta=(225^0-270^0)$, $\delta_{24}=(180^0-210^0)$.
$B_3(v)$(IH)	$\delta_{13}=\gamma=(0-90^0)$, $\alpha=(0-45^0)$, $\delta_{14}=\delta_{24}=(325^0-360^0)$, $\beta=(45^0-90^0)$
$B_4(iv)(a)$ (IH)	$\delta_{13}=(0-90^0)$, $\delta_{14}=(90^0-180^0)$, $\delta_{24}=(45^0-90^0)$ $\alpha=(0-45^0)$,$\beta=\gamma=(0-30^0)$
$D_1(ii)(a)$ (IH); $D_2(ii)(a)$ (IH)	$\delta_{13}=(0-45^0)$, $\delta_{14}=\delta_{24}=(0-30^0)$, $\alpha=(270^0-315^0)$, $\beta=(130^0-180^0)$, $\gamma=(225^0-270^0)$
$D_1(iii)$ (IH)	$\alpha=(0-45^0)$, $\delta_{13}=(45^0-90^0)$, $\delta_{14}=\beta=(0-30^0)$, $\delta_{24}=(315^0-360^0)$, $\gamma=(315^0-360^0)$
$D_1(iv)$ (IH)	$\delta_{13}=\delta_{24}=$ unconstrained, $\delta_{14}=(0-270^0)$, $\alpha=(0-90^0)$, $\beta=(0-90^0)$,$\gamma=(0-30^0)$
$D_2(v)(a)$ (IH)	$\delta_{13}=(45^0-90^0)$, $\beta=(0-45^0)$, $\alpha=\gamma=(180^0-225^0)$, $\delta_{14}=\delta_{24}=(0-45^0)$.
$F_3(iii)$ (IH)	$\delta_{24}=\alpha=(0-30^0)$, $\delta_{13}=(45^0-90^0)$, $\beta=(90^0-135^0)$, $\gamma=(270^0-315^0)$, $\delta_{14}=(315^0-360^0)$.

remain always viable within some ranges of $\sin\theta_{34}$ even if CP phases are constrained for any random segment of values.

We present the case of $D_1(iv)$ of this category. In the similar procedure of Category (I), we have plotted the Fig. 4.3. It shows the correlation plots of Eq. (4.14) for unconstrained (Plot (a)) and constrained (Plot (b)) CP phases (Normal Hierarchy). This figure tells that when CP phases are unconstrained, the texture is allowed for all ranges of $\sin\theta_{34} = (0.0 - 0.4)$. However, on constraining the phases to the ranges: $\delta_{13} = (45^0 - 90^0)$,$\delta_{14} = (270^0 - 315^0)$, δ_{24}= unconstrained, $\alpha = (180^0 - 225^0), \beta = (90^0 - 135^0), \gamma = (330^0 - 360^0)$, the allowed range of $\sin\theta_{34}$ has been found as $(0.06 - 0.40)$. On surveying the correlation with different ranges of CP phases, we find that the texture is always allowed at least for some values of $\sin\theta_{34}$, unlike the Category (I), and this is true even when CP phases are made to vanish.

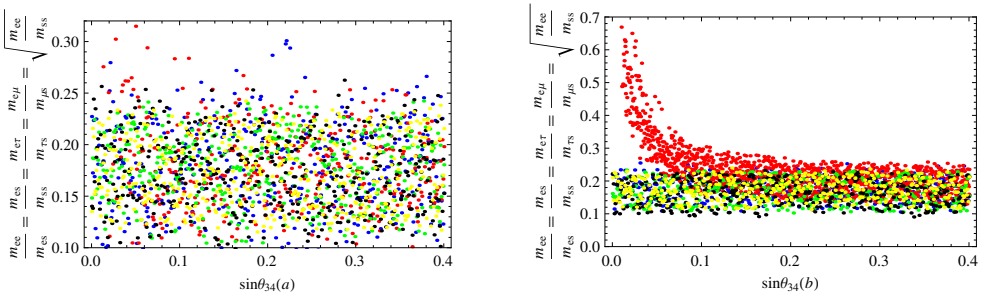

Fig. 4.3 Scatter plot for Eq. (4.14) against $\sin\theta_{34}$ for unconstrained (Plot (a)) and constrained (Plot (b)) ranges of CP phases: $\delta_{13} = (45^0 - 90^0), \delta_{14} = (270^0 - 315^0), \delta_{24}$ =unconstrained,$\alpha = (180^0 - 225^0), \beta = (90^0 - 135^0), \gamma = (330^0 - 360^0)$ (Texture $D_1(iv)$, NH). ■ $\frac{m_{ee}}{m_{es}}$, ■ $\frac{m_{es}}{m_{ss}}$, ■ $\frac{m_{e\tau}}{m_{\tau s}}$, ■ $\frac{m_{e\mu}}{m_{\mu s}}$, ■ $\sqrt{\frac{m_{ee}}{m_{ss}}}$.

Similar phenomenology has been observed for a number of textures. Table 4.10 shows the allowed ranges of $\sin\theta_{34}$ for each of those textures when CP phases are unconstrained and constrained to certain ranges. Their respective constrained ranges of CP phases are presented in Table 4.11.

Table 4.10 Allowed ranges of $\sin\theta_{34}$ for unconstrained and constrained CP phases for textures under Category (II). Here '*All*' represents that the texture allows all values of $\sin\theta_{34} = (0-0.4)$

Texture	Range of $\sin\theta_{34}$ for	
	Unconstrained CP phases	Constrained CP phases
$A_1(i)$ (NH)	$(0.04-0.4)$	$(0.08-0.4)$
$A_1(ii)(a)$ (NH)	>0.02	$(0.02-0.1)$
$A_2(ii)(a)$ (NH)	>0.08	>0.1
$A_2(ii)(b)$ (NH)	>0.08	>0.12
$A_2(iii),(v)$ (NH)	>0.04	>0.08
$A_2(iv)(a)$ (NH)	>0.04	>0.14
$B_3(iii)(a)$(NH)	*All*	>0.2
$B_3(v)$ (NH)	*All*	>0.06
$B_4(iv)(a)$(NH)	>0.02	<0.06
$B_4(iv)(a)$(IH)	>0.02	<0.18
$B_4(v)$(NH)	*All*	<0.14
$B_4(v)$(IH)	*All*	<0.06
$D_1(ii)(a)$(NH)	>0.02	>0.1
$D_1(iii)$(NH)	*All*	>0.04
$D_1(iv)$(NH)	*All*	>0.06
$D_1(v)(a)$(NH)	>0.02	>0.06
$D_1(v)(a)$(IH)	>0.06	>0.24
$F_1(iii)$(NH)	>0.04	>0.1
$F_1(iii)$(IH)	>0.04	>0.32
$F_1(iv)$(IH)	>0.04	$(0.02-0.06)$
$F_2(iv)$(NH)	>0.1	>0.14
$F_2(iv)$(IH)	>0.04	$(0.04-0.06)$

4.5.2 CP phase independent textures

The textures under this category are viable for all ranges of $\sin\theta_{34} = (0.0-0.4)$ while CP phases are (i) unconstrained, (ii) constrained to different ranges and (iii) even when CP phases are forced to be zero. For example the texture $B_4(iii)$ shows this type behaviour. The Fig. 4.4 is the scatter plot for Eq. (4.16) (NH) for unconstrained CP phases and the Fig. 4.5 the scatter plots for different ranges of CP phases. It is seen that the overlapping of the plots for the left-hand side and right-hand side of Eq. (4.16) maintains for the choice of different ranges of CP phases, thereby showing no dependence of CP phase change. Eq. (4.17) shows

Table 4.11 Constrained ranges of CP phases for textures under Category (II).

Texture	*Constrained CP phases*
$A_1(i)$ (NH)	$\delta_{13} = (45^0 - 90^0)$, $\delta_{14} = (180^0 - 225^0)$, $\delta_{24} = (0 - 45^0)$, $\alpha = \gamma = (225^0 - 270^0)$, $\beta = (135^0 - 180^0)$
$A_1(ii)(a)$ (NH)	$\delta_{13} = (135^0 - 180^0)$, $\delta_{14} = (325^0 - 360^0)$, $\beta = (0 - 30^0)$ $\delta_{24} = (90^0 - 135^0)$, $\alpha = (0 - 45^0)$, $\gamma = (120^0 - 160^0)$
$A_2(ii)(a)$ (NH)	$\delta_{13} = (135^0 - 180^0)$, $\alpha = \delta_{14} = (225^0 - 270^0)$, $\delta_{24} = (270^0 - 315^0)$, $\beta = (180^0 - 225^0), \gamma = (315^0 - 360^0)$
$A_2(ii)(b)$ (NH)	$\delta_{24} = (270^0 - 315^0)$, $\delta_{13} = (135^0 - 180^0)$, $\alpha = \delta_{14} = (225^0 - 270^0)$, $\beta = \delta_{24} = (0 - 45^0), \gamma = \delta_{13} = (0 - 30^0)$
$A_2(iii),(v)$ (NH)	$\alpha = (315^0 - 360^0)$, $\delta_{13} = (45^0 - 90^0)$,$\delta_{14} = (180^0 - 225^0)$ $\delta_{24} = (180^0 - 225^0)$, $\beta = \gamma = (0 - 30^0)$
$A_2(iv)(a)$ (NH)	$\gamma = (315^0 - 360^0)$, $\delta_{13} = (180^0 - 225^0)$, $\alpha = (135^0 - 180^0)$, $\delta_{14} = \delta_{24} = \beta = (0 - 30^0)$.
$B_3(iii)(a)$(NH)	$\delta_{13} = (160^0 - 200^0)$, $\alpha = (315^0 - 360^0)$, $\delta_{24} = (180^0 - 225^0)$, $\delta_{14} = \gamma = \beta = (330^0 - 360^0)$
$B_3(v)$ (NH)	$\delta_{13} = \delta_{24} < 45^0$, $\delta_{14} = (90^0 - 135^0)$, $\alpha = (180^0 - 225^0)$, $\beta = \gamma = (315^0 - 360^0)$
$B_4(iv)(a)$ (NH)	$\beta = \gamma = (315^0 - 360^0)$, $\delta_{14} = (0 - 20^0)$, $\alpha = \delta_{13} = (180^0 - 225^0)$, $\delta_{24} = (180^0 - 200^0)$
$B_4(iv)(a)$ (IH)	$\beta = \alpha = (315^0 - 360^0)$, $\delta_{14} = \delta_{24} = (0 - 30^0)$, $\gamma = (270^0 - 360^0)$,$\delta_{13} = (180^0 - 225^0)$
$B_4(v)$(NH)	$\beta = (225^0 - 270^0)$, $\delta_{13} < 45^0$, $\delta_{14} < 10^0$, $\delta_{24} = (45^0 - 90^0)$, $\alpha = \gamma = (30^0 - 45^0)$.
$B_4(v)$ (IH)	$\delta_{13} = (90^0 - 180^0)$, $\alpha = (0 - 45^0)$ $\delta_{14} = \delta_{24} = \gamma = \beta = (0 - 30^0)$
$D_1(ii)(a)$(NH)	$\alpha = (135^0 - 180^0)$, $\delta_{13} < 45^0$, $\delta_{14} < 30^0$, $\delta_{24} = (45^0 - 90^0)$, $\gamma = \beta = (315^0 - 360^0)$.
$D_1(iii)$(NH)	$\beta = (270^0 - 315^0)$, $\delta_{13} = \gamma = (135^0 - 180^0)$, $\delta_{14} < 30^0$, $\delta_{24} = (270^0 - 300^0)$, $\alpha = (315^0 - 360^0)$.
$D_1(iv)$(NH)	$\alpha = (180^0 - 225^0)$, $\delta_{13} = (45^0 - 90^0)$, $\delta_{14} = (270^0 - 315^0)$, $\gamma = (330^0 - 360^0)$, $\beta = (90^0 - 135^0)$.
$D_1(v)(a)$(NH)	$\alpha = (135^0 - 180^0)$, $\delta_{13} = (45^0 - 90^0)$, $\delta_{14} = (315^0 - 360^0)$, $\delta_{24} = \beta = (0 - 30^0)$, $\gamma = (225^0 - 315^0)$.
$D_1(v)(a)$(IH)	$\alpha = (90^0 - 135^0)$, $\delta_{13} = (45^0 - 90^0)$, $\delta_{14} = (180^0 - 225^0)$, $\delta_{24} = (225^0 - 270^0)$, $\beta = (0 - 30^0)$, $\gamma = (135^0 - 180^0)$.
$F_1(iii)$(NH)	$\delta_{13} = (135^0 - 180^0)$,$\gamma = (315^0 - 360^0)$, $\beta = (180^0 - 225^0)$, $\delta_{14} = \delta_{24} = (225^0 - 270^0)$, $\alpha = (270^0 - 315^0)$
$F_1(iii)$(IH)	$\delta_{13} = \delta_{24} = (0 - 45^0)$, $\delta_{14} = (180^0 - 225^0)$, $\gamma = \beta = \alpha = (0 - 30^0)$
$F_1(iv)$(IH)	$\delta_{13} = (0 - 90^0)$, $\delta_{14} = \gamma = (0 - 30^0)$, $\delta_{24} = \alpha = \beta = (0 - 45^0)$
$F_2(iv)$(NH)	$\delta_{13} = (0 - 45^0)$, $\delta_{14} = \delta_{24} = (0 - 30^0)$, $\gamma = \beta = \alpha = (315^0 - 360^0)$
$F_2(iv)$(IH)	$\delta_{13} = (45^0 - 90^0)$, $\delta_{14} = \beta = (0 - 30^0)$, $\delta_{24} = \alpha = (180^0 - 225^0)$,$\gamma = (0 - 45^0)$

similar phenomenology whereby the correlation remains insensitive to the variations of CP phases. We present the scatter plot for Eq. (4.17) in Fig. 4.6 for unconstrained CP phases. Thus such texture is CP phase independent texture. Similar phenomenology can be observed for the textures : $A_1(ii)(b), A_1(iv)(b); A_2(i); B_3(iii)(b),(iv)(b); B_4(iv)(b); D_1(v)(b);$ $D_2(ii)(b); D_2(v)(b)$.

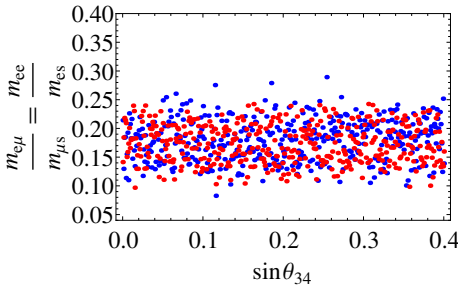

Fig. 4.4 Scatter plot for Eq. (4.16) against $\sin\theta_{34}$ for unconstrained CP phases (NH) (Texture $B_4(iii)(a)$). ■ $\frac{m_{e\mu}}{m_{\mu s}}$, ■ $\frac{m_{ee}}{m_{es}}$

4.6 Symmetry realization

For symmetry realization of texture zeros, the author of Ref. [100] discussed two methods of implementating Abelian symmetry group in the lepton sector with the seesaw mechanism and now we adopt the method-2 of the paper for symmetry realization of the textures studied here in the context of MES mechanism. We consider the charged lepton mass matrix M_l to be diagonal. For symmetry realization of all the viable textures we consider the Abelian symmetry group Z_8 which consists of the group elements

$$(1, \omega, \omega^2, \omega^3, \omega^4, \omega^5, \omega^6, \omega^7)$$

,

and $\omega = e^{\frac{i2\pi}{8}}$ is the generator of the group. We present the symmetry realization for texture $B_3(i)$ as a representative case.

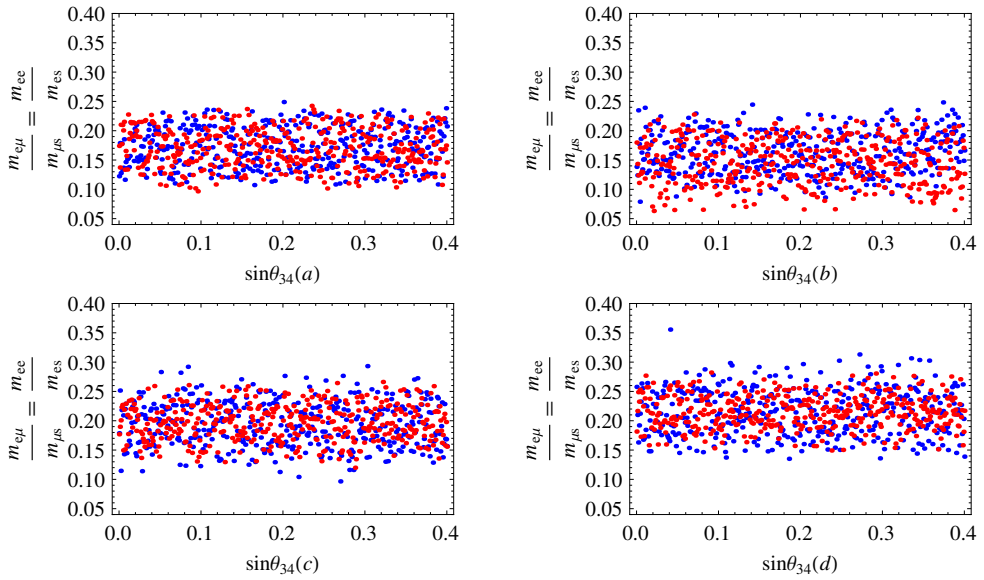

Fig. 4.5 Scatter plot for Eq. (4.16) against $\sin\theta_{34}$ for constrained ranges of CP phases: Plot (a) is for: $\delta_{13}=\beta=(45^0-90^0), \gamma<30^0, \delta_{14}=(90^0-130^0), \delta_{24}=(180^0-270^0), \alpha=(270^0-360^0)$. Plot (b) for: $\delta_{13}=\gamma=(135^0-180^0), \beta=(45^0-90^0), \delta_{14}=(180^0-225^0), \delta_{24}=(270^0-315^0), \alpha=(180^0-270^0)$. Plot (c) for: $\delta_{13}=\gamma=(135^0-180^0), \beta=(225^0-270^0), \delta_{14}=(180^0-225^0), \delta_{24}=(0-45^0), \alpha=(0-30^0)$. Plot (d) for: $\delta_{13}=(0-30^0), \gamma=(225^0-270^0), \beta=(135^0-180^0), \delta_{14}=(225^0-270^0), \delta_{24}=(45^0-90^0), \alpha=(90^0-135^0)$ (NH) (Texture $B_4(iii)(a)$). ■ $\frac{m_{e\mu}}{m_{\mu s}}$, ■ $\frac{m_{ee}}{m_{es}}$

We consider the leptonic fields to transform under Z_8 as-

$$\begin{aligned}
&\bar{D}_{e_L} \to \omega^7 \bar{D}_{e_L}, \qquad e_R \to \omega^3 e_R, \qquad \nu_{e_R} \to \omega \nu_{e_R} \\
&\bar{D}_{\mu_L} \to \omega \bar{D}_{\mu_L}, \qquad \mu_R \to \omega^2 \mu_R, \qquad \nu_{\mu_R} \to \omega^7 \nu_{\mu_R}. \\
&\bar{D}_{\tau_L} \to \omega^2 \bar{D}_{\tau_L}, \qquad \tau_R \to \omega^6 \tau_R, \qquad \nu_{\tau_R} \to \omega^3 \nu_{\tau_R}
\end{aligned} \tag{4.18}$$

Here, $\bar{D}_{j_L}$, l_R and ν_{k_R} represents the $SU(2)_L$ doublets, the RH $SU(2)_L$ singlets and the RH neutrino singlets respectively. The bilinears $\bar{D}_{j_L} l_R, \bar{D}_{j_L} \nu_{k_R}, \nu_{k_R}^T C^{-1} \nu_{j_R}$ relevant for M_l ,M_D

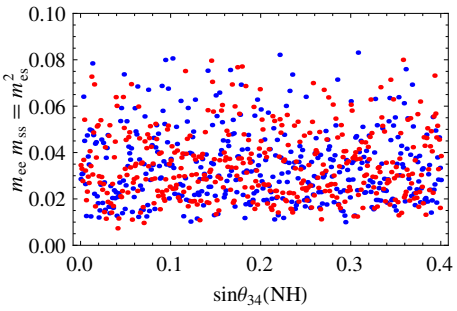

Fig. 4.6 Scatter plot for Eq. (4.17) against $\sin\theta_{34}$ for unconstrained CP phases (NH) (Texture $B_4(iii)(b)$). ■ $m_{ee}m_{ss}$, ■ m_{es}^2

and M_R respectively transforms as-

$$\bar{D}_{k_L} l_{j_R} = \begin{pmatrix} \omega^2 & \omega & \omega^5 \\ \omega^4 & \omega^3 & \omega^7 \\ \omega^5 & \omega^4 & 1 \end{pmatrix}, \quad \bar{D}_{k_L} \nu_{j_R} = \begin{pmatrix} 1 & \omega^6 & \omega^2 \\ \omega^2 & 1 & \omega^4 \\ \omega^3 & \omega & \omega^5 \end{pmatrix}, \nu_{k_R}^T C^{-1} \nu_{j_R} = \begin{pmatrix} \omega^2 & 1 & \omega^4 \\ 1 & \omega^6 & \omega^2 \\ \omega^4 & \omega^2 & \omega^6 \end{pmatrix}. \tag{4.19}$$

We consider three $SU(2)_L$ doublet Higgs (Φ_1, Φ_2, Φ_3) transforming under Z_8 as-

$$\Phi_1 \to \Phi_1\,, \qquad \Phi_2 \to \omega^6 \Phi_2\,, \qquad \Phi_3 \to \omega^5 \Phi_3. \tag{4.20}$$

The Z_8 invariant Yukawa Lagrangian becomes

$$\begin{aligned} -\mathscr{L} = {} & Y_{11}^l \bar{D}_{e_L} \Phi_2 e_R + Y_{22}^l \bar{D}_{\mu_L} \Phi_3 \mu_R + Y_{33}^l \bar{D}_{\tau_L} \Phi_1 \tau_R + Y_{11}^D \bar{D}_{e_L} \tilde{\Phi}_1 \nu_{\mu_R} \\ & + Y_{12}^D \bar{D}_{e_L} \tilde{\Phi}_2 \nu_{\mu_R} + Y_{22}^D \bar{D}_{\mu_L} \tilde{\Phi}_1 \nu_{\mu_R} + Y_{33}^D \bar{D}_{\tau_L} \tilde{\Phi}_3 \nu_{\tau_R} + h.c.. \end{aligned} \tag{4.21}$$

After acquiring a non-zero vacuum expectation value $<\phi_0>\neq 0$ by the Higgs fields, M_l and M_D takes the form

$$M_l = \begin{pmatrix} m_e & 0 & 0 \\ 0 & m_\mu & 0 \\ 0 & 0 & m_\tau \end{pmatrix}, \qquad M_D = \begin{pmatrix} a & b & 0 \\ 0 & e & 0 \\ 0 & 0 & l \end{pmatrix}. \tag{4.22}$$

We consider a scalar singlet χ transforming under Z_8 as-

$$\chi \to \omega^6 \chi_1, \tag{4.23}$$

which leads to the following form of M_R

$$M_R = \begin{pmatrix} A & B & 0 \\ B & 0 & E \\ 0 & E & 0 \end{pmatrix}. \tag{4.24}$$

We also consider transformation of the singlet chiral field 'S', so as to prevent bare mass term of the form $\bar{S^c}S$.

$$S \to \omega S. \tag{4.25}$$

Scalar singlet λ_1 transforming as

$$\lambda_1 \to \omega^4 \lambda_1, \tag{4.26}$$

leads to the following form of M_S

$$M_S = \begin{pmatrix} 0 & 0 & s_3 \end{pmatrix}, \tag{4.27}$$

which are the zero textures of the mass matrices in Eq. (4.9) for texture B_3.

It has been observed that, symmetry realization of the other five S_3 symmetric textures (Table 4.4) of the basic combination in Eq. (4.9) follows an interesting pattern. For instance, considering the textures in Case (b) of Table 4.4 obtained by tranforming the basic combination Eq. (4.9) by the element "B" of the S_3 group, where

$$B = \begin{pmatrix} 0 & 0 & 1 \\ 0 & 1 & 0 \\ 1 & 0 & 0 \end{pmatrix}, \tag{4.28}$$

There exist an interchange of the first and third column of the matrix "B". Following the similar pattern for symmetry realization of the textures of Case (b) (Table. 4.4), and interchanging only the Z_8 transformation of the right-handed neutrino singlets ($\nu_{e_R} \Leftrightarrow \nu_{\tau_R}$) of the basic combination in Eq. (4.18), that is

$$\nu_{e_R} \to \omega^3 \nu_{e_R}, \quad \nu_{\tau_R} \to \omega \nu_{\tau_R}, \tag{4.29}$$

meanwhile keeping the transformation of all the other fields, that is, ν_{μ_R}, $\bar{D}_{j_L}$,l_R,Φ,S,χ and λ same as that of basic combination, we arrive at the following set of matrices

$$M_D = \begin{pmatrix} 0 & b & c \\ 0 & e & 0 \\ g & 0 & 0 \end{pmatrix}, \quad M_R = M_R^{(3)}, \quad M_s^{(4)} = \begin{pmatrix} s_1 & 0 & 0 \end{pmatrix}. \tag{4.30}$$

Similarly, symmetry realization of all the other combinations (Table 4.4) can be obtained by simply interchanging the transformation of the RH neutrino singlets of the basic combination, according to the interchange of the columns of the elements of the S_3 group via which the

combinations are obtained.

In Table 4.12, we present the symmetry realization of all the basic combinations of M_D, M_R and M_S. The basic combinations for each textures involves only three basic forms of the right-handed Majorana mass matrix $M_R = M_R^{(7)}, M_R^{(9)}, M_R^{(10)}$. For those textures which are realized via $M_R^{(9)}$, we keep the Z_8 transformation of the RH neutrino singlets ν_{k_R} to be the same as in Eq. (4.18). The transformation for the scalar singlet χ, therefore, remains the same as in Eq. (4.23).

For textures obtained via $M_R^{(10)}$, we consider the transformation of the RH neutrino singlets and scalar singlet χ as:

$$\nu_{e_R} \to \omega \nu_{e_R}, \quad \nu_{\mu_R} \to \omega^7 \nu_{\mu_R}, \quad \nu_{\tau_R} \to \omega^5 \nu_{\tau_R}, \quad \chi \to \omega^6 \chi. \tag{4.31}$$

Textures that are realized by the diagonal RH Majorana mass matrix $M_R^{(7)}$, we consider the tranformations of ν_{kR}, χ as:

$$\nu_{e_R} \to \nu_{e_R}, \quad \nu_{\mu_R} \to \omega^4 \nu_{\mu_R}, \quad \nu_{\tau_R} \to \omega \nu_{\tau_R}, \quad \chi \to \omega^6 \chi. \tag{4.32}$$

Z_8 transformations of the left-handed $SU(2)_L$ doublets $\bar{D}_{j_L}$, right-handed $SU(2)_L$ singlets l_R, Higgs doublets ϕ, singlet field 'S' and scalar singlets λ of all the basic cases for each texture are presented in Table 4.12.

4.7 Conclusion

In this chapter have explored with (5+3) and (6+2) schemes of zeros in M_D and M_R along with required zero textures of M_S to realize the two-zero textures of $m_\nu^{4\times4}$ in the context

Table 4.12 Z_8 Symmetry realization of all the basic cases.

Texture	$\bar{\mathtt{D}}_{\mathtt{e}_L}, \bar{\mathtt{D}}_{\mu_L}, \bar{\mathtt{D}}_{\tau_L}$	$\mathtt{e}_R, \mu_R, \tau_R$	$\Phi'\mathtt{s}$	S	$\lambda' s$
$A_1(i)$	$\omega^7, \omega^3, \omega^2$	$\omega, \omega^4, \omega^7$	$1, \omega, \omega^7$	ω	$1, \omega^2$
(ii)	$\omega, \omega^2, \omega^5$	$\omega^4, \omega^6, \omega^5$	$1, \omega^3, \omega^6$	ω	ω^4
(iii)	$\omega, \omega^2, \omega^5$	$\omega^7, \omega^5, 1$	$1, \omega^3, \omega$	ω	ω^4
(iv)	$\omega^4, \omega^7, \omega$	$1, \omega^6, \omega^7$	$1, \omega^4, \omega^3$	ω	ω^4
(v)	$\omega^7, \omega^2, \omega$	$\omega, \omega^3, 1$	$1, \omega^3, \omega^7$	ω	1
$A_2(i)$	$\omega^7, \omega^2, \omega^3$	$\omega, \omega^7, \omega^4$	$1, \omega, \omega^7$	ω	$1, \omega^2$
(ii)	$\omega, \omega^5, \omega^2$	$\omega^4, \omega^5, \omega^6$	$1, \omega^3, \omega^6$	ω	ω^4
(iii)	$\omega, \omega^5, \omega^2$	$\omega^7, 1, \omega^5$	$1, \omega^3, \omega$	ω	ω^4
(iv)	$\omega^4, \omega, \omega^7$	$1, \omega^7, \omega^6$	$1, \omega^4, \omega^3$	ω	ω^4
(v)	$\omega^7, \omega, \omega^2$	$\omega, 1, \omega^3$	$1, \omega^3, \omega^7$	ω	1
$B_3(ii)$	$\omega^7, \omega^2, \omega$	$\omega, \omega^2, \omega^4$	$1, \omega^4, \omega^3$	ω	1
(iii)	$\omega^4, \omega, \omega^5$	$\omega^4, \omega^2, \omega^5$	$1, \omega^5, \omega^6$	ω	ω^4
(iv)	$\omega^7, \omega, \omega^4$	$\omega^6, \omega^7, \omega^5$	$1, \omega^7, \omega^3$	ω	ω^4
(v)	$\omega^3, \omega^7, \omega^2$	$\omega^4, \omega, \omega^7$	$1, \omega, \omega^7$	ω	$1, \omega^2$
$B_4(i)$	$\omega^7, \omega^2, \omega$	$\omega^3, \omega^6, \omega^2$	$1, \omega^6, \omega^5$	ω	ω^4
(ii)	$\omega^7, \omega, \omega^2$	$\omega, \omega^4, \omega^2$	$1, \omega^4, \omega^3$	ω	1
(iii)	$\omega^4, \omega^5, \omega$	$\omega^4, \omega^5, \omega^2$	$1, \omega^5, \omega^6$	ω	ω^4
(iv)	$\omega^7, \omega^4, \omega$	$\omega^6, \omega^5, \omega^7$	$1, \omega^2, \omega^3$	ω	ω^4
(v)	$\omega^3, \omega^2, \omega^7$	$\omega^4, \omega^7, \omega$	$1, \omega, \omega^7$	ω	$1, \omega^2$
$D_1(i)$	$\omega, \omega^5, 1$	$\omega, \omega^6, 1$	$1, \omega^6, \omega^5$	ω	$1, \omega^2$
(ii)	$\omega, 1, \omega^7$	$\omega^7, \omega^4, \omega^2$	$1, \omega^4, \omega^7$	ω	ω^4
(iii)	$\omega, \omega^7, \omega^2$	$1, \omega, \omega^3$	$1, \omega^7, \omega^3$	ω	1
(iv)	$\omega^5, \omega^2, \omega^7$	$\omega^2, \omega^4, \omega^7$	$1, \omega, \omega^2$	ω	ω^4
(v)	$\omega^5, \omega, 1$	$\omega^5, \omega^6, 1$	$1, \omega, \omega^6$	ω	ω^4
$D_2(i)$	$\omega, 1, \omega^5$	$\omega, 1, \omega^6$	$1, \omega^5, \omega^6$	ω	$1, \omega^2$
(ii)	$\omega, \omega^7, 1$	$\omega^7, \omega^2, \omega^4$	$1, \omega^4, \omega^7$	ω	ω^4
(iii)	$\omega, \omega^2, \omega^7$	$1, \omega^3, \omega$	$1, \omega^7, \omega^3$	ω	1
(iv)	$\omega^5, \omega^7, \omega^2$	$\omega^2, \omega^7, \omega^4$	$1, \omega, \omega^2$	ω	ω^4
(v)	$\omega^5, 1, \omega$	$\omega^5, 1, \omega^6$	$1, \omega, \omega^6$	ω	ω^4
$F_1(i)$	$\omega^3, \omega^7, \omega^2$	$\omega^4, \omega^3, \omega^6$	$1, \omega, \omega^6$	ω^3	$1, \omega^4$
(ii)	$\omega^3, \omega^2, \omega^7$	$\omega^4, \omega^6, \omega^3$	$1, \omega, \omega^6$	ω^3	$1, \omega^4$
(iii)	$1, \omega^4, \omega^2$	$\omega^2, \omega^4, \omega$	$1, \omega^6, \omega^5$	ω^4	$1, \omega^4$
(iv)	$1, \omega^4, \omega^2$	$\omega^2, \omega^4, \omega^3$	$1, \omega^6, \omega^3$	ω^4	$1, \omega^4$
$F_2(i)$	$\omega^7, \omega^3, \omega^2$	$\omega^3, \omega^4, \omega^6$	$1, \omega^6, \omega$	ω^3	$1, \omega^4$
(ii)	$\omega^2, \omega^5, \omega$	$\omega^4, \omega^2, \omega^7$	$1, \omega, \omega^2$	ω^3	$1, \omega^4$
(iii)	$\omega, \omega^3, 1$	$\omega^7, \omega^4, \omega$	$1, \omega, \omega^7$	ω^4	$1, \omega^4$
$F_3(i)$	$\omega^7, \omega^2, \omega^3$	$\omega^3, \omega^6, \omega^4$	$1, \omega^6, \omega$	ω^3	$1, \omega^4$
(ii)	$\omega^2, \omega, \omega^5$	$\omega^4, \omega^7, \omega^2$	$1, \omega^2, \omega$	ω^3	$1, \omega^4$
(iii)	$\omega, 1, \omega^3$	$\omega^7, \omega, \omega^4$	$1, \omega, \omega^7$	ω^4	$1, \omega^4$
(iv)	$\omega^4, \omega^6, \omega^5$	$\omega^4, \omega^5, \omega$	$1, \omega^2, \omega^5$	ω^4	$1, \omega^4$

of MES mechanism. We find that the (5+3) and (6+2) schemes are more constrained than the (4+4) scheme in chapter 3. It has been found that none of the two-zero textures can be realized within the (6+2) scheme. Out of 12 two-zero textures of rank 3, only 9 viable textures (A_1, A_2, B_3, B_4, D_1, D_2, F_1, F_2, F_3) can been realized in the (5+3) scheme. This is in contrast to the (4+4) scheme in chapter 3, where all the 12 two-zero textures have been realizable in the context of MES mechanism.

In realization of 9 two-zero textures under (5+3) scheme in MES mechanism we have found certain correlations among the elements of $m_\nu^{4\times4}$. The correlations have been scanned under recent neutrino oscillation data and plotted against $\sin\theta_{34}$ under two conditions (i) keeping the Dirac and Majorana CP phases unconstrained $(0-360^0)$ and (ii) constraining the CP phases to certain ranges. It has been observed that there are a number of textures whose viability gets affected when CP phases are constrained to certain ranges, while for a number of textures the phenomenology remains unchanged when CP phases are constrained to different segemnts of values or even when CP phases are made to be zero. Accordingly we have classified the textures under two categories (i) CP phase dependent textures and (ii) CP phase independent textures.

In our study we have seen that all textures are viable for some ranges of $\sin\theta_{34}$ when CP phases are unconstrained. However, for some selective ranges of CP phases, certain textures are not allowed within $\sin\theta_{34} = (0-0.4)$. For example, the phenomenology of the texture $B_3(i)$ is represented by the scatter plots for the correlations as shown in Fig. 4.1 and 4.2. Again, in case of the textures like $D_1(iv)$ of which the scatter plots are in (Fig. 4.3), it has been observed that for uncontrained CP phases, the texture is viable within the complete range of $\sin\theta_{34} = (0-0.4)$, while on constraining the CP phases, the allowed range of $\sin\theta_{34}$ have been squeezed to $(0.06-0.4)$. The texture has been found to be viable at least for some range of $\sin\theta_{34}$ whatever choice of the ranges of the CP phases. Viability of these

textures are affected on varying the CP phases and therefore they are categorised as CP phase dependent textures.

It has been observed that there are a number of textures which remain unaffected whether CP phases are unconstrained or constrained to different ranges. On surveying these textures for different segements of the six CP phases, it has been observed that the correlations are allowed for all values of $\sin\theta_{34}$. These textures are insensitive to variation of CP phases and are therefore categorised as CP phase independent textures. As a representative case realization of texture $B_4(iii)$ have been presented in section 4.5.2.

Also, it has been observed that there exist S_3 transformations of a given combination of M_D, M_R, M_S leading to a particular two-zero textures of $m_\nu^{4\times4}$ which give the same correlations. As a representative case Table 4.4 shows the combinations of M_D, M_R and M_S which are obtained via S_3 transformation from the basic combination in Eq. (4.9) for texture $B_3(i)$.

The viable textures have been finally realized by means of Z_8 Abelian flavor symmetry group by extending the SM with two additional Higgs doublet (Φ_2, Φ_3), scalar singlets χ and λ. We have presented the symmetry realization of texture $B_3(i)$ as a representative case. We have also demonstrated the symmetry realization of the Case (b) (Table 4.4) to show that all the S_3 symmetric textures also follow S_3 transformations of the fields of the basic combinations.

5

Conclusions

In this present work we have attempted to understand the issue of the LSND anomaly which has not been ruled out, but rather supported by MiniBooNE. The data indicate a fourth state of neutrino of about eV scale. The theoretical foundation of sterile neutrino is an important study from the point of view of physics. Again, eV scale sterile neutrinos may have significant implications in astrophysics and cosmology. The current promising neutrino models are built in the framework of seesaw mechanism beyond SM that can explain neutrino masses and mixing of three light active neutrinos barring the LSND discrepancy. The seesaw formula involves with 3×3 Dirac neutrino mass matrix, M_D of mass below electroweak scale, 200GeV, and 3×3 heavy right handed Majorana neutrino mass matrix,M_R of mass

scale about $\sim 10^{14}$ GeV. Again as per the experimental result of Z^0 decay width tells that the number of active neutrinos can never be more than 3. In this situation, natural objective of the work is to extend the type-I seesaw formula minimally to include an extra neutrino state which must not interact but mix only. In this purpose one right-handed gauge singlet chiral field 'S' represented by (1×3) row matrix M_S has been introduced to couple with the right-handed neutrinos. In construction of the extended version, a 7×7 m_ν matrix has been obtained which on block diagonalization with $M_R >> M_S > M_D$, we obtained a 4×4 neutrino mass matrix, and further block diagonalization with $M_S >> M_D$ has given us 3×3 neutrino mass matrix. So obtained m_ν (Eq. (1.30)) contains the type-I seesaw along with a second term having contribution from the sterile state. The MES has the following features: (i) M_D must possess its inverse along with M_R. (ii) MES neutrino mass matrices are of rank 3 which demand one of the active neutrino mass eigenvalues being zero. Hence only NH or IH mass orderings are allowed. (iii) An eV scale sterile neutrino has been a natural consequence without needing any tiny Yukawa coupling or mass scales.

The present study deals with the texture zeros of neutrino mass matrices in two folds: (i) of order 3×3 and (ii) of order 4×4 resulting from the zeros of (3×3) M_D, (3×3) M_R and M_S via MES. Texture zero models have been extensively studied in 3 active neutrino scenario as well as (3+1) scenario for two reasons; (i) enhancement of predictive power of models by reducing the number of free parameters and (ii) zero entries for underlying symmetries. In 3 neutrino scenario, there are a number of one and two-zero textures of m_ν which are compatible with oscillation data. Our motivation of work has been on realizing the zero textures of m_ν in presence of an additional eV-scale sterile neutrino i.e., (3+1) scenario. In order to realize zero textures of neutrino mass matrix m_ν we have considered the predictive scenario which leads to non-trivial fits for the lepton mixing (PMNS) matrix and/or for the neutrino mass ratios, whereby the sum of zeros of M_D and M_R is eight. In predictive scenario there are three possibilities: (4+4) scheme, (5+3) scheme and (6+2)

scheme, whereby the digits within the pair represent the zeros of M_D and M_R respectively. Also, we have considered suitable zero textures of M_S in the process. There are a number of possible combinations of M_D, M_R and M_S which cross over thousands in principle, but such complexity has been tackled with S_3 transformations demanding a set of only a small number of basic combinations. In the process we have obtained correlations among the matrix elements of neutrino mass matrices, which have been checked for their phenomenological consistencies under the current data of neutrino parameters of 3σ values by plotting scatter plots. Moreover, the zeros of the viable textures have been realized by the Abelian flavor symmetry group Z_N. The framework of the thesis has been elaborated in the **Chapter 1**.

In **Chapter 2**, we have systematically explored the one-zero and two-zero textures of three active neutrino sector, $m_\nu^{3\times3}$ in MES. To realize such texture zeros we have considered zeros of M_D, M_R and M_S as more fundamental, which finally propagate to the effective neutrino mass matrices $m_\nu^{3\times3}$ via MES. We explored all the three possible predictive scenarios: (4+4), (5+3) and (6+2) schemes along with suitable zero textures of M_S. In the (5+3) and (4+4) schemes one-zero textures of m_ν like $m_{e\tau}=0$, $m_{\tau\tau}=0$ and in (5+3) one more $m_{\mu\mu}=0$ have been generated. Interestingly the experimental compatibility allows the textures with $m_{\tau\tau}=0$ while the rest with $m_{e\tau}=0$, $m_{\mu\mu}=0$ are not allowed by recent neutrino oscillation data. Thus the presence of sterile state is more stringent for permissible textures. We have also observed that S_3 group transformations have reduced the tedious work for dealing with a large number of combinations to only a few basic combinations of M_D, M_R and M_S under each of (4+4) and (5+3) scheme.

Interestingly we have also found that in predictive scenario no two-zero textures, which are otherwise experimentally viable, survive in MES containing one sterile neutrino. Again all allowed one-zero textures of neutrino mass matrices represent only inverted hierarchical

neutrino models. So this is an important observation that $m_\nu^{3\times3}$ in MES framework favours only inverted hierarchy of mass ordering.

The viable textures in our study have been realized under Z_7 Abelian symmetry group by extending the Standard Model with 2 Higgs doublet (Φ_2, Φ_3) and 3 scalar singlets χ and λ_1, λ_2 to realize the viable structures of M_D, M_R and M_S respectively. We have also considered Z_7 transformations of the singlet chiral field 'S',in order to prevent bare mass term of 'S' as demanded by MES mechanism. We have also illustrated how other set of matrices obtained by permutation with the elements of S_3 can be realized by Z_7 by simply interchanging the transformations of the RH neutrino singlets from their respective basic cases.

In **Chapter 3** and **4** the phenomenology of MES mechanism for realization of two-zero textures in the 4×4 neutrino mass matrix has been explored. It is interesting to note that in chapter 2, two-zero textures in $m_\nu^{3\times3}$ in the framework of MES mechanism could not be realized under the predictive scenario. This motivated us to relook into the two-zero textures of m_ν in the 4×4 form in MES. As MES neutrino mass matrices must be of rank 3, so we have considered only those 12 textures $A_1, A_2, B_3, B_4, C, D_1, D_2, E_1, E_2, F_1, F_2, F_3$ which are of rank 3 for our study (Table 3.1), although we had 15 phenomenologically viable two zero textures of $m_\nu^{4\times4}$. We have undertaken the predictive scenarios of M_D and M_R: (4+4), (5+3) and (6+2) schemes for realization of two-zero textures of $m_\nu^{4\times4}$. Under (4+4) scheme (Chapter 3) we have found that two-zero texture of M_S cannot lead to non-zero sterile sector of $m_\nu^{4\times4}$. However, for (5+3) scheme (Chapter 4) both one and two-zero textures of M_S have been found to be useful for realizing the desired textures. The imposition of zeros has led us to certain correlations among the neutrino parameters for each texture. Then we have checked whether these correlations are consistent with the recent neutrino oscillation data.

Experimental bound on $\sin\theta_{34} < 0.4$. However, in our analysis, the lower limit has been taken to be 0. Furthermore, we have also considered the contributions of Dirac $(\delta_{13}, \delta_{14}, \delta_{24})$ and Majorana CP phases (α, β, γ) for the consistency test of the correlations of each texture. This is in contrast to the analysis of one-zero textures of $m_\nu^{3\times3}$ in chapter 2, whereby we considered a particular range of the CP phases (δ, α, β) for each texture. Although the methodology of chapter 3 and 4 are similar, the results are quite different.

In chapter 3 it has been observed that all the 12 two-zero textures can be realized under (4+4) scheme. However, we have found that for unconstrained CP phases $(0 - 360^0)$ the textures E_1, E_2 favoring normal hierarchy, are disfavored by neutrino oscillation data as its correlation remains inconsistent. Also, out of three combinations of M_D, M_R and M_S for texture D_2, two combinations for normal hierarchy are ruled out, as their respective correlations are inconsistent within 3σ range of oscillation data. This is an interestingly result that $m_\nu^{4\times4}$ in MES favors inverted hierarchy of mass ordering. Thus out of 12 only 10 textures are viable under (4+4) scheme

Again, in chapter 4 we have seen that (5+3) and (6+2) scheme are more constrained than that of the (4+4) scheme studied in chapter 3. Similar to chapter 2, here also the (6+2) scheme have not been found to be productive as none of the two-zero textures of $m_\nu^{4\times4}$ can be realized within MES. Again only 9 out of 12 textures are viable within the (5+3) scheme. Textures E_1, E_2 which were realizable in (4+4) scheme but ruled out by oscillation data, cannot be even realized within the (5+3) scheme. In addition we have seen that texture C which is an allowed texture within (4+4) scheme, cannot be realized with (5+3) scheme. Texture C has zeros in $\mu\mu$ and $\tau\tau$ entry of the mass matrix $m_\nu^{4\times4}$. Similarly for texture E_1 : $m_{ee} = 0; m_{\mu\mu} = 0$ and texture E_2: $m_{\mu\mu} = 0; m_{\tau\tau} = 0$. Thus, it is interesting to note that (5+3) scheme rules out those textures where both the zeros appears in the diagonal form of $m_\nu^{4\times4}$.

We have found that S_3 group transformations exist among different combinations of M_D, M_R and M_S which keep $m_\nu^{4\times4}$ invariant leading to same correlations and hence similar

phenomenology. We have tabulated the S_3 symmetric textures of (4+4) and (5+3) schemes in the respective chapters 3 and 4.

In both the schemes of (4+4) and (5+3) the viability of a texture have been checked by plotting the correlations against $\sin\theta_{34}$ under two conditions: (i) unconstrained $(0-360^0)$ Dirac and Majorana CP phases and (ii) constraining the CP phases to different segment of values. We have found that when CP phases are unconstrained, certain textures shows consistency in their correlation for all values of $\sin\theta_{34} = (0-0.4)$, while certain textures are allowed for some constrained ranges of $\sin\theta_{34}$.

We have found that there exist an interplay of Dirac and Majorana CP phases in determining the viability of a texture. Although experimental constraints on CP phases are yet not known, and remains unconstrained within 3σ range, still we have attempted to study the effect of the CP phases on the neutrino mass matrix $m_\nu^{4\times4}$. Accordingly we have checked the consistency of correlation(s) of each of the textures by considering smaller ranges of values of unknown CP phases from the complete range $(0-360^0)$. On constraining the CP phases we have observed that there are a number of textures for which (i) the allowed range of $\sin\theta_{34}$ gets squeezed to smaller values as compared to the values when CP phases are unconstrained (ii) the correlation(s) becomes inconsistent and the textures are not allowed for any range of $\sin\theta_{34} = (0-0.4)$ within that particular choice of combination of the six CP phases and (iii) viability of the textures remains unaffected for any choice of constrained ranges of CP phases and this holds even when CP phases are made to be zero. Textures of the type (i) and (ii) shows variation with the CP phases and are therefore categorised as CP phase dependent textures. On the other hand, textures of the type (iii) remains insensitive to the variations of CP phases and are therefore CP phase independent textures. Also, we have observed that most of the textures are allowed for values of $\sin\theta_{34} > 0$, thereby giving a lower limit on $\sin\theta_{34}$ which is still experimentally unknown.

Viable textures have been finally realized via Abelian flavor symmetry group Z_n by extending the Standard Model with some scalar fields. For (4+4) scheme we have undertaken Z_9 symmetry group while for (5+3) scheme textures are realized via the group Z_8. In symmetry realization of all the viable textures in chapter 2, 3 and 4, we have required three Higgs doublet (Φ_1, Φ_2, Φ_3) in which Φ_1 is the SM Higgs transforming trivially under the group Z_n. In addition we have required one singlet χ to realize the desired zero texture of M_R and one singlet λ to realize the two-zero textures of M_S while two scalars λ_1, λ_2 for realization of one-zero textures of M_S. Also we have given a transformation of the singlet chiral field 'S' so as to prevent bare mass term of the form $\bar{S}^c S$. We have also observed that symmetry realization of the other set of matrices obtained by permutation with the elements of S_3 can be achieved by simply interchanging the Z_9 field transformations of the RH neutrino singlets from their respective basic cases, meanwhile keeping the transformation of all the other fields unchanged.

Future scope of expansion of the present work:

It still awaits a watershed experimental proof for the existence of sterile neutrinos. Once it is established then some theoretical challenges shall stem before the theoretical particle physicists. The present study may be useful to understand light sterile states of neutrinos and may also be extended to the following which are not any way exhaustive lists:

• Our study has been confined to predictive scenario only, but there is a scope for study without restricting to predictive scenario as such study has been widely done in active neutrino scenario in literature.

• Neutrinoless double beta decay and leptonic CP violations may be explored.

• The M_R textures as predicted in our study may be used for study of baryogenesis in presence of sterile neutrinos as such study has been done in 3 active neutrino scenario to explain the matter-antimatter asymmetry in the early universe.

• The origin of zero textures have been studied in Z_N Abelian symmetry group but their study in other non-Abelian group symmetry realizations like A_4, S_N may be significant and useful.

• Study may be done on the scope for accommodating degenerate spectrum of active neutrino mass eigenvalues in presence of sterile state which is not allowed in the present form of MES as it demands one of the neutrinos being massless.

There are broader perspective of the thesis for expansion to address the following issues regarding sterile neutrinos:

• How many light sterile states of neutrinos may exist?

• What are the scales of sterile states: sub-eV, eV or KeV?

• What are the implications in astrophysics and cosmology particularly in structure formations?

• Are they candidates of dark matter?

Our understanding of the pertinent issues in neutrino physics is incomplete and so they require research in both theoretical and experimental perspectives for solutions.

References

[1] F. Reines and C. L. Cowan, Phys. Rev. **113**, 273 (1959).

[2] G. Danby, J. M. Gaillard, K. Goulianos, L.M.Lederman, N. Mistry, M. Schwartz and J. Steinberger, Phys. Rev. Lett. **9**, 36 (1962).

[3] K.Kodama et al., (DONUT Collaboration), Phys. Lett.**B 504**, 218 (2001), hep-ex/0012035.

[4] B T. Cleveland, T. Daily, R. Jr. Davis, J. R. Distel, K. Lande et al., Astrophys. J. **496**, 505, (1998).

[5] W. Hampel et al., (GALLEX Collaboration), Phys. Lett. B **447**, 127, (1999) .

[6] J. N. Abdurashitov et al., (SAGE Collaboration). J. Exp. Theor. Phys. **95**, 181,(2002) . astro-ph/0204245.

[7] Q.R. Ahmad et al., (SNO Collaboration), Phys. Rev. Lett. **89**, 011301, (2002),. nucl-ex/0204008.

[8] S. N. Ahmed et al., (SNO Collaboration), Phys. Rev. Lett. **92**, 181301, (2004). nucl-ex/0309004.

[9] Y. Fukuda et al., (Super-Kamiokande Collaboration), Phys. Rev. Lett. **81**, 1562 (1998). hep-ex/9807003.

[10] Y. Ashie et al., (Super-Kamiokande Collaboration), Phys. Rev. Lett. **93**, 101801, (2004).hep-ex/0404034.

[11] M. H. Ahn et al., (K2K Collaboration), Phys. Rev. Lett. **90**, 041801 (2003). hep-ex/0212007.

[12] M. Apollonio et al., (CHOOZ Collaboration), Eur. Phys. J.C **27**, (2003) 331; hep-ex/0301017.

[13] K. Eguchi et al. (KamLAND Collaboration), Phys. Rev. Lett. **90**, 021802 (2003).

[14] LSND: C. Athanassopoulos et al., Phys. Rev. Lett. **77**, 3082(1996).

[15] A. Aguilar et al., Phys. Rev. D **64**, 112007 (2001).

[16] MiniBooNE Collaboration: A. A. Aguilar-Arevalo et al., Phys. Rev. Lett. **110**, 161801 (2013).

[17] M. A. Acero, C. Giunti and M. Laveder, Phys. Rev. D **78**,073009 (2008).

[18] C. Giunti and M. Laveder, Phys. Rev. C **83**, 065504 (2011).

[19] G. Mention et al., Phys. Rev. D **83**, 073006 (2011).

[20] F. P. An et al., (Daya Bay Collaboration), Chin. Phys. C **37**, 011001 (2013); arXiv:1210.6327.

[21] F. P. An et al., Phys. Rev. D **90**, 071101, 2014.

[22] Y. Abe et al., (Double Chooz Collaboration), Phys. Rev. D **86**, 052008 (2012); arXiv:1207.6632.

[23] S.Abe et al.,(The KamLAND Collaboration) Phys. Rev. Lett. **100**, 221803; arxiv: 0801.4589[hep-ex] 2008.

[24] MINOS Collab. (P. Adamson et al.), Phys. Rev. Lett. **110**, 171801 (2013).

[25] D. S. Ayres et al., [NOvA Collaboration], hep-ex/0503053.

[26] J. K. Ahn et al., (RENO collaboration), Phys. Rev. Lett. **108**, 191802 (2012); arXiv:1204.0626.

[27] K. Abe et al., [T2K Collaboration], Phys. Rev. Lett. **107**, 041801 (2011); [arXiv:1106.2822 [hep-ex]].

[28] M. Agostini et al., [GERDA Collaboration], Phys. Rev. Lett. **111**, 122503 (2013) [arXiv:1307.4720 [nucl-ex]];

[29] K. H. Ackermann et al., [GERDA Collaboration], Eur. Phys. J. C **73**, 2330 (2013) [arXiv:1212.4067 [physics.ins-det]];

[30] M. Agostini et al., [GERDA Collaboration], Eur. Phys. J. C **74**, 2764 (2014); arXiv:1306.5084 [physics.ins-det];

[31] K. T. Knpfle [GERDA Collaboration],PoS TIPP 2014, **109** (2014).

[32] A. Gando et. al., [KamLAND-Zen Collaboration], Phys. Rev. Lett. **110**, 062502 (2013).

[33] M. Haag [KATRIN Collaboration], PoS EPS- **HEP 2013**, 518 (2013).

[34] C. Jarlskog, Phys. Rev. Lett. **55**, 1039 (1985).

[35] J. C. Pati and A. Salam, Phys. Rev. D **10** (1974) 275.

[36] R. N. Mohapatra and J. C. Pati, Phys. Rev. D **11** (1975) 566; G. Senjanovic and R. N. Mohapatra, Phys. Rev. D **12** (1975) 1502.

[37] R. N. Mohapatra and R. E. Marshak, Phys. Lett. B **91** (1980) 222; A. Davidson, Phys. Rev. D **20** (1979) 776.

[38] P. Minkowski, Phys. Lett. B **67** (1977) 421

[39] T. Yanagida, *Proceedings of the Workshop on the Unified Theory and the Baryon Number in the Universe* (O. Sawada and A.Sugamoto, eds), KEK Report, Tsukuba, Japan, 1979, p.95.

[40] M. Gell-Mann, P. Ramond, R. Slansky, *Complex spinors and unified theories in supergravity* (P. van Nieuwenhuizen and D.Z. Freedman, eds.), North-Holland, Amsterdam, 1979, p. 315.

[41] R. N. Mohapatra, G. Senjanovic, Phys. Rev. Lett. **44** (1980) 912.

[42] K. N. Abazajian et. al., arXiv:1204.5379 [hep-ph].

[43] G. Hinshaw et al.; arXiv:1212.5226.

[44] S. Schael et al., Phys. Rept. **427**, 257 (2006)[hep-ex/0509008].

[45] B. Armbruster et al., Phys. Rev. D **65**, 2002; arXiv: hep-ex/0203021 [hep-ex].

[46] P. Adamson et al., Phys. Rev. Lett., **107**, 011802, 2011; arXiv: 1104.3922 [hep-ex].

[47] MAntonello et al.; arXiv:1209.0122 [hep-ex].

[48] J. M. Conrad and M. H. Shaevitz, Phys. Rev. D **85**, 013017 (2012); arXiv:1106.5552 [hep-ex].

[49] P. A. R. Ade et al., [Planck Collaboration], A & A, **594**, A13, 2016; arXiv:1502.01589 [astro-ph.CO].

[50] NEOS Collab. (Y. J. Ko et al.), Phys. Rev. Lett. **118**, 121802 (2017).

[51] MiniBooNE Collab. (A. A. Aguilar-Arevalo et al.), Phys. Rev. Lett. **121**, 221801 (2018); arXiv:1805.12028 [hep-ex].

[52] P. W. Gorham et al., Phys. Rev. Lett. **117**, 071101 (2016).

[53] G. Y. Huang, Phys. Rev. D **98**, 043019 (2018).

[54] J. Kopp, M. Maltoni and T. Schwetz, Phys. Rev. Lett. **107**, 091801 (2011); arXiv:hep-ph/1103.4570.

[55] S. Joudaki, K. N. Abazajian and M. Kaplinghat; arXiv:astro-ph.CO/1208.4354.

[56] C. Giunti and M. Laveder, Phys. Rev. D **84** (2011)073008; arXiv:1107.1452.

[57] R. H. Cyburt et al., Astropart. Phys. **23**, 313 (2005), astro-ph/0408033.

[58] G. Mangano and P. D. Serpico, Phys. Lett. B **701**, 296 (2011); arXiv:1103.1261.

[59] J. J. Gomez-Cadenas and M. C. Gonzalez-Garcia, Z. Phys. C **71** (1996) 443-454, [hep-ph/9504246].

[60] S. Goswami, Phys. Rev. D **55** (1997) 2931-2949, [hep-ph/9507212].

[61] M. Maltoni et al., Phys. Rev. D **67** (2003) 013011, [hep-ph/0207227].

[62] J. Hamann et al., Phys. Rev. Lett. **105** (2010) 181301; arXiv:1006.5276.

[63] E. Giusarma et al., Phys. Rev. D **83** (2011) 115023; arXiv:1102.4774.

[64] S. Goswami and W. Rodejohann, Phys. Rev. D **73** (2006)113003 [hep-ph/0512234].

[65] J. Beringer et al., [Particle Data Group Collaboration], Phys. Rev. D **86**, 010001 (2012).

[66] A. Merle and V. Niro, JCAP 1107, **023** (2011).

[67] J. Barry, W. Rodejohann and H. Zhang, JHEP **1107**, 091 (2011).

[68] H. Zhang, Phys. Lett. B **714**, 262 (2012).

[69] J. Barry, W. Rodejohann and H. Zhang, JCAP 1201, **052** (2012).

[70] J. Heeck and H. Zhang, JHEP **1305**, 164 (2013).

[71] P. S. Bhupal Dev and A. Pilaftsis, Phys. Rev. D **87**, 053007(2013).

[72] Y. Zhang, X. Ji and R. N. Mohapatra, JHEP **1310**, 104 (2013).

[73] M. Frank and L. Selbuz, Phys. Rev. D **88**, 055003 (2013).

[74] D. Borah and R. Adhikari, Phys. Lett. B **729**, 143 (2014).

[75] R. Adhikari, D. Borah and E. Ma, Phys. Lett. B **755**, 414 (2016).

[76] A. Y. Smirnov and R.Zukanovich Funchal, Phys. Rev. D **74**, 013001 (2006), hep-ph/0603009.

[77] H. Fritzsch, Z. Z. Xing, Prog. Part. Nucl. Phys. **45** (2000) 1 [hep-ph/9912358].

[78] P. H. Frampton, S. L. Glashow, D. Marfatia, Phys. Lett. B **536** (2002) 79 [hep-ph/0201008].

[79] Z. Z. Xing, Phys. Lett. B **530** (2002) 159 [hep-ph/0201151]; Z. Z. Xing, Phys. Lett. B **539** (2002) 85 [hep-ph/0205032].

[80] R. R. Gautam, M. Singh, and M. Gupta, Phys. Rev. D **92** (2015) 013006; arXiv:1506.0486.

[81] L. Lavoura, Phys. Lett. B **609** (2005) 317 [hep-ph/0411232]; W. Grimus et. al, JHEP **0601** (2006) 110, hep-ph/0510326.

[82] L. Lavoura, J. Phys. G **42** (2015) 105004; arXiv:1502.0300.

[83] S. Choubey, W. Rodejohann and P. Roy, Nucl. Phys. B **808**, 272 (2009) [Erratum: ibid. 818, 136 (2009)]; arXiv:0807.4289.

[84] S. Goswami and A. Watanabe, Phys. Rev. D **79**, 033004 (2009); arXiv:0807.3438.

[85] R. N. Mohapatra and J. W. F. Valle, Phys. Rev. D **34** ,1642 (1986).

[86] J. Bernabeu, A. Santamaria, J. Vidal, A. Mendez and J. W. F. Valle, Phys. Lett. B **187**, 303 (1987).

[87] R. N. Mohapatra, Phys. Rev. Lett. **56**, 561 (1986).

[88] J. Schechter and J. W. F. Valle, Phys. Rev. D **25**, 774 (1982).

[89] J. Schechter and J. W. F. Valle, Phys. Rev. D **22**, 2227 (1980).

[90] S. Fraser, E. Ma and O. Popov, Phys. Lett. B **737**, 280(2014); arXiv:1408.4785 [hep-ph].

[91] B. Adhikary, A. Ghosal and P. Roy, Indian J. Phys.**88**, 979 (2014); arXiv:1311.6746 [hep-ph].

[92] Roopam Sinha, Rome Samanta, Ambar Ghoshal, Phys. Lett. B **759**, 206 (2016); arXiv: 1508.05227[hep-ph].

[93] Rome Samanta, Ambar Ghoshal; Nuc. Phys. B **911**; arXiv: 1507.02582 [hep-ph].

[94] Ambar Ghoshal, Rome Samanta, JHEP **05** 077 (2015); arXiv: 1501.00916.

[95] Monojit Ghosh et al., Phys. Rev. D **88** (2013) 3, 033009; arXiv:1305.0180 [hep-ph].

[96] M. Ghosh, S. Goswami and S. Gupta, JHEP **1304** (2013) 103 ; arXiv:1211.0118 [hep-ph].

[97] N. Nath et al., JHEP **03** (2017) 075; arXiv:1610.09090.

[98] M. Patgiri, P. Kumar, D. Sarma, Int. J. Mod.Phys. A, **32**, 27 (2017) 1750168.

[99] M. Patgiri and P. Kumar, Int. J. Mod.Phys. A, **34**, 11 (2019) 1950059.

[100] Walter Grimus, *Neutrino mass matrices, texture zeros, and family symmetries*, Talk presented at HEP2005, 2005, Lisbon, Portugal; arXiv:hep-ph/0511078 (2005).

[101] W. Grimus et al., Eur. Phys. J. C **36** (2004) 227 [hep-ph/0405016].

[102] R. Gonzalez Felipe and H. Serodio, Nucl.Phys. B **886** (2014) 75; arXiv:1405.4263[hep-ph].

[103] C. I. Low, Phys. Rev. D **70** (2004) 073013 [hep-ph/0404017].

[104] C. I. Low, Phys. Rev. D **71** (2005) 073007 [hep-ph/0501251].

[105] Satoru Kaneko et al.; arXiv: hep-ph/0703250 (2007).

[106] F. Capozzi et al., Nucl. Phys. B **908** (2016) 218-234; arXiv:1601.07777.

[107] S. Gariazzo et al., J.Phys. G **43** (2016) 033001; arXiv:1507.0820.

[108] C. Giunti, *Oscillations beyond three-neutrino mixing*, 2016. Talk given at Proceedings of Neutrino 2016, London, UK.

[109] T. Schwetz, *Global oscillation fits with sterile neutrinos, 2011*. Talk given at Proceedings of Sterile Neutrino Crossroads, 2011, Virginia Tech, USA.

[110] P. O. Ludl, W. Grimus, JHEP **07** 090 (2014); arXiv: 1406.3546.

[111] A. Kageyama et al., Phys. Lett. B **538** (2002) 96 [hep-ph/0204291].

[112] B. R. Desai, D. Roy, and A. R. Vaucher, Mod. Phys. Lett. A **18** (2003) 1355-1366; [hep-ph/0209035].

[113] S. Dev et al., Phys. Lett. B **656** (2007) 79-82; arXiv:0708.3321.

[114] W. Grimus and L. Lavoura, J. Phys.G **31** (2005) 693 [hep-ph/0412283].

[115] S. Dev et al., Nucl. Phys. B **784** (2007) 103 [hep-ph/0611313].

[116] S. Dev et al., Nucl. Phys. B **784** (2007) 103-117, [hep-ph/0611313].

[117] W. Grimus and P. O. Ludl, Phys. Lett. B **700** (2011) 356; arXiv:1104.4340.

[118] S. Kumar, Phys. Rev. D **84** (2011) 077301; arXiv:1108.2137.

[119] P. O. Ludl, S. Morisi and E. Peinado, Nucl. Phys. B **857** (2012) 411; arXiv:1109.3393.

[120] B. Adhikary, M. Chakraborty and A. Ghosal, Phys. Rev. D **86** (2012) 013015; arXiv:1205.1355.

[121] D. Meloni and G. Blankenburg, Nucl. Phys. B **867** (2013) 749; arXiv:1204.2706.

[122] J. Liao, D. Marfatia and K. Whisnant, JHEP **09** (2014) 013; arXiv:1311.2639.

[123] D. Meloni, A. Meroni and E. Peinado, Phys. Rev. D **89** (2014) 053009; arXiv:1401.3207.

[124] S. Dev, R.R. Gautam, L. Singh and M. Gupta, Pramana **86** (2016) 379.

[125] P. Kumar and M. Patgiri, *Minimal extended seesaw and group symmetry realization of two-zero textures of neutrino mass matrices* (Under Review)

[126] Y. Zhang, Phys.Rev. D **87** (2013), 053020; arXiv:1301.7302.

[127] D. Borah et al., Phys. Rev. D **94**, 113001 (2016); arXiv:1606.0207.

A

A.1 Light neutrino mass matrix elements

$$m_{ee} = c_{12}^2 c_{13}^2 c_{14}^2 m_1 + e^{-i\alpha} c_{13}^2 c_{14}^2 m_2 s_{12}^2 + e^{-i\beta} c_{14}^2 m_3 s_{13}^2 + e^{-i\gamma} m_4 s_{14}^2, \tag{A.1}$$

$$\begin{aligned} m_{e\mu} = {} & e^{i(\delta - 14 - \delta_{24} - \gamma)} c_{14} m_4 s_{14} s_{24} + c_{12} c_{13} c_{14} m_1 (-c_{23} c_{24} s_{12} - e^{i\delta_{13}} c_{12} c_{24} s_{13} s_{23} - e^{i(\delta_{14} - \delta_{24})} \\ & c_{12} c_{13} s_{14} s_{24}) + e^{-i\alpha} c_{13} c_{14} m_2 s_{12} (c_{12} c_{23} c_{24} - e^{i\delta_{13}} c_{24} s_{12} s_{13} s_{23} - e^{i(\delta_{14} - \delta_{24})} c_{13} s_{12} s_{14} s_{24}) \\ & + e^{-i(\beta + \delta_{24})} c_{14} m_3 s_{13} (e^{i(\delta_{13} + \delta_{24})} c_{13} c_{24} s_{23} - e^{i\delta_{14}} s_{13} s_{14} s_{24})), \end{aligned} \tag{A.2}$$

$$
\begin{aligned}
m_{e\tau} = {} & e^{-\frac{i\gamma}{2}-\frac{1}{2}i(\gamma-2\delta_{14})}c_{14}c_{24}m_4 s_{14}s_{34} + c_{12}c_{13}c_{14}m_1(-e^{i\delta_{13}}c_{12}c_{23}c_{34}s_{13} + c_{34}s_{12}s_{23} \\
& - e^{i\delta_{14}}c_{12}c_{13}c_{24}s_{14}s_{34} + e^{i\delta_{24}}(c_{23}s_{12} + e^{i\delta_{13}}c_{12}s_{13}s_{23})s_{24}s_{34}) - e^{-i\alpha}c_{13}c_{14}m_2 s_{12} \\
& (e^{i\delta_{13}}c_{23}c_{34}s_{12}s_{13} + c_{12}c_{34}s_{23} + e^{i\delta_{14}}c_{13}c_{24}s_{12}s_{14}s_{34} + e^{i\delta_{24}}(c_{12}c_{23} - e^{i\delta_{13}}s_{12}s_{13}s_{23})s_{24}s_{34}) \\
& + e^{-i\beta}c_{14}m_3 s_{13}(-e^{i\delta_{14}}c_{24}s_{13}s_{14}s_{34} + e^{i\delta_{13}}c_{13}(c_{23}c_{34} - e^{i\delta_{24}}s_{23}s_{24}s_{34})),
\end{aligned}
\tag{A.3}
$$

$$
\begin{aligned}
m_{es} = {} & e^{-\frac{i\gamma}{2}-\frac{1}{2}i(\gamma-2\delta_{14})}c_{14}c_{24}c_{34}m_4 s_{14} + e^{-i\beta}c_{14}m_3 s_{13}(-e^{i\delta_{14}}c_{24}c_{34}s_{13}s_{14} - e^{i\delta_{13}}c_{13} \\
& (e^{i\delta_{24}}c_{34}s_{23}s_{24} + c_{23}s_{34})) + c_{12}c_{13}c_{14}m_1(-e^{i\delta_{14}}c_{12}c_{13}c_{24}c_{34}s_{14} + e^{i\delta_{24}}c_{23}c_{34}s_{12}s_{24} \\
& - s_{12}s_{23}s_{34} + e^{i\delta_{13}}c_{12}s_{13}(e^{i\delta_{24}}c_{34}s_{23}s_{24} + c_{23}s_{34})) + e^{-i\alpha}c_{13}c_{14}m_2 s_{12}(-e^{i\delta_{14}}c_{13}c_{24}c_{34}s_{12}s_{14} \\
& - e^{i\delta_{24}}c_{12}c_{23}c_{34}s_{24} + c_{12}s_{23}s_{34} + e^{i\delta_{13}}s_{12}s_{13}(e^{i\delta_{24}}c_{34}s_{23}s_{24} + c_{23}s_{34})),
\end{aligned}
\tag{A.4}
$$

$$
\begin{aligned}
m_{\mu\mu} = {} & e^{-i(\gamma-2\delta_{14}+2\delta_{24})}c_{14}^2 m_4 s_{24}^2 + m_1(-c_{23}c_{24}s_{12} - e^{i\delta_{13}}c_{12}c_{24}s_{13}s_{23} - e^{i(\delta_{14}-\delta_{24})}c_{12}c_{13}s_{14}s_{24})^2 \\
& + e^{-i\alpha}m_2(c_{12}c_{23}c_{24} - e^{i\delta_{13}}c_{24}s_{12}s_{13}s_{23} - e^{i(\delta_{14}-\delta_{24})}c_{13}s_{12}s_{14}s_{24})^2 \\
& + e^{-i(\beta+2\delta_{24})}m_3(e^{i(\delta_{13}+\delta_{24})}c_{13}c_{24}s_{23} - e^{i\delta_{14}}s_{13}s_{14}s_{24})^2),
\end{aligned}
\tag{A.5}
$$

$$
\begin{aligned}
m_{\mu\tau} = {} & e^{-\frac{1}{2}i(\gamma-2\delta_{14})-\frac{1}{2}i(\gamma-2\delta_{14}+2\delta_{24})} c_{14}^2 c_{24} m_4 s_{24} s_{34} m_1 (-c_{23}c_{24}s_{12} + -e^{i\delta_{13}} c_{12}c_{24}s_{13}s_{23} \\
& - e^{i(\delta_{14}-\delta_{24})} c_{12}c_{13}s_{14}s_{24})(-e^{i\delta_{13}} c_{12}c_{23}c_{34}s_{13} + c_{34}s_{12}s_{23} - e^{i\delta_{14}} c_{12}c_{13}c_{24}s_{14}s_{34} \\
& + e^{i\delta_{24}}(c_{23}s_{12} + e^{i\delta_{13}} c_{12}s_{13}s_{23})s_{24}s_{34}) - e^{-i\alpha} m_2 (c_{12}c_{23}c_{24} - e^{i\delta_{13}} c_{24}s_{12}s_{13}s_{23} - e^{i(\delta_{14}-\delta_{24})} \\
& c_{13}s_{12}s_{14}s_{24})(e^{i\delta_{13}} c_{23}c_{34}s_{12}s_{13} + c_{12}c_{34}s_{23} + e^{i\delta_{14}} c_{13}c_{24}s_{12}s_{14}s_{34} + e^{i\delta_{24}}(c_{12}c_{23} \\
& - e^{i\delta_{13}} s_{12}s_{13}s_{23})s_{24}s_{34}) + e^{-\frac{i\beta}{2}-\frac{1}{2}i(\beta+2\delta_{24})} m_3 (e^{i(\delta_{13}+\delta_{24})} c_{13}c_{24}s_{23} - e^{i\delta_{14}} s_{13}s_{14}s_{24}) \\
& (-e^{i\delta_{14}} c_{24}s_{13}s_{14}s_{34} + e^{i\delta_{13}} c_{13}(c_{23}c_{34} - e^{i\delta_{24}} s_{23}s_{24}s_{34})),
\end{aligned}
\tag{A.6}
$$

$$
\begin{aligned}
m_{\mu s} = {} & e^{-\frac{1}{2}i(\gamma-2\delta_{14})-\frac{1}{2}i(\gamma-2\delta_{14}+2\delta_{24})} c_{14}^2 c_{24} c_{34} m_4 s_{24} + e^{-\frac{i\beta}{2}-\frac{1}{2}i(\beta+2\delta_{24})} m_3 (e^{i(\delta_{13}+\delta_{24})} \\
& c_{13}c_{24}s_{23} - e^{i\delta_{14}} s_{13}s_{14}s_{24})(-e^{i\delta_{14}} c_{24}c_{34}s_{13}s_{14} - e^{i\delta_{13}} c_{13}(e^{i\delta_{24}} c_{34}s_{23}s_{24} + c_{23}s_{34})) + \\
& m_1 (-c_{23}c_{24}s_{12} - e^{i\delta_{13}} c_{12}c_{24}s_{13}s_{23} - e^{i(\delta_{14}-\delta_{24})} c_{12}c_{13}s_{14}s_{24})(-e^{i\delta_{14}} c_{12}c_{13}c_{24}c_{34}s_{14} \\
& + e^{i\delta_{24}} c_{23}c_{34}s_{12}s_{24} - s_{12}s_{23}s_{34} + e^{i\delta_{13}} c_{12}s_{13}(e^{i\delta_{24}} c_{34}s_{23}s_{24} + c_{23}s_{34})) + \\
& e^{-i\alpha} m_2 (c_{12}c_{23}c_{24} - e^{i\delta_{13}} c_{24}s_{12}s_{13}s_{23} - e^{i(\delta_{14}-\delta_{24})} c_{13}s_{12}s_{14}s_{24})(-e^{i\delta_{14}} c_{13}c_{24}c_{34}s_{12}s_{14} \\
& - e^{i\delta_{24}} c_{12}c_{23}c_{34}s_{24} + c_{12}s_{23}s_{34} + e^{i\delta_{13}} s_{12}s_{13}(e^{i\delta_{24}} c_{34}s_{23}s_{24} + c_{23}s_{34})),
\end{aligned}
\tag{A.7}
$$

$$
\begin{aligned}
m_{\tau\tau} = {} & e^{-i(\gamma-2\delta_{14})} c_{14}^2 c_{24}^2 m_4 s_{34}^2 + m_1 (-e^{i\delta_{13}} c_{12}c_{23}c_{34}s_{13} + c_{34}s_{12}s_{23} - e^{i\delta_{14}} c_{12}c_{13}c_{24}s_{14}s_{34} \\
& + e^{i\delta_{24}}(c_{23}s_{12} + e^{i\delta_{13}} c_{12}s_{13}s_{23})s_{24}s_{34})^2 + e^{-i\alpha} m_2 (e^{i\delta_{13}} c_{23}c_{34}s_{12}s_{13} + c_{12}c_{34}s_{23} \\
& + e^{i\delta_{14}} c_{13}c_{24}s_{12}s_{14}s_{34} + e^{i\delta_{24}}(c_{12}c_{23} - e^{i\delta_{13}} s_{12}s_{13}s_{23})s_{24}s_{34})^2 + e^{-i\beta} m_3 \\
& (-e^{i\delta_{14}} c_{24}s_{13}s_{14}s_{34} + e^{i\delta_{13}} c_{13}(c_{23}c_{34} - e^{i\delta_{24}} s_{23}s_{24}s_{34}))^2,
\end{aligned}
\tag{A.8}
$$

$$
\begin{aligned}
m_{\tau s} = {} & e^{-i(\gamma-2\delta_{14})}c_{14}^2c_{24}^2c_{34}m_4s_{34} + m_1(-e^{i\delta_{13}}c_{12}c_{23}c_{34}s_{13} + c_{34}s_{12}s_{23} - e^{i\delta_{14}}c_{12}c_{13}c_{24}s_{14}s_{34} \\
& + e^{i\delta_{24}}(c_{23}s_{12} + e^{i\delta_{13}}c_{12}s_{13}s_{23})s_{24}s_{34})(-e^{i\delta_{14}}c_{12}c_{13}c_{24}c_{34}s_{14} + e^{i\delta_{24}}c_{23}c_{34}s_{12}s_{24} \\
& - s_{12}s_{23}s_{34} + e^{i\delta_{13}}c_{12}s_{13}(e^{i\delta_{24}}c_{34}s_{23}s_{24} + c_{23}s_{34})) - e^{-i\alpha}m_2(e^{i\delta_{13}}c_{23}c_{34}s_{12}s_{13} + c_{12}c_{34}s_{23} \\
& + e^{i\delta_{14}}c_{13}c_{24}s_{12}s_{14}s_{34} + e^{i\delta_{24}}(c_{12}c_{23} - e^{i\delta_{13}}s_{12}s_{13}s_{23})s_{24}s_{34})(-e^{i\delta_{14}}c_{13}c_{24}c_{34}s_{12}s_{14} \\
& - e^{i\delta_{24}}c_{12}c_{23}c_{34}s_{24} + c_{12}s_{23}s_{34} + e^{i\delta_{13}}s_{12}s_{13}(e^{i\delta_{24}}c_{34}s_{23}s_{24} + c_{23}s_{34})) + e^{-i\beta}m_3(-e^{i\delta_{14}} \\
& c_{24}c_{34}s_{13}s_{14} - e^{i\delta_{13}}c_{13}(e^{i\delta_{24}}c_{34}s_{23}s_{24} + c_{23}s_{34}))(-e^{i\delta_{14}}c_{24}s_{13}s_{14}s_{34} \\
& + e^{i\delta_{13}}c_{13}(c_{23}c_{34} - e^{i\delta_{24}}s_{23}s_{24}s_{34})),
\end{aligned}
\tag{A.9}
$$

$$
\begin{aligned}
m_{ss} = {} & e^{-i(\gamma-2\delta_{14})}c_{14}^2c_{24}^2c_{34}^2m_4 + e^{-i\beta}m_3(-e^{i\delta_{14}}c_{24}c_{34}s_{13}s_{14} - e^{i\delta_{13}}c_{13}(e^{i\delta_{24}}c_{34}s_{23}s_{24} + c_{23}s_{34}))^2 \\
& + m_1(-e^{i\delta_{14}}c_{12}c_{13}c_{24}c_{34}s_{14} + e^{i\delta_{24}}c_{23}c_{34}s_{12}s_{24} - s_{12}s_{23}s_{34} + e^{i\delta_{13}}c_{12}s_{13}(e^{i\delta_{24}}c_{34}s_{23}s_{24} \\
& + c_{23}s_{34}))^2 + e^{-i\alpha}m_2(-e^{i\delta_{14}}c_{13}c_{24}c_{34}s_{12}s_{14} - e^{i\delta_{24}}c_{12}c_{23}c_{34}s_{24} + c_{12}s_{23}s_{34} \\
& + e^{i\delta_{13}}s_{12}s_{13}(e^{i\delta_{24}}c_{34}s_{23}s_{24} + c_{23}s_{34}))^2.
\end{aligned}
\tag{A.10}
$$

Study of different texture zeros of neutrino mass matrices in seesaw mechanism and their group symmetry realization

Priyanka Kumar

Department of Physics

Cotton College (currently Cotton University)

This thesis is submitted to

Gauhati University as requirement for the degree of

Doctor of Philosophy

Faculty of Science

March 2020

5

Conclusions

In this present work we have attempted to understand the issue of the LSND anomaly which has not been ruled out, but rather supported by MiniBooNE. The data indicate a fourth state of neutrino of about eV scale. The theoretical foundation of sterile neutrino is an important study from the point of view of physics. Again, eV scale sterile neutrinos may have significant implications in astrophysics and cosmology. The current promising neutrino models are built in the framework of seesaw mechanism beyond SM that can explain neutrino masses and mixing of three light active neutrinos barring the LSND discrepancy. The seesaw formula involves with 3×3 Dirac neutrino mass matrix, M_D of mass below electroweak scale, 200GeV, and 3×3 heavy right handed Majorana neutrino mass matrix,M_R of mass

scale about $\sim 10^{14}$ GeV. Again as per the experimental result of Z^0 decay width tells that the number of active neutrinos can never be more than 3. In this situation, natural objective of the work is to extend the type-I seesaw formula minimally to include an extra neutrino state which must not interact but mix only. In this purpose one right-handed gauge singlet chiral field 'S' represented by (1×3) row matrix M_S has been introduced to couple with the right-handed neutrinos. In construction of the extended version, a 7×7 m_ν matrix has been obtained which on block diagonalization with $M_R >> M_S > M_D$, we obtained a 4×4 neutrino mass matrix, and further block diagonalization with $M_S >> M_D$ has given us 3×3 neutrino mass matrix. So obtained m_ν (Eq. (1.30)) contains the type-I seesaw along with a second term having contribution from the sterile state. The MES has the following features: (i) M_D must possess its inverse along with M_R. (ii) MES neutrino mass matrices are of rank 3 which demand one of the active neutrino mass eigenvalues being zero. Hence only NH or IH mass orderings are allowed. (iii) An eV scale sterile neutrino has been a natural consequence without needing any tiny Yukawa coupling or mass scales.

The present study deals with the texture zeros of neutrino mass matrices in two folds: (i) of order 3×3 and (ii) of order 4×4 resulting from the zeros of (3×3) M_D, (3×3) M_R and M_S via MES. Texture zero models have been extensively studied in 3 active neutrino scenario as well as (3+1) scenario for two reasons; (i) enhancement of predictive power of models by reducing the number of free parameters and (ii) zero entries for underlying symmetries. In 3 neutrino scenario, there are a number of one and two-zero textures of m_ν which are compatible with oscillation data. Our motivation of work has been on realizing the zero textures of m_ν in presence of an additional eV-scale sterile neutrino i.e., (3+1) scenario. In order to realize zero textures of neutrino mass matrix m_ν we have considered the predictive scenario which leads to non-trivial fits for the lepton mixing (PMNS) matrix and/or for the neutrino mass ratios, whereby the sum of zeros of M_D and M_R is eight. In predictive scenario there are three possibilities: (4+4) scheme, (5+3) scheme and (6+2)

scheme, whereby the digits within the pair represent the zeros of M_D and M_R respectively. Also, we have considered suitable zero textures of M_S in the process. There are a number of possible combinations of M_D, M_R and M_S which cross over thousands in principle, but such complexity has been tackled with S_3 transformations demanding a set of only a small number of basic combinations. In the process we have obtained correlations among the matrix elements of neutrino mass matrices, which have been checked for their phenomenological consistencies under the current data of neutrino parameters of 3σ values by plotting scatter plots. Moreover, the zeros of the viable textures have been realized by the Abelian flavor symmetry group Z_N. The framework of the thesis has been elaborated in the **Chapter 1**.

In **Chapter 2**, we have systematically explored the one-zero and two-zero textures of three active neutrino sector, $m_\nu^{3\times3}$ in MES. To realize such texture zeros we have considered zeros of M_D, M_R and M_S as more fundamental, which finally propagate to the effective neutrino mass matrices $m_\nu^{3\times3}$ via MES. We explored all the three possible predictive scenarios: (4+4), (5+3) and (6+2) schemes along with suitable zero textures of M_S. In the (5+3) and (4+4) schemes one-zero textures of m_ν like $m_{e\tau}=0$, $m_{\tau\tau}=0$ and in (5+3) one more $m_{\mu\mu}=0$ have been generated. Interestingly the experimental compatibility allows the textures with $m_{\tau\tau}=0$ while the rest with $m_{e\tau}=0$, $m_{\mu\mu}=0$ are not allowed by recent neutrino oscillation data. Thus the presence of sterile state is more stringent for permissible textures. We have also observed that S_3 group transformations have reduced the tedious work for dealing with a large number of combinations to only a few basic combinations of M_D, M_R and M_S under each of (4+4) and (5+3) scheme.

Interestingly we have also found that in predictive scenario no two-zero textures, which are otherwise experimentally viable, survive in MES containing one sterile neutrino. Again all allowed one-zero textures of neutrino mass matrices represent only inverted hierarchical

neutrino models. So this is an important observation that $m_\nu^{3\times3}$ in MES framework favours only inverted hierarchy of mass ordering.

The viable textures in our study have been realized under Z_7 Abelian symmetry group by extending the Standard Model with 2 Higgs doublet (Φ_2, Φ_3) and 3 scalar singlets χ and λ_1, λ_2 to realize the viable structures of M_D, M_R and M_S respectively. We have also considered Z_7 transformations of the singlet chiral field 'S',in order to prevent bare mass term of 'S' as demanded by MES mechanism. We have also illustrated how other set of matrices obtained by permutation with the elements of S_3 can be realized by Z_7 by simply interchanging the transformations of the RH neutrino singlets from their respective basic cases.

In **Chapter 3** and **4** the phenomenology of MES mechanism for realization of two-zero textures in the 4×4 neutrino mass matrix has been explored. It is interesting to note that in chapter 2, two-zero textures in $m_\nu^{3\times3}$ in the framework of MES mechanism could not be realized under the predictive scenario. This motivated us to relook into the two-zero textures of m_ν in the 4×4 form in MES. As MES neutrino mass matrices must be of rank 3, so we have considered only those 12 textures $A_1, A_2, B_3, B_4, C, D_1, D_2, E_1, E_2, F_1, F_2, F_3$ which are of rank 3 for our study (Table 3.1), although we had 15 phenomenologically viable two zero textures of $m_\nu^{4\times4}$. We have undertaken the predictive scenarios of M_D and M_R: (4+4), (5+3) and (6+2) schemes for realization of two-zero textures of $m_\nu^{4\times4}$. Under (4+4) scheme (Chapter 3) we have found that two-zero texture of M_S cannot lead to non-zero sterile sector of $m_\nu^{4\times4}$. However, for (5+3) scheme (Chapter 4) both one and two-zero textures of M_S have been found to be useful for realizing the desired textures. The imposition of zeros has led us to certain correlations among the neutrino parameters for each texture. Then we have checked whether these correlations are consistent with the recent neutrino oscillation data.

Experimental bound on $\sin\theta_{34} < 0.4$. However, in our analysis, the lower limit has been taken to be 0. Furthermore, we have also considered the contributions of Dirac $(\delta_{13}, \delta_{14}, \delta_{24})$ and Majorana CP phases (α, β, γ) for the consistency test of the correlations of each texture. This is in contrast to the analysis of one-zero textures of $m_\nu^{3\times3}$ in chapter 2, whereby we considered a particular range of the CP phases (δ, α, β) for each texture. Although the methodology of chapter 3 and 4 are similar, the results are quite different.

In chapter 3 it has been observed that all the 12 two-zero textures can be realized under (4+4) scheme. However, we have found that for unconstrained CP phases $(0 - 360^0)$ the textures E_1, E_2 favoring normal hierarchy, are disfavored by neutrino oscillation data as its correlation remains inconsistent. Also, out of three combinations of M_D, M_R and M_S for texture D_2, two combinations for normal hierarchy are ruled out, as their respective correlations are inconsistent within 3σ range of oscillation data. This is an interestingly result that $m_\nu^{4\times4}$ in MES favors inverted hierarchy of mass ordering. Thus out of 12 only 10 textures are viable under (4+4) scheme

Again, in chapter 4 we have seen that (5+3) and (6+2) scheme are more constrained than that of the (4+4) scheme studied in chapter 3. Similar to chapter 2, here also the (6+2) scheme have not been found to be productive as none of the two-zero textures of $m_\nu^{4\times4}$ can be realized within MES. Again only 9 out of 12 textures are viable within the (5+3) scheme. Textures E_1, E_2 which were realizable in (4+4) scheme but ruled out by oscillation data, cannot be even realized within the (5+3) scheme. In addition we have seen that texture C which is an allowed texture within (4+4) scheme, cannot be realized with (5+3) scheme. Texture C has zeros in $\mu\mu$ and $\tau\tau$ entry of the mass matrix $m_\nu^{4\times4}$. Similarly for texture E_1 : $m_{ee} = 0; m_{\mu\mu} = 0$ and texture E_2: $m_{\mu\mu} = 0; m_{\tau\tau} = 0$. Thus, it is interesting to note that (5+3) scheme rules out those textures where both the zeros appears in the diagonal form of $m_\nu^{4\times4}$.

We have found that S_3 group transformations exist among different combinations of M_D, M_R and M_S which keep $m_\nu^{4\times4}$ invariant leading to same correlations and hence similar

phenomenology. We have tabulated the S_3 symmetric textures of (4+4) and (5+3) schemes in the respective chapters 3 and 4.

In both the schemes of (4+4) and (5+3) the viability of a texture have been checked by plotting the correlations against $\sin\theta_{34}$ under two conditions: (i) unconstrained $(0-360^0)$ Dirac and Majorana CP phases and (ii) constraining the CP phases to different segment of values. We have found that when CP phases are unconstrained, certain textures shows consistency in their correlation for all values of $\sin\theta_{34} = (0-0.4)$, while certain textures are allowed for some constrained ranges of $\sin\theta_{34}$.

We have found that there exist an interplay of Dirac and Majorana CP phases in determining the viability of a texture. Although experimental constraints on CP phases are yet not known, and remains unconstrained within 3σ range, still we have attempted to study the effect of the CP phases on the neutrino mass matrix $m_\nu^{4\times4}$. Accordingly we have checked the consistency of correlation(s) of each of the textures by considering smaller ranges of values of unknown CP phases from the complete range $(0-360^0)$. On constraining the CP phases we have observed that there are a number of textures for which (i) the allowed range of $\sin\theta_{34}$ gets squeezed to smaller values as compared to the values when CP phases are unconstrained (ii) the correlation(s) becomes inconsistent and the textures are not allowed for any range of $\sin\theta_{34} = (0-0.4)$ within that particular choice of combination of the six CP phases and (iii) viability of the textures remains unaffected for any choice of constrained ranges of CP phases and this holds even when CP phases are made to be zero. Textures of the type (i) and (ii) shows variation with the CP phases and are therefore categorised as CP phase dependent textures. On the other hand, textures of the type (iii) remains insensitive to the variations of CP phases and are therefore CP phase independent textures. Also, we have observed that most of the textures are allowed for values of $\sin\theta_{34} > 0$, thereby giving a lower limit on $\sin\theta_{34}$ which is still experimentally unknown.

Viable textures have been finally realized via Abelian flavor symmetry group Z_n by extending the Standard Model with some scalar fields. For (4+4) scheme we have undertaken Z_9 symmetry group while for (5+3) scheme textures are realized via the group Z_8. In symmetry realization of all the viable textures in chapter 2, 3 and 4, we have required three Higgs doublet (Φ_1, Φ_2, Φ_3) in which Φ_1 is the SM Higgs transforming trivially under the group Z_n. In addition we have required one singlet χ to realize the desired zero texture of M_R and one singlet λ to realize the two-zero textures of M_S while two scalars λ_1, λ_2 for realization of one-zero textures of M_S. Also we have given a transformation of the singlet chiral field 'S' so as to prevent bare mass term of the form $\bar{S}^c S$. We have also observed that symmetry realization of the other set of matrices obtained by permutation with the elements of S_3 can be achieved by simply interchanging the Z_9 field transformations of the RH neutrino singlets from their respective basic cases, meanwhile keeping the transformation of all the other fields unchanged.

Future scope of expansion of the present work:

It still awaits a watershed experimental proof for the existence of sterile neutrinos. Once it is established then some theoretical challenges shall stem before the theoretical particle physicists. The present study may be useful to understand light sterile states of neutrinos and may also be extended to the following which are not any way exhaustive lists:

• Our study has been confined to predictive scenario only, but there is a scope for study without restricting to predictive scenario as such study has been widely done in active neutrino scenario in literature.

• Neutrinoless double beta decay and leptonic CP violations may be explored.

• The M_R textures as predicted in our study may be used for study of baryogenesis in presence of sterile neutrinos as such study has been done in 3 active neutrino scenario to explain the matter-antimatter asymmetry in the early universe.

• The origin of zero textures have been studied in Z_N Abelian symmetry group but their study in other non-Abelian group symmetry realizations like A_4, S_N may be significant and useful.

• Study may be done on the scope for accommodating degenerate spectrum of active neutrino mass eigenvalues in presence of sterile state which is not allowed in the present form of MES as it demands one of the neutrinos being massless.

There are broader perspective of the thesis for expansion to address the following issues regarding sterile neutrinos:

• How many light sterile states of neutrinos may exist?

• What are the scales of sterile states: sub-eV, eV or KeV?

• What are the implications in astrophysics and cosmology particularly in structure formations?

• Are they candidates of dark matter?

Our understanding of the pertinent issues in neutrino physics is incomplete and so they require research in both theoretical and experimental perspectives for solutions.